Helsinki University of Technology Laboratory of Steel Structures Publications 20

Teknillisen korkeakoulun teräsrakennetekniikan laboratorion julkaisuja 20

Espoo 2000 TKK-TER-20

BEHAVIOUR OF A SEMI-CONTINUOUS BEAM-COLUMN CONNECTION FOR COMPOSITE SLIM FLOORS

Mikko Malaska

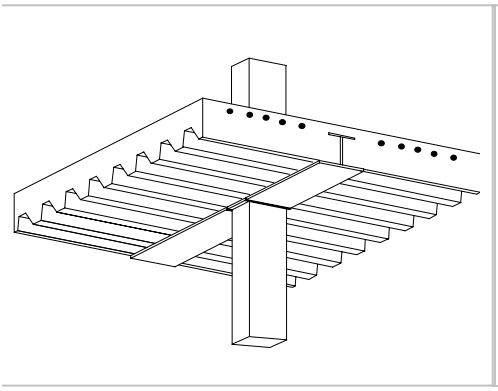

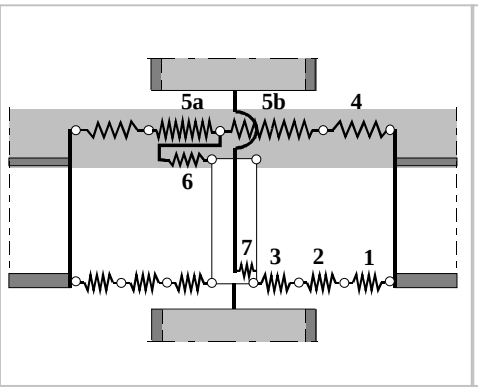

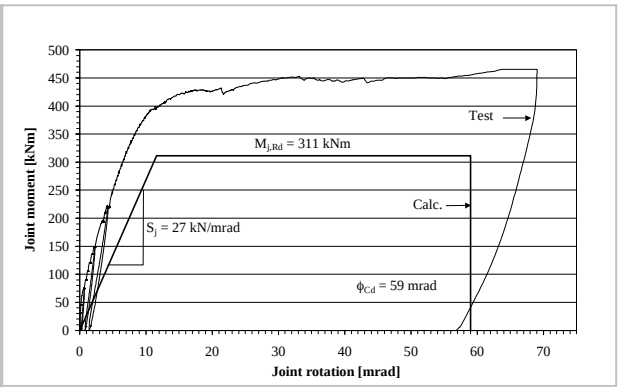

TEKNILLINEN KORKEAKOULU
TEKNISKA HÖGSKOLAN
HELSINKI UNIVERSITY OF TECHNOLOGY
TECHNISCHE UNIVERSITÄT HELSINKI
UNIVERSITE DE TECHNOLOGIE D'HELSINKI

Helsinki University of Technology Laboratory of Steel Structures Publications 20

Teknillisen korkeakoulun teräsrakennetekniikan laboratorion julkaisuja 20

Espoo 2000 TKK-TER-20

BEHAVIOUR OF A SEMI-CONTINUOUS BEAM-COLUMN CONNECTION FOR COMPOSITE SLIM FLOORS

Mikko Malaska

Dissertation for the degree of Doctor of Science in Technology to be presented with due permission for public examination and debate in Auditorium R1 at Helsinki University of Technology (Espoo, Finland) on the 11th of December, 2000, at 12 o'clock noon.

Helsinki University of Technology

Department of Civil and Environmental Engineering

Laboratory of Steel Structures

Teknillinen korkeakoulu

Rakennus- ja ympäristötekniikan osasto

Teräsrakennetekniikan laboratorio

Distribution:
Helsinki University of Technology
Laboratory of Steel Structures
P.O. Box 2100
FIN-02015 HUT
Tel. +358-9-451 3701
Fax. +358-9-451 3826
E-mail: sinikka.rahikainen@hut.fi

ISBN 951-22-5224-4
ISSN 1456-4327

Otamedia Oy

ABSTRACT

The flooring system with its connections to the supporting column significantly influences the technical quality and performance of the steel-concrete composite design and the overall economic viability of the construction. Expectations of technical and economic flexibility and cost-effectiveness that alternative feasible solutions may offer motivate research and development in this field. This study focuses on the behaviour of beam-column connections in a building frame consisting of slim floor beams. The principal purpose was to gain a better understanding of the engineering features of semi-continuous composite joints and to apply this knowledge in the design of structures frequently used in Finland.

A new advanced structural design connecting a slim floor beam to a tubular steel column section filled with concrete was designed using an application of the semi-continuous concept. The design was implemented and the construction tested in a thorough empirical study. Experimental work included two tests on bare steel connections and four tests on composite connections with full-scale specimens. The two tests on the bare steel connections demonstrated the joint behaviour during the erection and concreting work of the floor. Four specimens of composite connections were then tested in order to learn the influence of the slab characteristics on the connection behaviour in terms of the amount of reinforcement used in the slab, the shear-to-moment ratio, and the concrete strength.

A mathematical model for predicting the moment-rotation characteristics of the joint response was formulated based on the geometrical and mechanical joint properties and findings from the empirical study. In the model formulation the basic mechanism of force transfer within the components of a composite connection was applied. Derived from the model and validated by the experimental results simple and robust methods that can be used by the designers are proposed.

Keywords: composite; slim floor; structural joints; characterisation; modelling; classification; continuous; semi-rigid; experimentation; idealisation; mechanical model; analytical model

PREFACE

This research was carried out in the Laboratory of Steel Structures at Helsinki University of Technology (HUT). The work was done mainly in the frame of an extensive research project *Steel-concrete Composite Slim Floor Frame System* belonging to the TEKES/Finnsteel technology programme conducted to investigate and improve the existing methods in composite frame design and construction.

Financial support to this research project was provided by the National Technology Agency of Finland (TEKES), the Finnish Constructional Steelwork Association Ltd (FCSA) and the Finnish companies Rautaruukki Oyj and PPTH Teräs Oy. The preparation of this doctoral thesis has been supported by personal research grants from the Association of Finnish Civil Engineers (RIL), the Foundation of Oskar Öflund, Tekniikan edistämissäätiö, The Academy of Finland and Helsinki University of Technology. The financiers and sponsors are gratefully acknowledged.

I am very grateful for the support given by my supervisor, Professor Pentti Mäkeläinen, during this work. I would like to thank him for directing me to this challenging and interesting field of research, for the possibilities to introduce the results of the study in many international research forums and his trustful support throughout the work. The constructive criticism of the preliminary examiners, Professor Johansson and Dr. Matti Leskelä, has greatly improved the consistency and reliability of the thesis. I also wish to thank Mr. Nigel Kimberley who carried out the linguistic revision.

The members of the steering committee of the TEKES/Finnsteel project were Mr. Tarmo Mononen (Rautaruukki Oyj), Mr. Tom Warras (National Technology Agency, TEKES), Mr. Jouko Kouhi (Finnsteel Technology Program), Mrs. Heli Koukkari (VTT Building Technology), Mr. Reino Hänninen (Ins.tsto P. Kaista & Co Oy), Mr. Jouko Kansa (PR-Steel Oy), Mr. Tapio Leino (VTT Building Technology), Mr. Allan Savola (Rannila Steel Oy), Mr. Markku Varis (Finnmap Consulting Oy) and Mr. Casper Ålander (Fundia-Betoniteräkset). The discussions with the committee have

been particularly fruitful, bringing the producers' and designers' viewpoints into consideration.

All the tests have been carried out at Helsinki University of Technology in the test hall of the Department of Civil and Environmental Engineering by Mr. Veli-Antti Hakala, Mr. Pekka Tynnilä, Mr. Hannu Kaartinaho and Mr. Esko Varis. Mr. Pertti Alho from the Laboratory of Material Technology gave valuable help in testing the material properties of concrete.

I wish to thank Mr. Aki Vuolio, who carried out finite element calculations, which, even though not documented here, formed the basis for the connection design at the early stage of the work. My warmest thanks also to my colleagues at Helsinki University of Technology. I would like to thank them for their support and for making the laboratory a good and innovative environment for research.

I want especially to thank Professor Karin Holstius and Professor Pentti Malaska for thorough support in the process of transforming the results of research into dissertation form. I am also grateful to my parents, grandmother and brother for their encouragement and support in both the difficult and the exciting moments of my studies. Special thanks go to my father, Martti Malaska, who has endured endless discussions about structural mechanics, statics and steel design over the years.

November 2000

Mikko Malaska

TABLE OF CONTENTS

LIST OF SYMBOLS

a	distance from the column face to the first shear connector
b	Breadth, width
d	Depth
e	Eccentricity
f	Strength
h	Thickness
k	Coefficient of translational stiffness
k_c	Coefficient that allows for the self-equilibrating stresses and the stress distribution in the slab prior to cracking
p	Distance between the shear connectors
s	Slip
y	Distance
z	Distance

A	Cross-sectional area
D_s	Distance between the centroid of the reinforcement and the upper layer of the steel beam
E	Modulus of elasticity
F	Force
I	Second moment of area of cross-section
L	Length
M	Bending moment
S	Rotational stiffness
V	Shear force

δ	Deflection
ε	Strain
ϕ	Diameter, rotation
γ	Partial safety factor
η	Modification factor
μ	Factor of imbalance
ρ	Reinforcement ratio
σ	Stress
τ	Bond stress, shear stress

Δ	Deformation capacity, difference

Subscripts

a	Structural steel
b	Beam
c	Column, compression, concrete
cp	Contact plate
cs	Concrete slab
d	Design value
eff	Effective value

exp	Experimental
fl	Flange
ini	Initial
j	Joint
k	Characteristic value
l	Left
m	Mean, average value
pl	Plastic
pred	Predicted
ps	Profiled steel decking
r	Right
s	Reinforcement
sh	Shear flat, strain hardening
stiff	Stiffener
t	Tensile, transnission
u	Ultimate value
unl	Unloading
v	Shear connection
y	Yield

C	Capacity
L	Longitudinal
R	Resistance
S	Shear, Effect of actions
T	Tension
Xd	Threshold of the inelastic stage

1 INTRODUCTION

A slim floor beam system with the steel beams contained within the depth of the floor and supported by circular or rectangular hollow steel columns filled with concrete is a frequently used construction in office and residential building frames in Finland. In the conventional design of these buildings, the connections between the beams and columns are treated as nominally pinned or as rigid, resulting in a simple or continuous construction, respectively. However, the design guidance and rules of application for the steel-concrete composite connections treated as semi-continuous are now proposed and implemented in design codes. Guidelines for the design of building frames are also available including the connection behaviour and methods for the evaluation of the mechanical properties and of the non-linear moment-displacement relationship of the connections. Satisfactory design concepts have already been proposed for the most conventional composite connections, e.g. a structural steel section located beneath the slab, and manuals providing tabulated connection capabilities for the standard connections have recently been published for designers (Anderson (ed), 1997, Couchman and Way, 1998 and Anderson et al., 1999, Huber, 1999).

The flooring system with its connections to the supporting column significantly influences the technical quality and performance of the steel-concrete composite design and the overall economic viability of the construction. Alternative feasible solutions of the floor beam system and its connection to the supporting column offer technical and economic flexibility in different applications, and furthermore expectations of improved cost-effectiveness motivate research and development in this field. A design principle of semi-continuity provided with multi-span continuous structures or with beam-column connection structures has been studied and found to promise more advanced designs. Extensive research of composite connections with slim floor systems has been carried out at Helsinki University of Technology (HUT) from 1997 – 2000 (Malaska and Mäkeläinen, 1999, Mäkeläinen and Malaska, 1999, Vuolio, 2000 and Malaska et al., 2000). A slim floor beam system of semi-continuous constructions provides shallower beam and floor sections, larger clear beam spans and better performance of beams in service conditions with reduced problems in cracking,

deflections and vibration. A structural configuration of a beam-column connection in a slim floor system, as illustrated in Fig. 1.1, was developed and constructed for this study by the author. The building frame consists of a concrete-filled composite column and a composite floor. The system utilizes an asymmetric floor beam connected to the column by bolts. Compared to conventional floor systems, the system studied offers also advantages of providing a floor system of minimum depth and a flat soffit, which facilitates easy installation of services and the free positioning of building partition walls. Both the beam and the steelwork connection are encased in the concrete, which significantly enhances their resistance at ambient and fire temperatures.

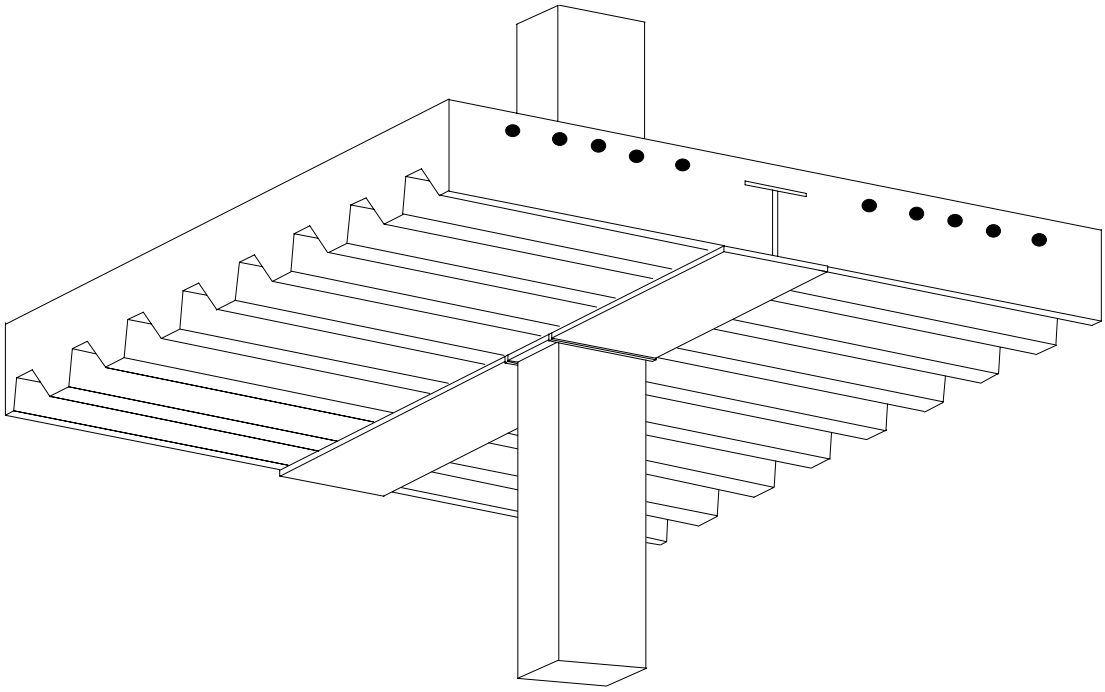

Figure 1.1 The slim floor beam system.

Compared with the conventional composite connections, the available lever arm between compression and tension components of the connection is decreased in the slim flooring systems while the amount of the slab reinforcement required to get moment resistance equal to the capacity of the conventional connections is increased. The higher amount of reinforcement in the tension region increases the forces in the

compression region. However, the joints in the slim flooring systems have better performance concerning the stability problems of the steel beam in compression because the beam is partially encased in the concrete of the slab.

Only few references are available on the behaviour and design of connections between slim floor beams and composite columns (Leino, 1994, Bernuzzi et al., 1995, Tschemmernegg, 1998, Charbrolin & Bitar, 1998, Huber, 1999). In order to enable the use of a semi-continuous concept in the design and construction of the new flooring system, more information on the deformability and the resistance of the beam-column connection is required. This work focuses on researching of the connections between slim floor beam and concrete-filled composite column members with special regard to their design characterisation.

2 SCOPE OF THE WORK AND OBJECTIVES

2.1 Aim of the research

The aim of the research is to implement the design idea of the connection in test specimens, to determine empirically the static strength of the connection constructed, to identify the parameters and mechanical properties which govern the connection behaviour, and to translate this knowledge into a calculation method that can be used by designers. The problem is firstly studied by laboratory testing. The results are then used to identify possible failure modes, the mechanisms of load transfer and hence to determine the basis for a design approach. The experimental work, including full-scale beam-column connection tests on two bare steel connections and four composite connections, was performed by the author in the TEKES/Finnsteel project reported in ”*Steel-Concrete Composite Slim Floor Frame System*” (Malaska et al., 2000) at Helsinki University of Technology. The results are analyzed and presented in detail in this work. Mathematical modelling of the connection behaviour is performed and analytical calculation methods for designing the composite connection studied are presented and validated against the experimental test results. The effects of variable reinforcement and shear-to-moment ratios are studied and the aspects of the model in design practice are discussed.

2.2 Research tasks and methods

The behaviour of the beam-column connection of the slim floor beam system is investigated. The principal purpose is to gain a better understanding of the engineering features of semi-continuous composite joints and to apply this design knowledge to the structures frequently used in construction in Finland. The research tasks for the study are set as follows:

- to develop a new structural joint connecting a slim floor beam to a tubular steel column section filled with concrete;

- to identify the behavioural model and its essential parameters and determine analytically and experimentally the mechanical properties which govern the connection behaviour;
- to derive and present simple analytical and numerical methods that can be used by designers.

In the preliminary stage of the research, as well as during the main work, a member of experts in research, design offices, construction and steel workshops were consulted in order to specify the relevant requirements for the structural and economical features and for validating the author's ideas of design and to specify the relevant construction conditions. Internationally recognized research reports and other relevant literature was also carefully studied before the test arrangements were designed and carried out.

The research methodology of the study on the connection behaviour and the joint characteristics consisted of experimental investigations, mathematical modelling resulting in predictions of the characteristics, and derivation of the design formulae. New knowledge was accumulated with each of the mutually supporting methodological means. The main methodological contributions are summarized below.

Experimental investigations of two bare steel connections were first carried out in order to demonstrate the joint behaviour during the erection and concreting work of the floor. Four specimens with composite connections were then tested so as to understand the influence of the slab characteristics on the connection behaviour in terms of the amount of reinforcement used in the slab, the shear-to-moment ratio, and the concrete strength.

The purpose of the experimental approach provided information, which was then used in deriving the proposals for the mechanical joint model and analytical calculation methods for the joint characteristics. From the experimental results, a concept for the joint design was developed for the beam-column composite joint configuration between a slim floor beam and a concrete-filled tubular column section exposed to static bending and shear force. The behaviour of the individual material components

in the joint was determined from the material test results and models for the component behaviour were developed in the form of translational springs. From the individual spring components and principles of equilibrium and compatibility, the overall behaviour of the joint was derived.

The influence of connections on the behaviour of a building frame performance depends on the type of the frame, the mode of failure and the limit state considered. The scope of this work is limited to the partial strength connections in braced frames, where the connection is designed to resist the support moments resulting only from gravity loads after the slab has cured and the members are acting compositely. Generally, the design guides recommend that continuous composite connections only be used to connect the beams to internal columns. In perimeter columns, the use of bare steel details are preferred so as to avoid the need to design adequate anchorage of the reinforcement at the edge of the slab. Thus, the prediction methods proposed in this work are applicable only to the connections to internal columns.

2.3 Outline of the thesis

The structural details of the new connection configuration developed in this work, the terminology and the methodology of experimental and numerical research are first described in Chapter 3, in which the floor system, the connection studied and its components are introduced.

In Chapter 4, the experimental work carried out is described and the results obtained from the experiments are reported. A distinction is made between the full-scale beam-column connection tests on bare steel connections and tests on composite connections. The important aspects of the empirical results are discussed.

Based on the experimental results, a simplified mechanical model and mathematical formulae defining the connection response and the connection moment-deformation characteristics are proposed in Chapter 5.

The summary and conclusions, as well as suggestions for further research, are given in Chapter 6.

In the Appendices, the following information is included:

Appendix I: Material test results of reinforcing steel and structural steel

Appendix II: Experimental moment-rotation curves

Appendix III: Measured reinforcement strains

Appendix IV: Measured strains in the shear flat

Appendix V: Calculation example

3 RESEARCH ISSUES IN THE ANALYSES OF SEMI-CONTINUOUS CONNECTIONS

3.1 Beam-column connection of the slim floor system

The design of the frames should be based on the satisfactory performance criteria beginning from the erection, to the serviceability and ultimate state conditions. The following demands for the advanced connection system in this study have influenced the design of the connection configuration to meet the best possible performance at all the limit states discussed not forgetting the fabrication and erection:

- Simple detailing in steelwork.
- Welding on site should be minimized.
- In order to keep composite beam design easy, the steel beam is designed as simply supported during the erection and concreting work. This means that the bare steelwork connections should be designed as hinges and they are employed to resist only vertical shear. According to the numerical frame analysis, the steelwork connections should have capability to rotate as a hinge up to 10-15 mrad rotation.
- The moment resistance and flexural stiffness of the composite joint is provided by the tensile action of the slab reinforcement and the balancing compression is transferred to the column by the steel beam. Any contribution of the steelweb elements to moment-rotation behaviour of the composite joint should be avoided.
- In the composite state, the joint should have sufficient rotation capacity so as to ensure the redistribution of bending moments required by the plastic global analysis of the composite floor beam.

SLIM FLOOR BEAM: Taking into account the structural and the technological requirements identified in the previous studies by Malaska and Mäkeläinen (1999), an asymmetric built-in steel beam section, as shown in Fig. 3.1, is selected. The system consists of a composite floor with a depth of 300 mm and it utilizes a 258 mm-deep welded built-in steel beam partially encased in the slab. The slab consists of *in situ* concrete and a profiled metal decking with a depth of 117 mm. The decking is supported on the lower flange of an asymmetric, I-shaped steel beam.

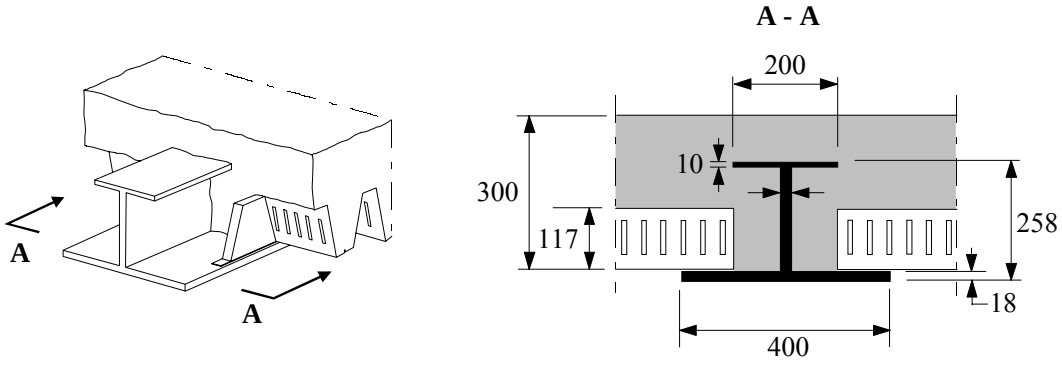

Figure 3.1 Studied composite slim floor system.

STEEL-CONCRETE INTERACTION: Transverse bars having a diameter of 16 mm and length of 500 mm, adopted as shear connectors, are welded on the top flange of the steel beam for resisting the vertical separation and the shear slip between the steel beam and the slab under hogging moment, see Fig 3.2. The first bar is located at a distance of 100 mm from the face of the column, so that the longitudinal reinforcing bars are strained over a substantial length and sufficient rotation can take place. In addition, longitudinal reinforcing bars (ϕ 12 mm) of the composite slab were anchored through the beam web using 16 mm diameter holes.

COMPOSITE COLUMN: In the structural frame system considered, concrete-filled rectangular hollow steel sections are used as columns. This type of a column is very common in office and residential buildings in Finland. The columns are provided with longitudinal reinforcing bars at the column corners and stirrups already in the workshop.

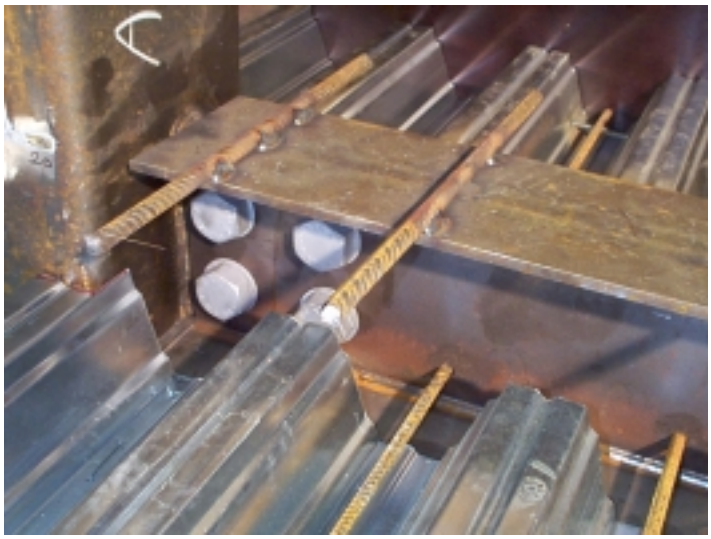

Figure 3.2 Shear connectors resisting vertical separation and slip between steel beam and concrete slab.

STEELWORK CONNECTION: The steelwork connection consists of a shear flat slotted through the wall of the hollow column section and bolted to the steel beam web, see Fig. 3.3. The plate of size 800x210x25 mm is fillet-welded to the web of the column section. To improve the rotation capacity of the connection, a 25x25 mm bevel was cut from the top corner of the plate. The idea is to prevent the corner from getting in contact with the top flange or the fillet weld seam of the steel beam while the connection rotates.

The beam web is connected to the shear flat with four bolts and the bottom flange of the beam is connected to the column web using a contact plate. A bolt connection with 4 ϕ 38 mm (60x38) slotted bolt-holes for the M36 bolts of grade 8.8 was used. The slotted holes are required so as to account for assembly tolerances and to improve the connection rotation capacity. The holes are filled with elastic material before concreting to prevent the concrete from filling the empty slots. The holes in the beam web are round with a diameter of 38 mm. Hexagonal screws with a total length of 140 mm and an 84 mm of thread length were used provided with washers of 65 mm diameter. As the bolts are not subjected to any tensile forces, there are no special

requirements for tightening. A contact plate is used to transmit the compressive force resulting from the beam end moment from the lower beam flange to and through the column. The plate is wedged in tightly and spot-welded on site after the beam is installed and supported by the bolts.

At the same level with the bottom flanges of the steel beams, two steel plates of size 300x50x18 mm are fillet-welded on both sides of the column to strengthen the composite column against the local compression applied from the bottom flanges and through the contact plate. These stiffeners also strengthen the hollow steel section against local buckling effects and offer support for the steel decking.

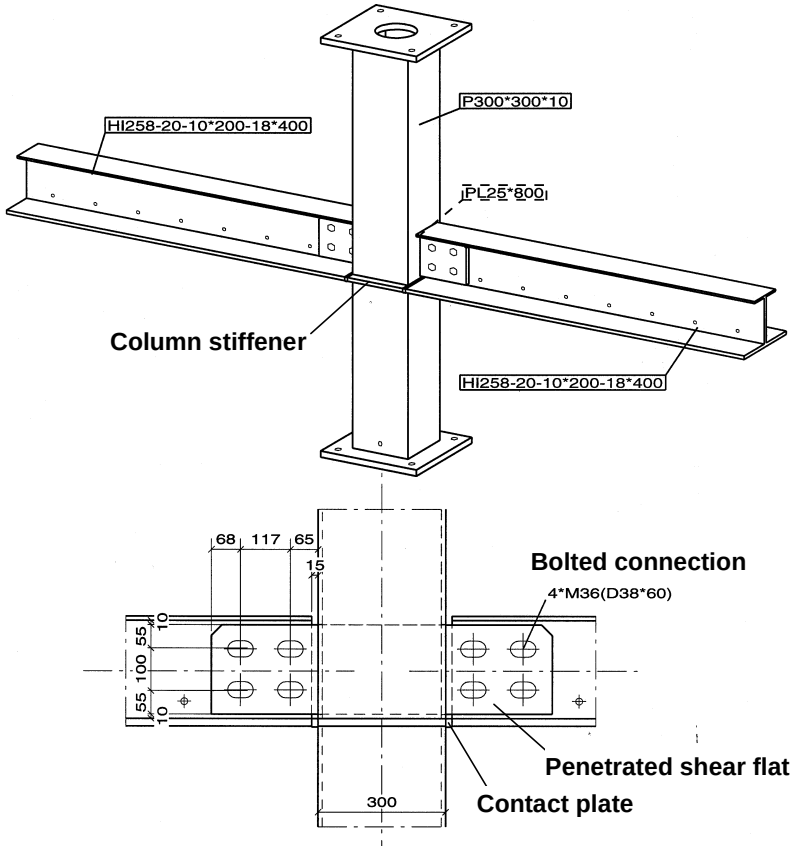

Figure 3.3 Steelwork connection between asymmetric steel beams and a rectangular hollow steel section.

Finplate type of connections that are fillet-welded only on the outer wall of the column section are easy to manufacture and, therefore, often used in beam-column connections of a tubular column section. However, the shear capacity of a connection is significantly improved when the plate is penetrated through the column section and the concrete core. The vertical shear capacities of the penetrated shear flat and finplate connections are compared in the following example.

The governing shear resistance of a shear flat is determined as that of the net section of the shear flat reduced by the slotted bolt-holes and taking into account the interaction of shear (F) and moment due to the eccentric load introduction (F·e) from the beam to the shear flat, see Fig. 3.4 (a). The ultimate strength can be approximately obtained by applying the Von Mises yield criterion:

$$F \le \frac{f_{y,sf}}{\sqrt{\left(\frac{e}{W_{sf}}\right)^2 + 3\left(\frac{1}{A_{sf}}\right)}}. \qquad (3.1)$$

For a finplate connection a simplified chord face yield line model is shown in Fig. 3.4 (b). The deformation of the compression loaded edge of the plate into the column face is assumed as zero because of the concrete filling. Neglecting the influence of membrane action and strain hardening, the following strength formula is obtained:

$$F \le \frac{f_{y,c} \cdot t_c^2 \cdot h_{sf}}{e}\left(2 + 2 \cdot \frac{h_{sf}}{h_c} + 0.5 \cdot \frac{h_c}{h_{sf}}\right). \qquad (3.2)$$

Using the real dimensions and strengths of the connection studied and partial safety factors equal to unity, the predicted shear capacities for the penetrated shear flat and finplate connections are 447 kN and 173 kN, respectively. The results show that the shear capacity is significantly increased if the plate is penetrated through the column.

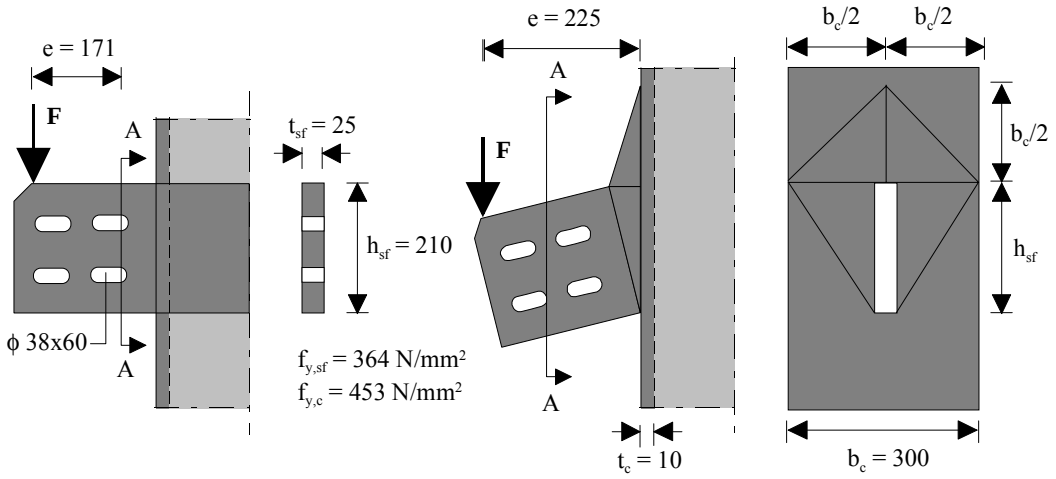

Figure 3.4 Assumed failure modes of a penetrated shear flat and a finplate connection.

REINFORCEMENT: In the composite state, the tension force resulting from the beam end moment is resisted by the longitudinal reinforcement of the composite floor beam, see Fig. 3.5. Grade A500HW ductile reinforcing bars are used. Sufficient transverse reinforcement as ϕ 12 mm bars is supplied on both sides of the column to prevent longitudinal splitting failure of the concrete slab. A layer of welded fabric mesh reinforcement (ϕ 6 mm, cc 150 mm) is placed over the longitudinal bars for resisting shrinkage and for controlling the cracking behaviour in the concrete.

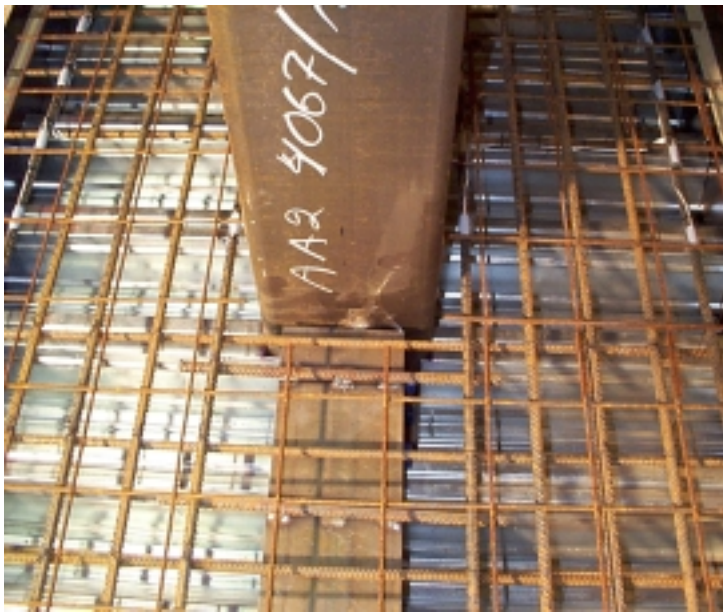

Figure 3.5 Slab reinforcement.

3.2 Terminology

In this section, the essential terms frequently used are defined. Some of them are well established and have a unique meaning, while others are used in different meanings by various authors. The definitions of the main terms used in this thesis are provided so as to set basis for their consistent use in the later chapters.

CONNECTION: The interconnection between the composite slim floor beam and the composite column in which the reinforced composite slab is intended to contribute to the resistance of the connection is called a ‘composite connection’. A steelwork connection refers to the physical steel component part, which mechanically links the steel beam and the column.

JOINT: The assembly of the connection components including a concrete-filled composite column, the adjacent end of a composite beam, steelwork connection and a reinforced composite slab, as shown in Fig. 3.6.

JOINT CONFIGURATION: Type or layout of the joint in a zone within which the axes of two or more inter-connected members intersect.

BASIC JOINT COMPONENT: Specific part of a joint that makes an identified contribution to one or more of the joint's structural properties. The characteristics of a basic joint component may be defined by its resistance, stiffness and deformation capacity.

The behaviour of beam-column connections affects the structural frame response and shall therefore be modelled for the frame analysis and design. In the joint model used in the Eurocodes, the overall joint response is simulated by so called *concentrated joint model*. The model adopts the deformation in the connection area by concentrating sources of deformability into single flexural springs arranged to an infinite small point at the intersection point of the axes of the connected members. The joint response is simulated by combined springs representing bending and shear together. In the case of a double-sided connection configuration, two separate but interacting springs are used, as is shown in Fig. 3.6(a). The transformation process linking the shear and bending into a one combined spring characteristic is, however, complicated. Therefore, it is more convenient to regard the joint as a separate member with finite size and with infinite stiffness. In this so called *finite joint model* the sources of deformation are assigned to rotational springs located at the joint edges, separately for bending, S_j, and shear, S_s, influences, see Fig. 3.6(b) (Tschemmernegg, 1994, Huber, 1999). The shear spring is only activated when the joint is exposed to unbalanced hogging moments. In this work, the principles of the finite joint model are followed.

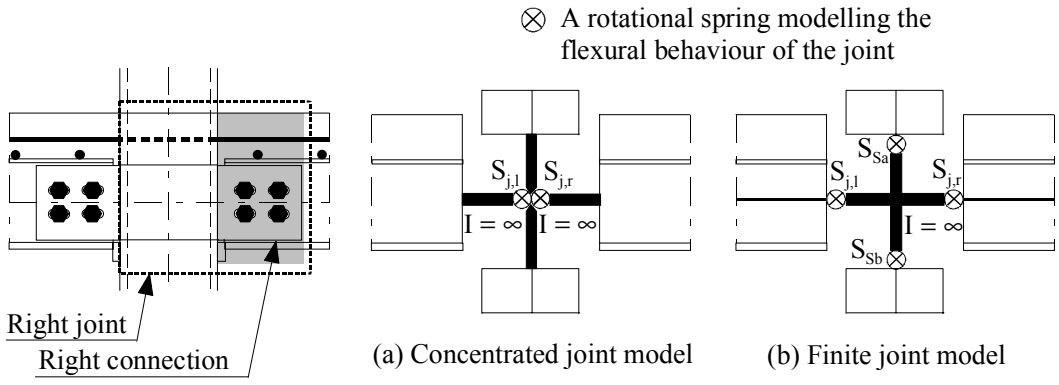

Figure 3.6 Applications of joint modelling.

JOINT CHARACTERISTICS: Throughout this thesis, the overall response of a joint is described by a concept of the moment-rotation curve that takes into account the behaviour of the column as well as the influence of the connection. The curve, indicating the moment-rotation characteristics, is simply the relationship between the moment transmitted by the joint, M_j, and the corresponding rotation, ϕ_j, within the joint. The actual moment-rotation curve of the joint is frequently non-linear. However, for practical design purposes the joint characteristics are idealized by bi-linear shapes or multi-linear simplification so as to fit with the specific analysis approaches used in frame analysis systems, see Fig. 3.7.

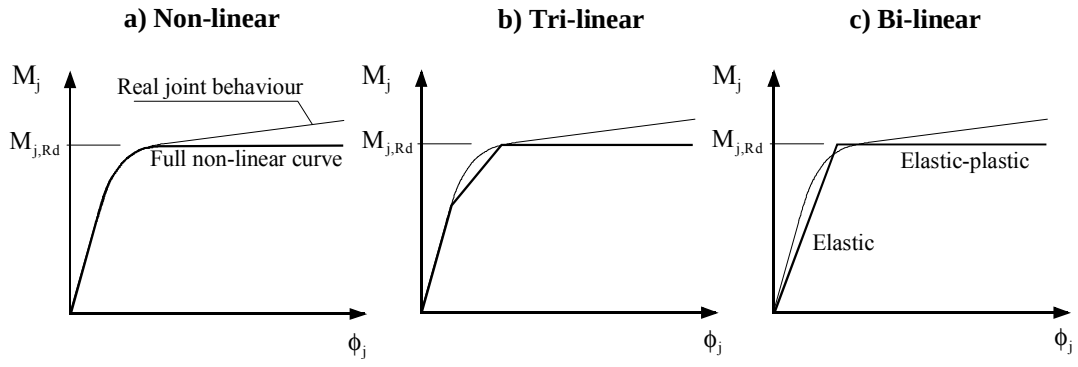

Figure 3.7 Possibilities for moment-rotation curve idealization.

PREDICTION METHODS: Simple mathematical models aimed at predicting the joint characteristics for the purpose of being used in practical design.

The concept of semi-continuous construction requires a statement of the joint behaviour to help the designer to choose a suitable basis on which to carry out the overall frame analysis. This is provided by a classification system. In the system adopted in Eurocode 3 and by Anderson et al. (1999) the joints are classified by two criteria separately: stiffness and strength. Depending on the stiffness of the joints relative to the stiffness of the connected beams, joints are classified as pinned, semi-rigid and rigid. Depending on the moment capacity of the joints relative to the connected beams, connections are classified as pinned, partial-strength and full-strength.

PINNED: A nominally frictionless hinge that prevents any rotational continuity between the connected members.

RIGID: No relative rotations occur between the members connected at the joint.

SEMI-RIGID: The transmitted moment in a joint will result in a difference between the absolute rotations of the two connected members.

FULL-STRENGTH: Joint is stronger than the weaker of the connected members.

PARTIAL-STRENGTH: The moment capacity of the joint is less the hogging bending resistance of the adjacent beam.

CONTINUOUS: The joint ensures a full rotational continuity between the connected members, covering the rigid/full-strength cases.

SEMI-CONTINUOUS: The joint ensures only partial rotational continuity between the connected members, covering the rigid/partial-strength, the semi-rigid/full-strength and the semi-rigid/partial-strength cases.

3.3 Definitions of various characteristics

3.3.1 Prediction of a joint moment-rotation curve

In the experiments, the joint moment, $M_{j,exp}$, is defined as a moment at the column face, resulting as the product of the applied load and the distance from the centre of the load to the outside surface of the column. The rotation of a joint, $\phi_{j,exp}$, is defined according to Fig. 3.8. Bar studs ϕ 8 mm are welded to the upper and lower flanges of the beam and inductive transducers are used to measure the horizontal displacements between the measurement points at the end of the bars and the column face. The rotation of a joint is then calculated dividing the sum of the measured vertical displacements by the vertical distance, 718 mm, between the measurement points. The horizontal deflection values are measured within a calibrated horizontal length of the beam, at a cross-section of 182 mm from the column face. The rotation of the joint is evaluated and deduced from the displacement measurements obtained by transducers 3 and 4 in Fig. 3.8:

$$\phi_{j,exp} = (\delta_4 - \delta_3) / 718 . \qquad (3.3)$$

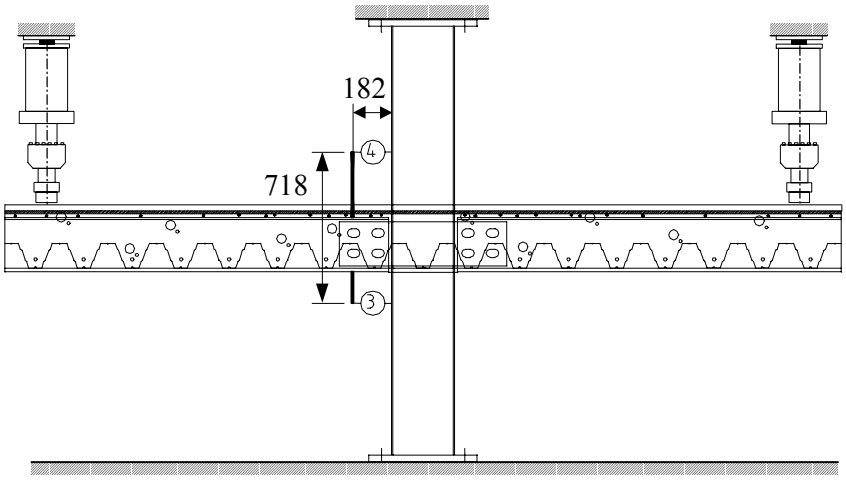

Figure 3.8 Measurement system used for determining the joint rotation.

The rotations due to the moment of the column and the short length of the beam up to the point of rotation measurement are very small, and are ignored.

3.3.2 Prediction of joint characteristics

The definitions of the joint moment-rotation characteristics used in this work are shown in Fig. 3.9. The initial rotational stiffness of the joint, $S_{j,ini}$, is assumed to be equal with the gradient of the unloading and reloading part of the curve, $S_{j,unl}$. The joint moment when all the reinforcing bars in the slab section are plastic is assumed to define the threshold of the inelastic stage of the joint, i.e. the plastic design moment resistance of a joint, $M_{j,Rd}$. ϕ_{Xd} is the joint rotation at which the joint moment first reaches $M_{j,Rd}$. The ultimate moment capacity of the connection in the joint, $M_{j,u}$, is defined as the maximum moment obtained. The rotation capacity, ϕ_{Cd}, of a joint is defined as the rotation that can develop without the bending moment falling below the design moment resistance, $M_{j,Rd}$. If the moment-rotation curve of the experimental results does not indicate a clear point for defining the ultimate connection strength and the curve is still rising at the end of the test, the rotation capacity is equal to the maximum rotation achieved.

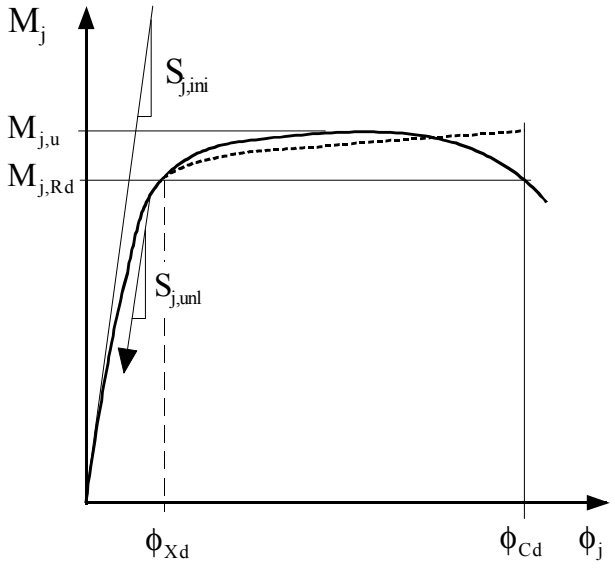

Figure 3.9 Definitions of moment-rotation characteristics in a joint.

3.3.3 Definition of reinforcement ratio

The moment capacity of a joint is controlled by the longitudinal reinforcement in the composite slab. In this work, the amount of reinforcement in the slab is defined by the ratio of reinforcement area to the cross-sectional area of the concrete slab, shown by grey hatching in Fig. 3.10:

$$\rho = \frac{A_s}{A_c} = \frac{A_s}{d_{eff}(b_{eff} - b_c)}, \tag{3.4}$$

where:

$A_s = A_{s,l} + A_{s,r}$ is the cross-sectional area of the longitudinal slab reinforcement in the joint excluding the mesh reinforcement. $A_{s,l}$ and $A_{s,r}$ are the areas on the left and right sides of a column, respectively;

b_{eff} is the effective width of the concrete slab;

b_c is the column width;

d_{eff} is the depth of the solid concrete slab above the metal decking.

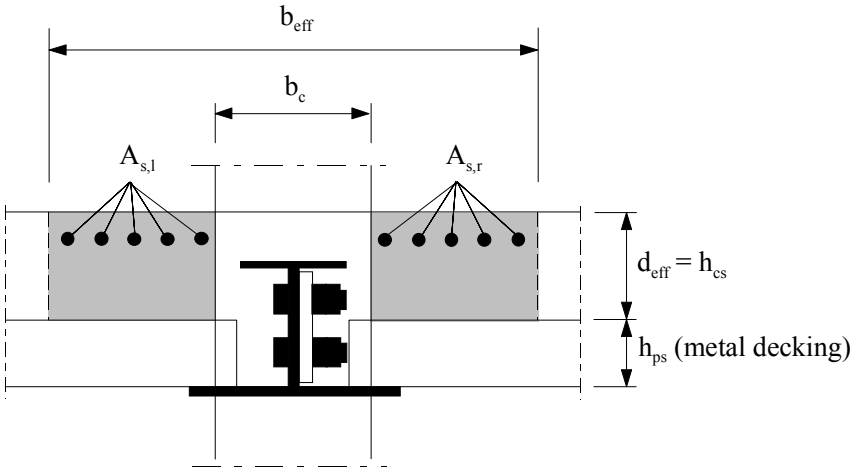

Figure 3.10 Concrete cross-section and reinforcement used in the definition of reinforcement ratio.

In the experimental research programme, one of the parameters varied is the amount of slab reinforcement. The longitudinal reinforcement used is 10 ϕ 16 mm and 10 ϕ 20 mm, corresponding to reinforcement ratios of 0.92 % and 1.43 %, respectively.

4 EXPERIMENTAL RESEARCH

4.1 Objective

With the experimental research, the static strength of the connection was determined and the relevant parameters and mechanical properties that govern the connection behaviour were identified from the results. Most important results of each test are the moment-rotation curve, the pattern of cracking in the concrete and distribution of stresses in the longitudinal reinforcement, as well as the failure mode.

4.2 Research programme

The specimens, which modelled the internal joints in a braced frame, were subjected to in-plane bending and a shear force. Overviews of the specimens are shown in Fig. 4.1. The experimental programme consists of tests with specimens where the geometrical size is fixed and the reinforcement ratio of the slab, concrete strength and the shear-to-moment ratio are as parameters. Two bare steel connections and four composite connections were tested under static loading. The main features of the specimens are given in Table 4.1.

TABLE 4.1

THE CONNECTION SPECIMENS.

Specimen	Connection type	Load position *	Reinforcement / ρ [%]	Concrete
SC1	Bare steel	1650 mm	-	-
SC2	Bare steel	1150 mm	-	-
CC1	Composite	1650 mm	10 ϕ 16 mm / 0.92	C35/45
CC2	Composite	1650 mm	10 ϕ 16 mm / 0.92	C25/30
CC3	Composite	1650 mm	10 ϕ 20 mm / 1.43	C25/30
CC4	Composite	1150 mm	10 ϕ 16 mm / 0.92	C25/30

* Distance from the column flange

a) Bare steel connection b) Composite connection

Figure 4.1 Test specimens.

In order to interpret the connection behaviour during the construction stage, the beam-column connections were first tested without the presence of the reinforced concrete slab (tests SC1 and SC2). The bare steel connections were tested only for bending moments with applied values much less than those of the failure load. After the tests, the connections and the measurement system were restored to the initial state and the same test set-up was used for the composite connection test to follow.

In the composite connection tests (CC1, CC2, CC3 and CC4), the effects of different reinforcement areas on reinforcing bar force and hence moment capacity for a symmetrically loaded connection with two different shear-to-moment ratios were investigated. The reinforcement percentage of the slabs in the composite joint tests CC1, CC2 and CC4 was 0.92 %, and in test CC3 1.43 %. The corresponding longitudinal reinforcements were 10 ϕ 16 mm and 10 ϕ 20 mm, respectively. In one

test, CC1, a higher concrete strength was used. In order to investigate the connection behaviour with different shear-to-moment ratios, the location of the applied load was varied.

4.3 Dimensions of the specimens

All the specimens were designed to have exactly the same steel details and the same composite slab as introduced in Section 3.1. The geometrical dimensions of the specimens including the layouts of the steel reinforcements are shown in Fig. 4.2. The width of the slab was 1500 mm, and it does not exceed the limiting value for the joint effective width of seven times the column width as proposed by Leon and Zandonini (1992). The longitudinal bars were continuous along the beams and over the joint region and they were evenly spaced across the width of twice the column width as proposed by Couchman and Way (1998). The vertical distance between the top of the slab and the centroid of the reinforcement was 40 mm and 38 mm for the 16 mm and 20 mm bars, respectively. Sufficient transverse reinforcement of ϕ 12 mm straight bars, as 1500 mm-long, was supplied on both sides of the column, with the nearest bars situated 50 mm from the column edge so as to prevent longitudinal splitting failure of the concrete slab. The bars were placed below the longitudinal bars on the beam top flange and they were evenly spaced across the width of three times the column width, as proposed by Couchman and Way (1998). The mesh reinforcement (ϕ 6 mm cc 150 mm) was placed above the longitudinal bars with approximately a 20 mm cover from the upper surface of the slab. The hollow square column section was reinforced at the workshop with ϕ 16 mm longitudinal bars at the column corners and ϕ 6 mm stirrups with 240 mm spacing.

Transverse bars of ϕ 16 mm and length 500 mm as welded on the top flange of the steel beam were employed as shear connectors. Eight bars were placed on each cantilever beam and the first one was located at a distance of 100mm from the face of the column.

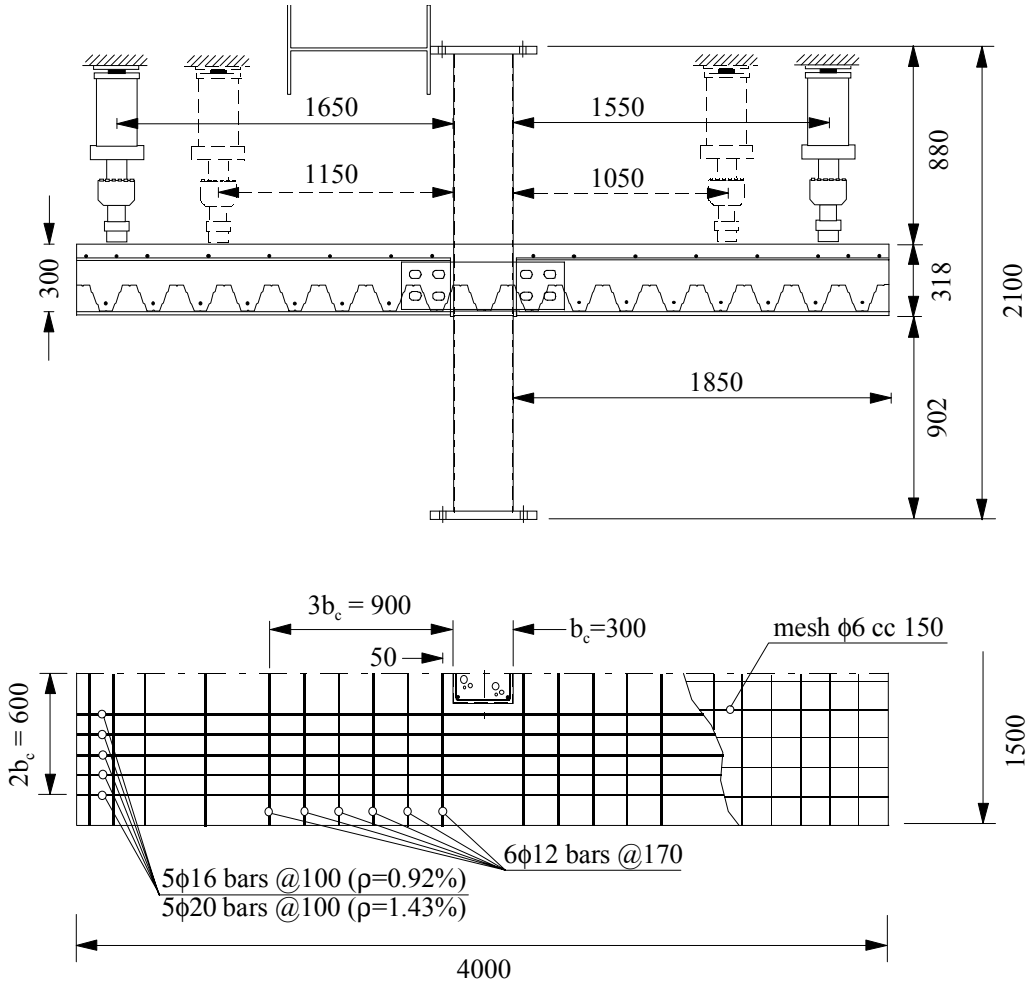

Figure 4.2 General arrangement of the test set-up and the reinforcements.

4.4 Mechanical properties

Material tests were carried out on samples of structural steel, the concrete of the slab, reinforcing bars and welded wire mesh in accordance with standard methods. The detailed test results for steel materials are listed in Appendix I and the main results are also shown below. The bolts were of grade 8.8. Their mechanical properties were not experimentally determined, however.

4.4.1 Structural steel

The mechanical properties of the structural steel components were determined from coupon tests in accordance with standard SFS-EN 10 002-1 "*Metallic materials. Tensile testing. Part 1: Method of test (at ambient temperature)"* (1990). The shear flat and the asymmetric steel beam sections used for the tests were all of grade S355K2G3 steel (Raex moniteräs) and the cold-formed welded column section was of grade S355J2H steel (Raex moniteräs). The mean values for the yield and tensile strength of the steel members are given in Table 4.2.

TABLE 4.2

MEAN VALUES OF MEASURED MATERIAL PROPERTIES OF STEEL MEMBERS.

Element	$f_{y,0.2}$ [N/mm^2]	f_u [N/mm^2]	E [N/mm^2]	ε_y [%]	ε_{sh} [%]	ε_u [%]	ε [%]
Beam flange	387	542	212567	0.18	1.4	14.9	25.4
Beam web	376	548	212012	0.18	1.3	14.5	24.0
Shear flat	364	531	211708	0.17	1.5	15.5	26.1
Column flange	453*	528*	-	-	-	-	24*

$f_{y,0.2}$ mean yield strength — f_u mean tensile strength

ε_y mean strain at yielding — ε_{sh} mean strain at hardening

ε_u mean strain at ultimate load — ε mean strain at rupture

* value given by the manufacturer

4.4.2 Concrete

For the reinforced concrete slab and the infill of the composite column, ready-mixed normal weight concrete with a maximum aggregate size of 16mm was used in the test specimens. The mechanical properties of the concrete were determined using compression tests on 150x150x150 mm cubes according to the standard SFS 4474

"*Concrete. Compressive strength*" (1988). The specimen and 10 cubes were cured under wet foam plastic. In addition, 6 cubes were kept in relative humidity of 95 % and an average temperature of 20 °C. The compressive strength was measured on the day of testing and after 28 days. For the concrete, the mean values of the measured compressive cubic strength on the test day are given in Table 4.3. In specimen CC2 the ready-mix concrete had a high water-to-cement ratio and the top surface of the concrete slab cracked significantly due to the shrinkage.

TABLE 4.3

MEASURED CONCRETE CUBIC PROPERTIES ON THE DAY OF TESTING.

Test specimen	Concrete age on the day of testing (days)	Average cube compression strength $f_{c,c}$ (N/mm^2)
CC1	15	46.8
CC2	12	34.5
CC3	18	35.5
CC4	13	33.9

4.4.3 Reinforcing steels

The reinforcement used in the slab and column was of with hot-rolled bars of grade A500HW. The tensile tests for reinforcing bars and mesh were carried out according to the standard SFS-EN 10 002-1 "*Metallic materials. Tensile testing. Part 1: Method of test (at ambient temperature)"* (1990). The material properties of the steel reinforcements are given in Tables 4.4 and 4.5. The surfaces of the rebars were ground smooth where the strain gauges were fixed, which reduces the cross-sectional area of the bars locally. Therefore, also longitudinal bars ground equally were tested so as to interpret the reduction in strength and ductility. In the appropriate tables, the bars with reduced cross-section are indicated with an asterisk.

TABLE 4.4

MATERIAL PROPERTIES OF THE STEEL REINFORCEMENTS IN TEST CC1.

Diameter [mm]	$f_{y,0.2}$ [N/mm^2]	f_u [N/mm^2]	E [N/mm^2]	ε_y [%]	ε_{sh} [%]	ε_u [%]	ε [%]
12	546	664	196587	-	-	8.4	11.4
16	575	682	205437	0.28	1.5	11.7	16.7
mesh ϕ6	625	670	199509	0.31	-	1.8	2.6

$f_{y,0.2}$ mean yield strength — f_u mean tensile strength

ε_y mean strain at yielding — ε_{sh} mean strain at hardening

ε_u mean strain at ultimate load — ε mean strain at rupture

TABLE 4.5

MATERIAL PROPERTIES OF THE STEEL REINFORCEMENTS IN TESTS CC2, CC3 AND CC4.

Diameter [mm]	$f_{y,0.2}$ [N/mm^2]	F_u [N/mm^2]	E [N/mm^2]	ε_y [%]	ε_{sh} [%]	ε_u [%]	ε [%]
12	546	664	196587	-	-	8.4	11.4
16	532	645	204329	0.27	1.9	12.1	18.1
20	553	657	199389	0.27	1.6	11.7	17.9
16*	524	639	198694	0.26	2.8	10.4	12.9
20*	552	654	202608	0.28	2.4	10.9	13.8
mesh ϕ6	625	670	199509	0.31	-	1.8	2.6

$f_{y,0.2}$ mean yield strength — f_u mean tensile strength

ε_y mean strain at yielding — ε_{sh} mean strain at hardening

ε_u mean strain at ultimate load — ε mean strain at rupture

* bars with a reduced cross-section

The reinforcement employed is of high ductility type in order to prevent premature failure due to rupture of the longitudinal bars. For all the bars, the total elongation at maximum force exceeded the Eurocode requirement of 5 % strain. The mesh

reinforcement behaved in a very brittle manner, with elongation being of the order of 1.8 % only.

4.5 Test set-up and measurement system

The tested connection configuration comprises a concrete-filled tubular column with nominal dimensions 300x300x10 mm connected on both sides to two identical composite slim floor cantilever beams of length 1850 mm, see Fig. 4.2. The length of the column was 2100 mm and it was plumbed vertical and fixed to the laboratory floor and to a test rig by base-plates. The bolted connection to the laboratory floor allows no rotation, but the connection to the horizontal beam section of the rig is assumed to behave as a hinge. The horizontal rig beam section with a flexural stiffness value of $1.571*10^9$ mm^4 is assumed to be stiff enough to prevent horizontal deflections.

Two concentrated loads were employed by independently servo-controlled hydraulic jacks each of which having a capacity of 500 kN. The jacks were mounted on the test rigs, which were themselves attached to the strong walls of the laboratory. The loading condition on the joint was very close to symmetry. The connection was instrumented only on the left side of the column centre-line and therefore the jacks were located at a slightly different distance from the column in order to ensure that the collapse would occur on the instrumented side of the connection. The distances were 1650 mm and 1550 mm from the face of the column flange at the left and the right cantilever beams, respectively. In test CC4, the load positions were moved closer to the column at 1150 and 1050 mm to produce a higher shear to check the effect of a higher shear-to-moment ratio on the moment-rotation behaviour. The loads were applied through spreader plates (150x150 mm^2) positioned on the slab. The load cells fixed at the jacks were used to record the applied loads.

A comprehensive set of displacement components and of strains was measured at each step of the loading history so as to enable the evaluation of both the global response of specimens, the local behaviour in the joint and the strains in the

reinforcement. Inductive linear variation transducers and electrical strain gauges were used.

The locations of the displacement measurements are shown in Fig. 4.3. The transducers used are for measuring:

- The vertical deflection of the composite beam at different locations, relative to the laboratory floor (transducers 0, 2, 5, 6, 7 and 9);
- The slip between the concrete slab and the steel beam at the free end of the cantilever. The transducer was placed horizontally on the concrete slab (fixed part) and on the steel beam (moving part) (transducer 8);
- The rotation, relative to the column, of the cross-sections of the steel beam at 182 mm and 25 mm from the column outer face by the use of bar studs ϕ 8 mm welded to the upper and lower flanges of the steel beam, to which transducers were connected (transducers 1, 3 and 4). Plastic tubes ϕ 20 mm were installed around the bar studs so as to keep the bars not embedded in the concrete slab.

Sixteen electrical strain gauges were placed on the innermost and outermost reinforcing bars at four sections, as indicated in Fig. 4.4, to monitor the variation in stress distribution in the reinforcing bars during testing. The four sections selected (A,B,C and D) are: the column centre-line and the cross-sections at 175 mm, 332 mm and 482 mm apart from it. The sections are equivalent to the positions of the inductive transducers at the joint region. Strain gauges were applied also on the steel beam bottom flange in section B (gauges b1,b2,b3), on the shear flat (gauges g3 and g4) and on the column face below the shear flat (gauge c1), as shown in Fig. 4.5, to allow for the evaluation of the local effects due to load introduction. Strain gauge rosettes were used in order to resolve the strain state in the shear flat (gauges g1 and g2).

The development of cracks was marked and the maximum crack widths on the top surface of the concrete slab were measured using a microscope as the loading progressed. After the tests, the state of specimens was thoroughly inspected, which included the disassembly of the connection, removal of the bolts, and checking of the deformations in the shear flat and holes.

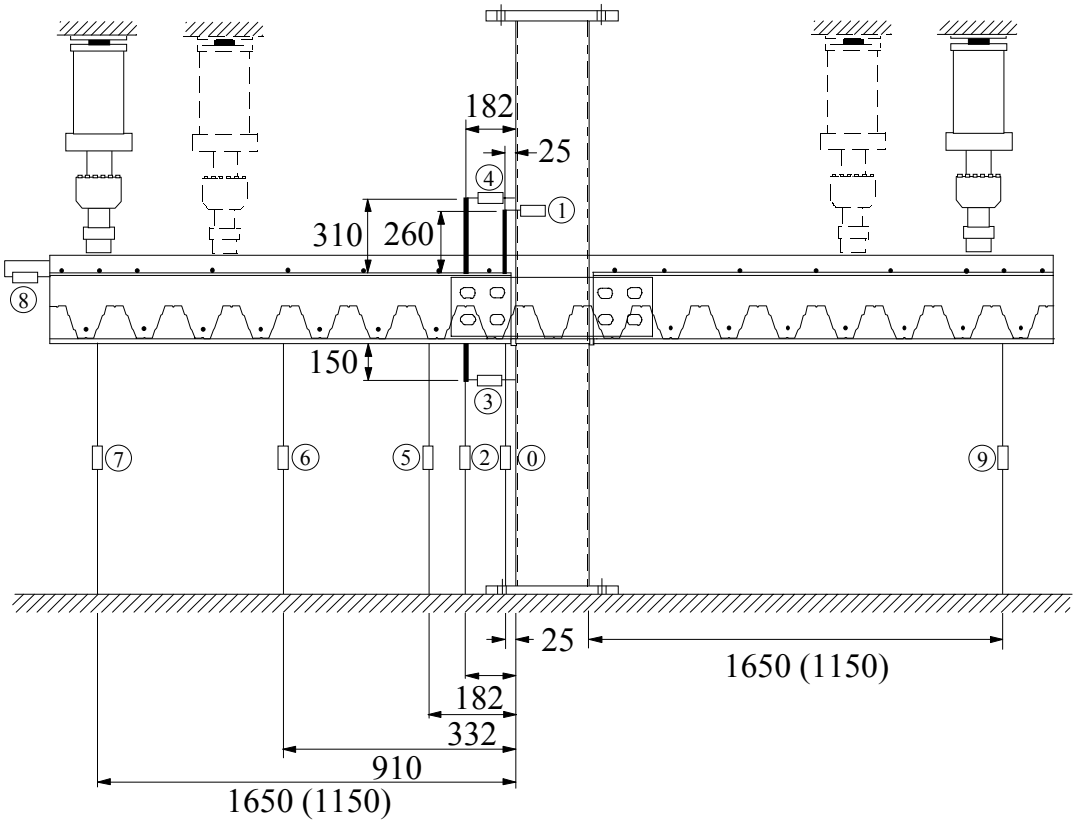

Figure 4.3 Inductive transducers monitoring deflection components.

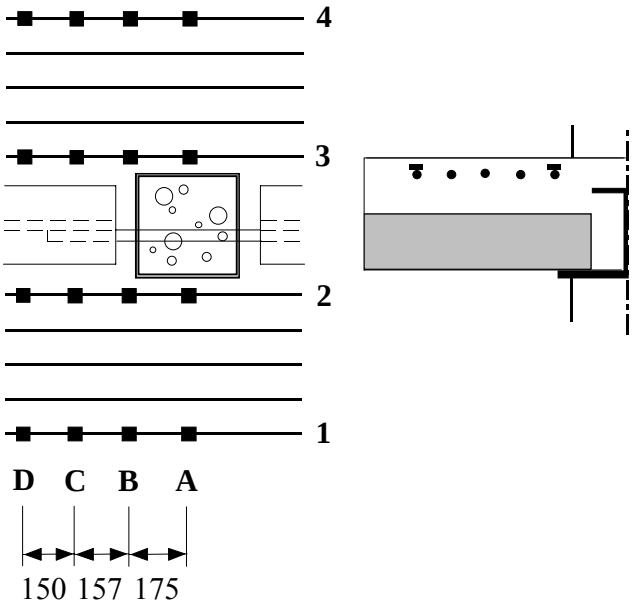

Figure 4.4 Instrumentation of the steel reinforcements.

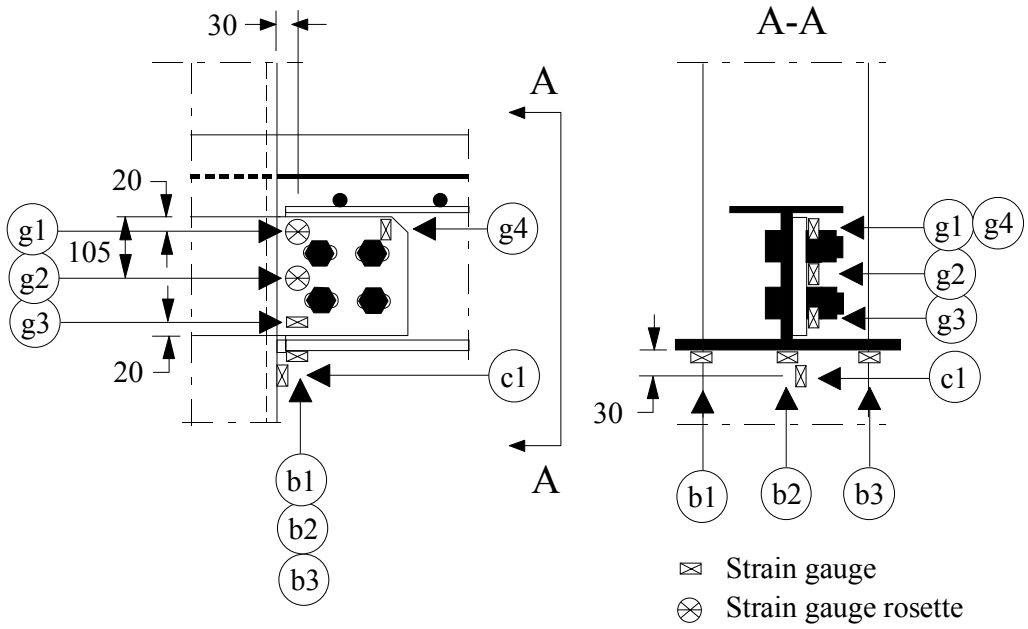

Figure 4.5 Strain gauges on steel members.

4.6 Testing procedure

4.6.1 Bare steel connection tests

Two connection tests were carried out without the presence of the reinforced concrete slab. The tests were carried out as the displacement controlled and the loading rate was 1-4 mm/mim. The connections were tested only for bending moments that are much smaller than the failure load, and the tests were terminated well before the specimens showed plastic deformation.

4.6.2 Composite connection tests

All tests were carried out following a step-by-step procedure. This means, for load control tests, that the external load was applied by increments and at each step the load was kept constant until full development of the deformations was achieved. In the elastic state, the tests were carried out as load controlled. The loading increment

was 12.5 kN and the loading rate 10 kN/min. Readings were recorded every 10 seconds and a time interval of 5-10 minutes elapsed between each load stage in order to make a visual inspection for failure and to take measurements. A loading history included three loading and unloading cycles. The loading and unloading rates were 20 kN/min.

The deflections due to the dead weight of the composite beam were measured at the beginning of each test. The specimens were loaded to 50 kN (82.5 kNm) and the displacement transducers and the strain gauges were checked to ensure that they were functioning correctly. The specimens were then unloaded to 3 kN. Load was subsequently applied up to 40-50 % of the predicted ultimate resistance of the connections. The specimens were then unloaded again to 3 kN to monitor their unloading stiffness. The specimens were then loaded again and unloaded once more when the load-deformation behaviour of the joint started to become non-linear.

When the joint behaviour became non-linear, the vertical displacement at the load application point was assumed as the control parameter in order to ensure the possibility to follow the specimen response also beyond the attainment of the ultimate capacity. The displacement rate was first adjusted to 0.5 mm/min and then 3 mm/min.

4.7 Bare steel connection test results and observations

The detailed test results considering the moment-rotation curves and the shear flat strains are reported in the Appendices II and IV. The main observations are summarised below.

The moment-rotation curves for the connection specimens SC1 and SC2 are shown in Fig. 4.6. The moment-rotation curves can be divided into three stages. Up to a rotation value of 15 mrad (23 mrad for SC2), the overall response of the bare steel connections indicates very flexible behaviour. The beam end tends to deflect upwards during the test. The spot-welds between the steel beam bottom flange and the contact plate, used only to attach the plate, resisted this deflection. However, in test SC1 the welds fractured with a rotation of 30 mrad and the load fell rapidly. After this, the increase

in joint moment was linear until the test was interrupted at the rotation of about 40 mrad. The results showed that the centre of rotation of the steelwork connection does not lie at the intersection of the beam bottom flange and column flange, and also that the location moves as the level of loading changes. No deformation in the bolt-holes and bolts were observed after the tests.

The principal strains in the shear flat, calculated from strains in the rosette gauges, g1 and g2 in Fig. 4.5, are shown plotted with respect to the joint rotations in Figs. 4.7 and 4.8.

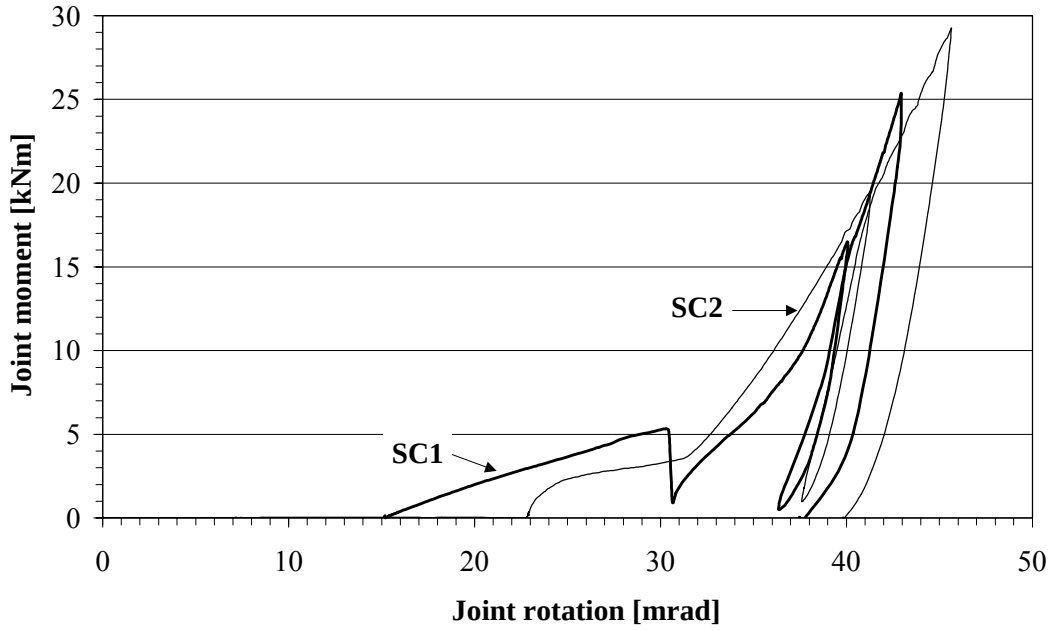

Figure 4.6 Moment-rotation (M_j-ϕ_j) curve for bare steel connection specimens.

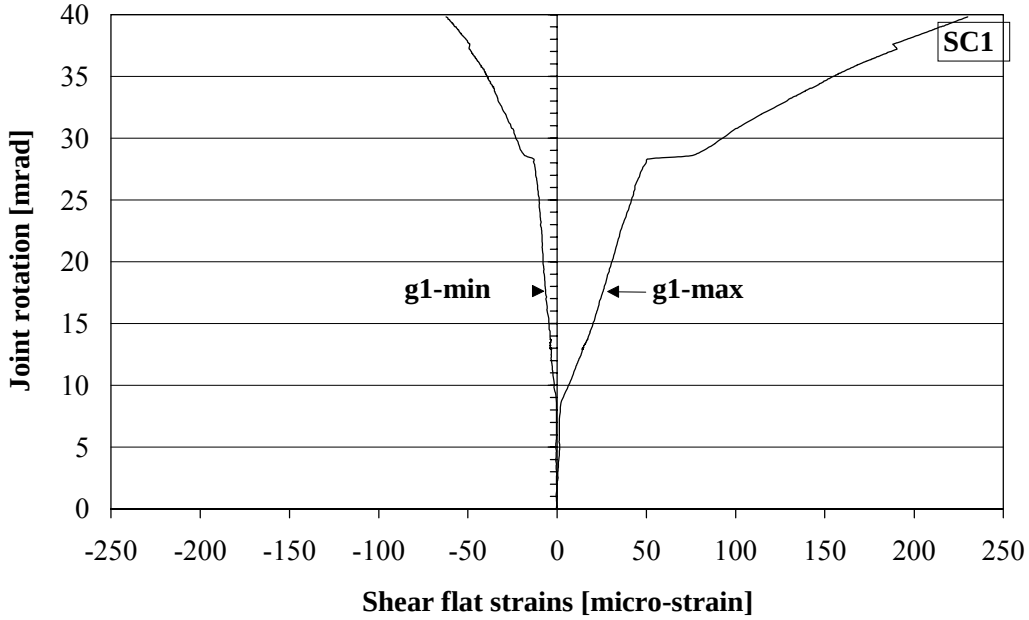

Figure 4.7 Principal strains in the shear flat (specimen SC1).

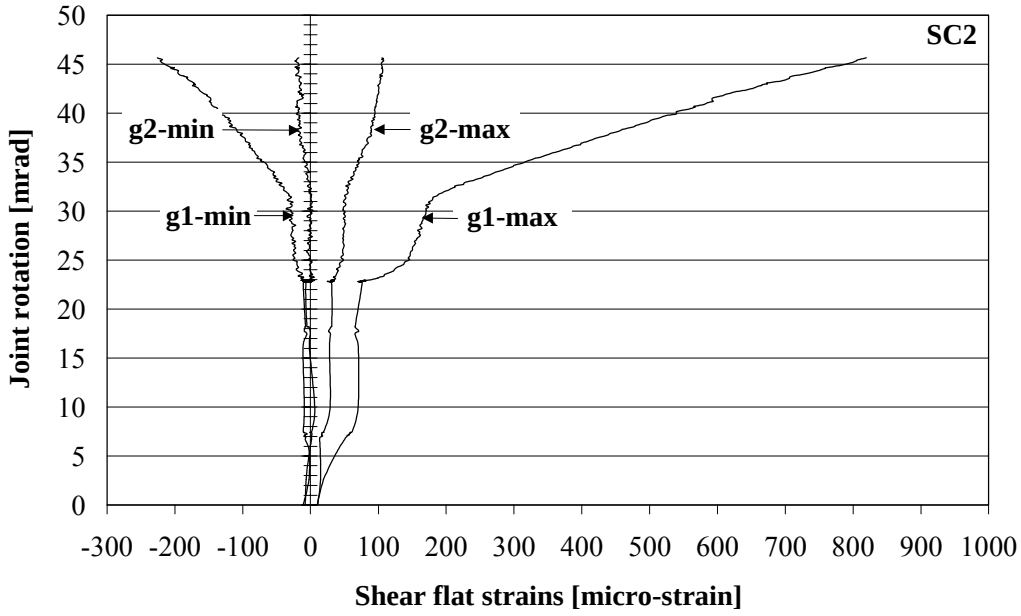

Figure 4.8 Principal strains in the shear flat (specimen SC2).

4.8 Composite connection test results and observations

Any actual indication of collapse in all the tested composite connections could not be observed and the tests were terminated when the beam deformation was out of the practical range. In all tests, only negligible slips were found in the slab relative to the steel beam at the free end of the cantilever, which confirms the full interaction behaviour. The detailed test results considering the moment-rotation curves, the reinforcement and the shear flat strains are reported in the Appendices II to IV. The main results and observations concerning the connection component behaviour are summarised below.

4.8.1 Moment-rotation curves

The moment-rotation relationships, M_j-ϕ_j, of the four tested composite connections are plotted in Fig. 4.9. The joint response is calculated directly from the recorded data, as explained in Section 3.3.1.

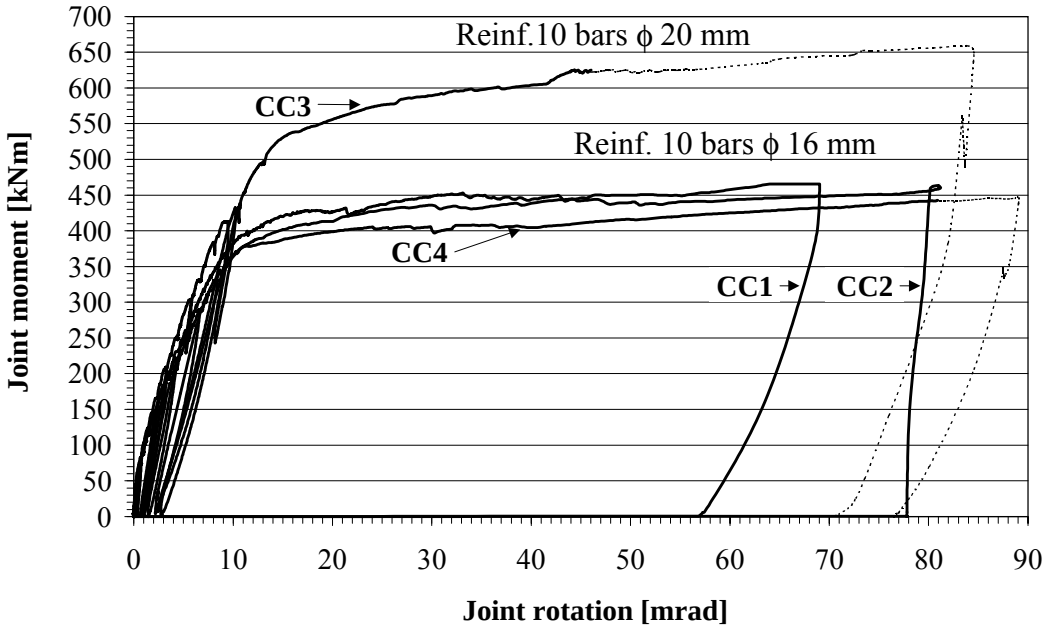

Figure 4.9 Moment-rotation curves for composite specimens.

All experimental moment-rotation curves exhibit a high rotational stiffness, a high moment resistance and a good rotation capacity. No great differences in the overall responses of joints CC1, CC2 and CC4 were observed. The joint ultimate moment capacity is only slightly decreased (about 4 %), as indicated in Fig. 4.9, for the higher shear-to-moment ratio in specimen CC4. The measured ultimate moment capacities achieved range from 446 to 466 kNm. In test CC3, the corresponding capacity is 659 kNm. The joint rotational stiffnesses were defined from the gradient of the unloading and reloading part of the moment-rotation curve. The curves show a joint rotational stiffness of the order of 65.8-99.0 kNm/rad. The measured joint rotational stiffness and ultimate moment capacity values are reported in columns (4) and (7) in Table 4.6.

4.8.2 Concrete cracking

The cracking pattern on the top of the concrete slab was remarkably similar in all the specimens. A typical distribution of the crack pattern of the slab is presented in Fig. 4.10. The cracking of the concrete slab started at the column corners, and expanded transversely to the longitudinal edges of the slab. The cracks were approximately equally spaced and the cracked zone extended towards the loaded end of the beam, with the final cracking patterns in all tests being spread up to 900-1100 mm on both sides of the column. The width of the main crack was about 12-17 mm when the tests were interrupted. The inclination of the cracks was modest and occurred only in the vicinity of the column. This is because the stress flow in the central part of the slab must divert to the external part. The crack pattern and the inclination of the cracks depends on the type of shear flow in the slab, i.e. on the distribution and flexibility of shear connectors in the beam (Zandonini, 1989). Stiffer connection increase the shear lag and this is reflected in the inclined pattern of cracks. More flexible connections lead to almost straight cracks running transversely across the slab. Therefore, it can be assumed that the shear lag effect is limited in all the specimens. Slight longitudinal cracking appeared also over the longitudinal reinforcement. The formation and distribution of the cracks were not remarkably affected by the shear-to-moment ratio of the connection and concrete strength.

Fig. 4.11 shows the side view of the crack pattern near the column. The first crack through the slab grew at the column line. Further cracks appeared thereby increasing the elongation length of the slab. The maximum crack widths on the top surface of the concrete slab were measured using a microscope and the results are presented in Fig. 4.12, plotted with respect to joint moment and average strain in reinforcement. The maximum crack widths were quite consistent with the joint moment until the crack exceeded a width of 0.4 mm. After this, the crack widths varied for the same connection moment. If the maximum crack width is limited to 0.3 mm in the serviceability limit state (Eurocode 2, 1992), the joint moments under service loads must be limited to values of 290 kNm and 330 kNm for the specimens CC4 and CC3, respectively. Corresponding to this crack width, the average stress in the reinforcement was at least 390 N/mm^2.

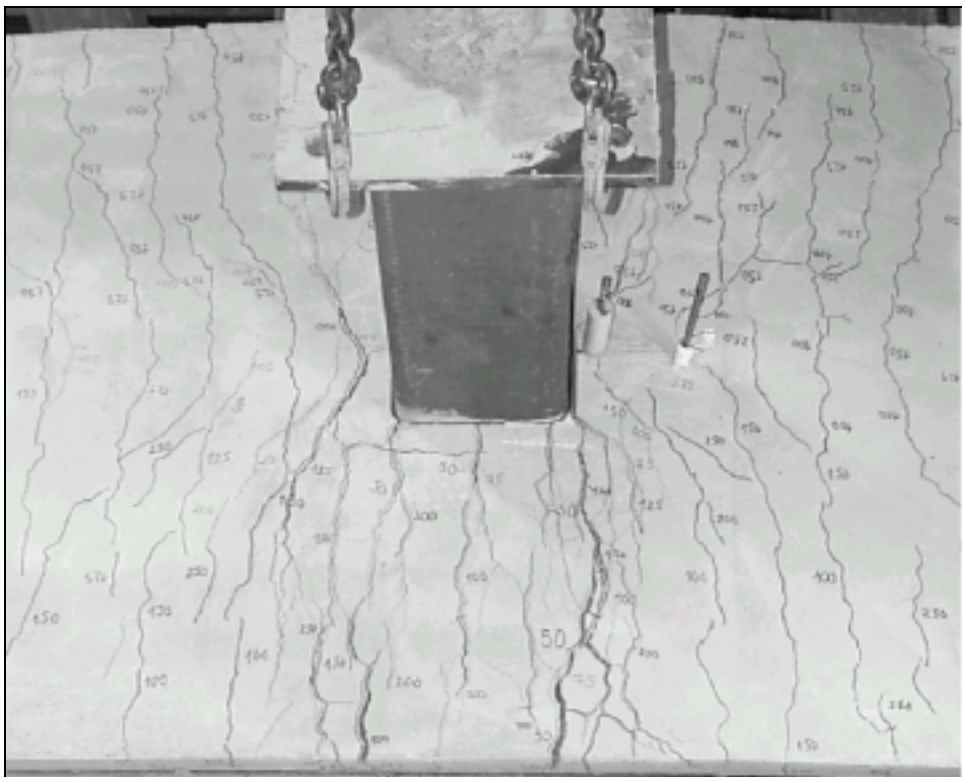

Figure 4.10 Typical crack pattern of the concrete slab (specimen CC3 after testing).

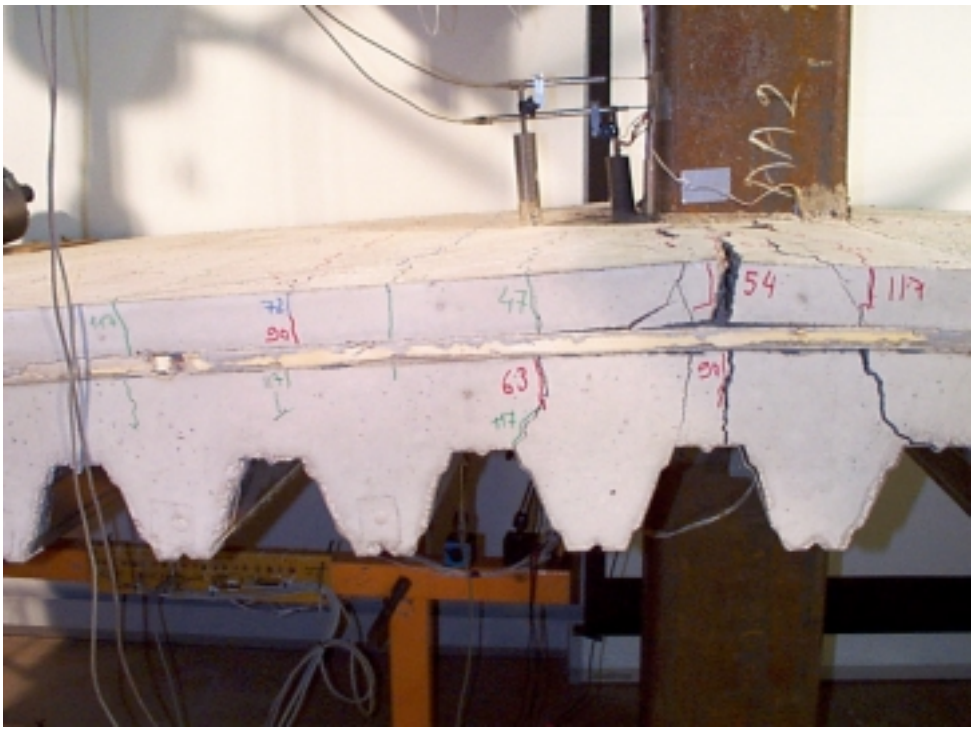

Figure 4.11 Cracking of concrete slab after test (specimen CC1).

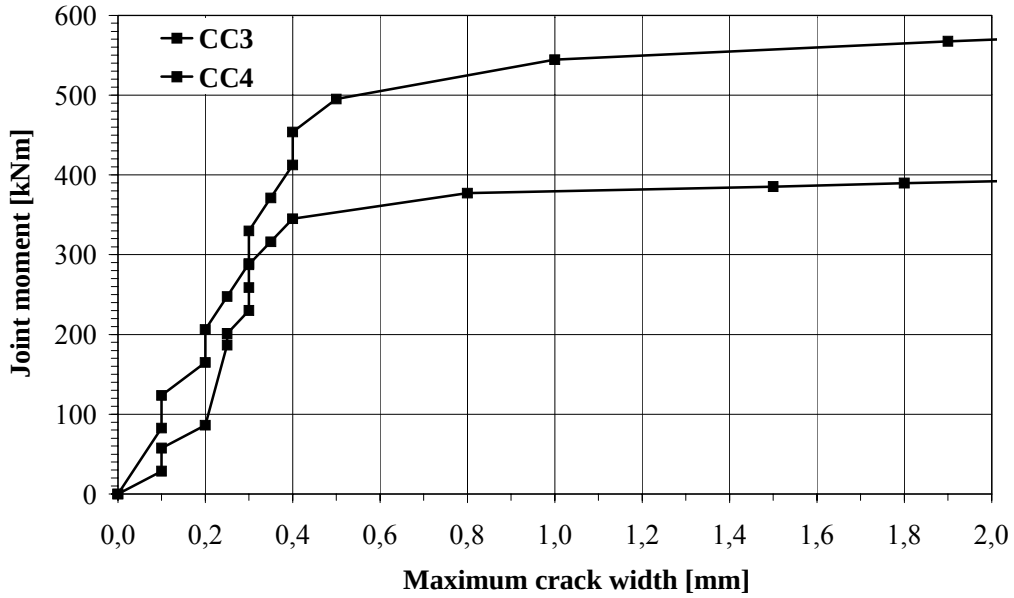

(a) Maximum crack width with respect to the connection moment.

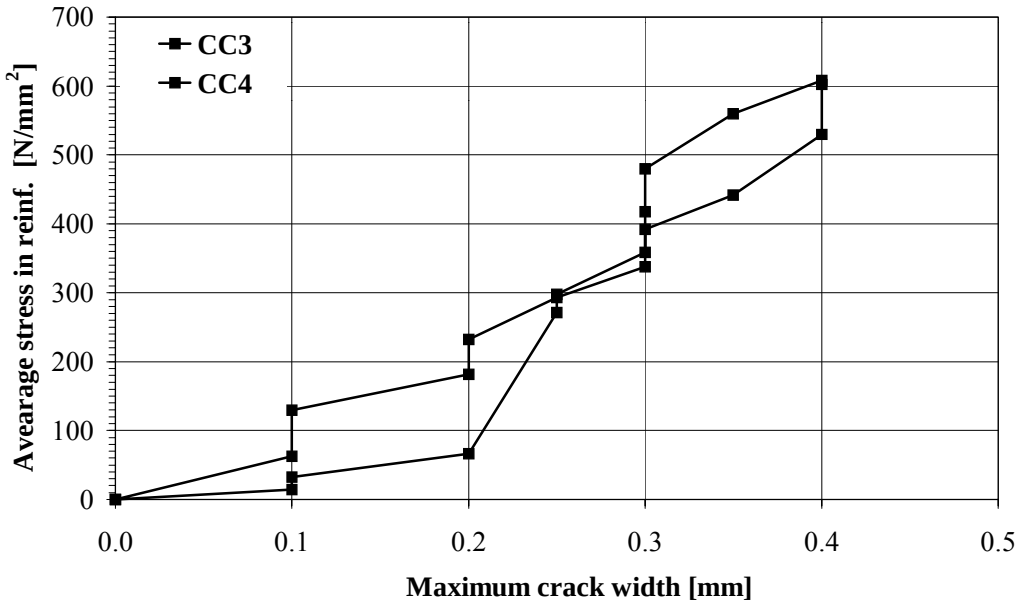

(b) Maximum crack width with respect to the average stress in reinforcement.

Figure 4.12 Maximum crack widths of the top surface of concrete slab.

4.8.3 Reinforcement

Strains in the reinforcement were measured on four sections, as shown in Fig. 4.4. In Figs. 4.13 to 4.16, the strains on the first yielded beam sections are presented with respect to the joint moment. These sections are: section B in the specimens CC1, CC2 and CC3 and section A in the specimen CC4. The nominal yield limit of the reinforcement strain is indicated in the figures by a dashed line.

The effects of concrete cracking on the strains of the reinforcement can be seen at a connection moment of about 30 kNm, which corresponds to the point after which the rate of the straining in the reinforcement increases more. After the concrete slab starts cracking, the force sustained mainly by the concrete is redistributed to the reinforcement and this causes the change in the rate of straining.

First yielding occurred in the bars close to the column when the bending moment is approximately 250 kNm, when ρ=0.92 % and 370 kNm when ρ=1.43 %. With higher moments the yielding spread transversely to neighbouring bars and also longitudinally. The joint moment when all the reinforcing bars in the slab section are plastic is assumed to define the threshold of the inelastic stage of the joint, i.e. it is the plastic moment capacity $M_{j,Rd}$ of the joint and it varied between 347 kNm and 375 kNm when ρ=0.92 %, and it was 489 kNm when ρ=1.43 %, see column (5) in Table 4.6. The ratio between $M_{j,Rd}$ and the ultimate moment capacity of the joint $M_{j,u}$ ranged from 0.70 to 0.80 when ρ=0.92 %, and it was 0.71 when ρ=1.43 %. The results indicate that the moment capacity was not decreased when shear-to-moment ratio decreased from 1.65 to 1.15. The joint rotations measured at $M_{j,Rd}$ range from 9.0 mrad to 10.5 mrad when ρ=0.92 %, and it is 12.0 mrad when ρ=1.43 %, see column (6) in Table 4.6. The higher shear-to-moment ratio increased the joint rotation from 9.0 mrad (CC2) to 10.5 mrad (CC4).

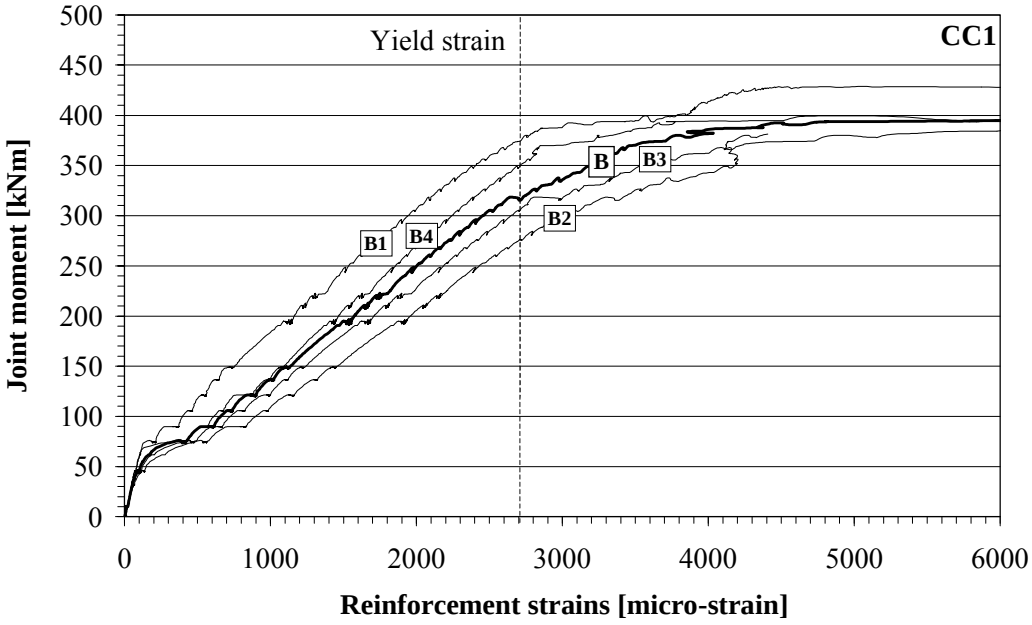

Figure 4.13 Measured reinforcement strains with respect to the joint moment in section B of specimen CC1.

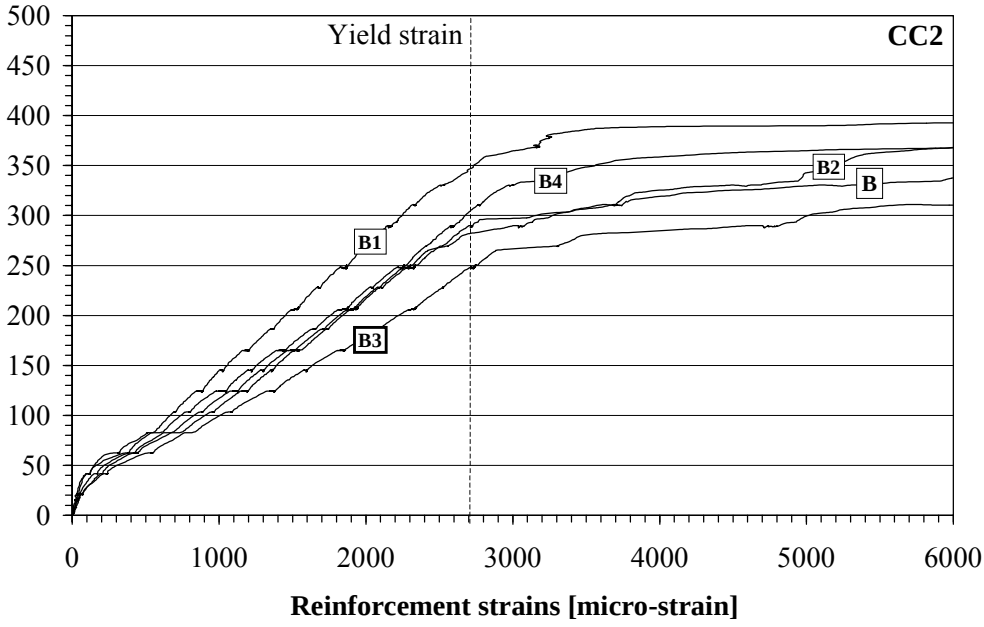

Figure 4.14 Measured reinforcement strains with respect to the joint moment in section B of specimen CC2.

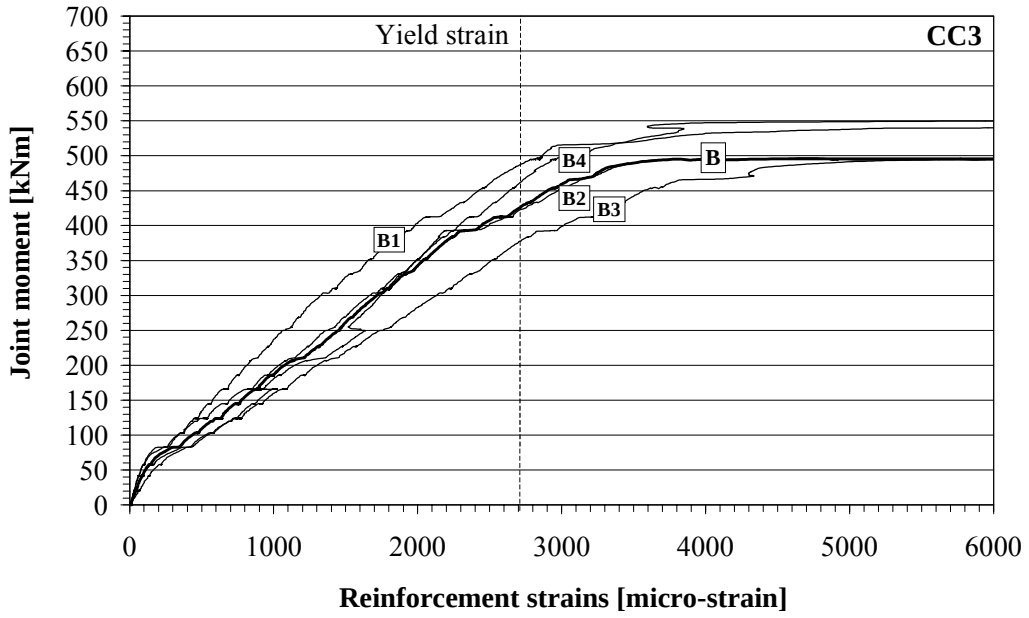

Figure 4.15 Measured reinforcement strains with respect to the joint moment in section B of specimen CC3.

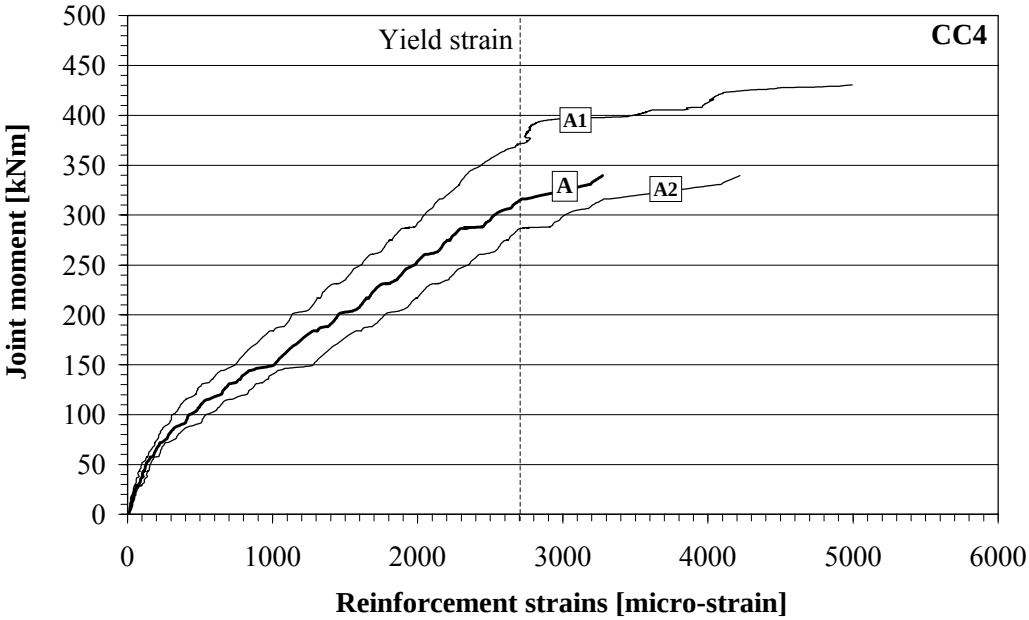

Figure 4.16 Measured reinforcement strains with respect to the joint moment in section A of specimen CC4.

In all the specimens, the yielding of the reinforcing bars spread transversely through the whole width of the slab section, demonstrating that the used width of the slab cross-section, twice the column width both sides of the column (see Fig. 4.2), does not exceed its effective width. All the specimens were tested into large rotations of up to 80-90 mrads. The mesh reinforcement fractured already at low rotation, but the longitudinal and transverse bars exhibited no visible rupture strains or damage after the tests, see Fig. 4.17. The strains and stresses in the bars were not affected by the connection shear-to-moment ratio, as the curves for CC1, CC2 and CC4 are similar.

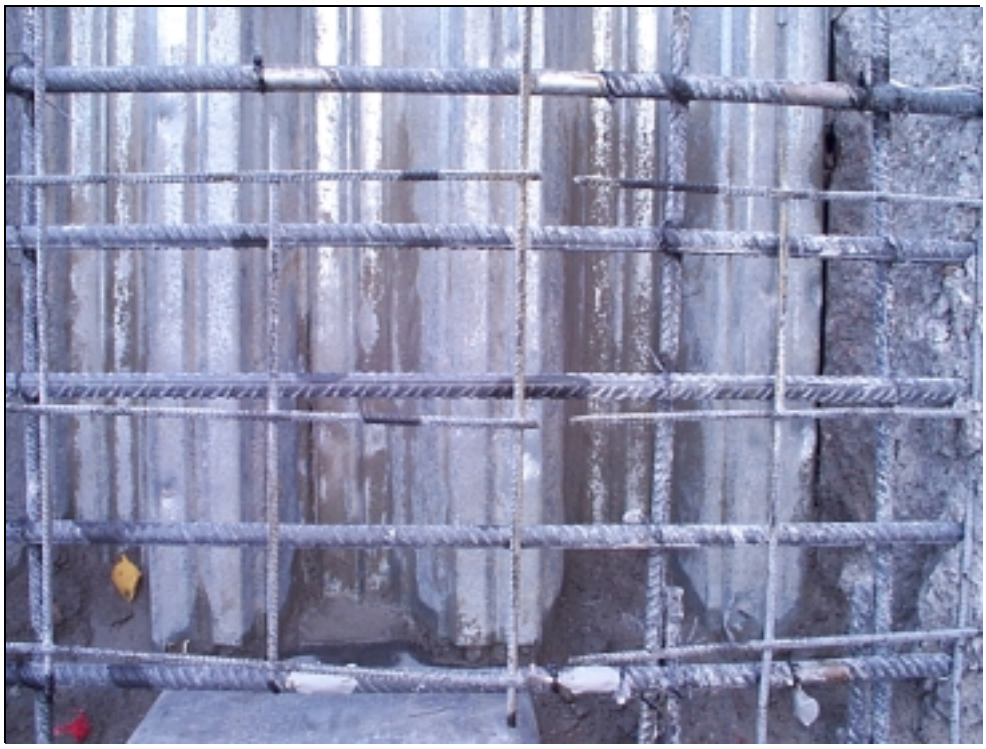

Figure 4.17 Reinforcement after test (specimen CC2).

4.8.4 Steel beam

The bottom flange strains in the steel beam at the cross-section B are plotted with respect to the joint moments and joint rotations in Figs. 4.18 and 4.19, respectively. The figures indicate that the strains do not exceed the yield limit before the plastic

moment resistance of the joint was reached, but the yield strain is exceeded in all the specimens before the ultimate moment capacity. The joint rotation with which the flange yielded varies significantly, ranging from 23 to 47 mrad.

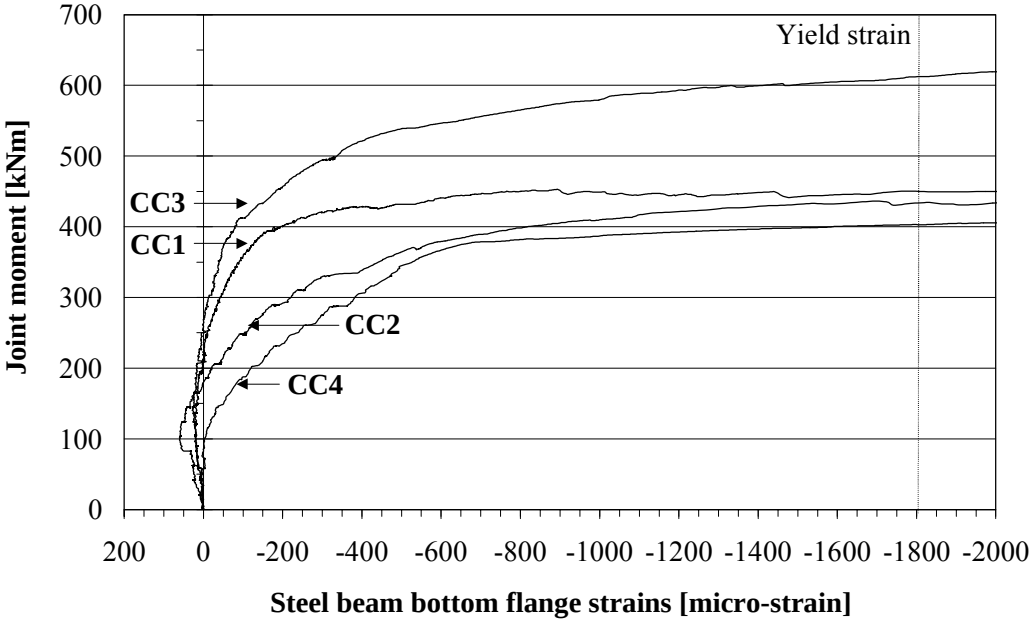

Figure 4.18 Measured steel beam bottom flange strains with respect to joint moment.

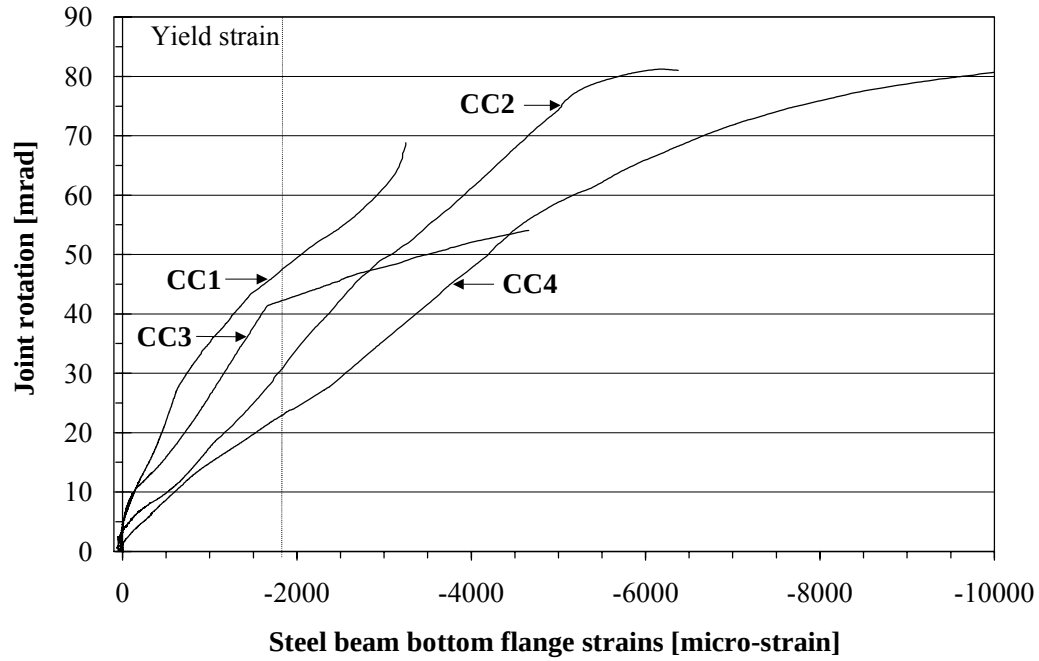

Figure 4.19 Measured steel beam bottom flange strains with respect to joint rotation.

4.8.5 Steelwork connection

Large deformations were present in the shear flat after the tests as shown in Fig. 4.20. The vertical deflections measured at the free end (top corner) of the shear flat were about 10 mm. However, there were minor deformations in the circular or slotted bolt-holes, or in the bolts.

It is obvious that the corner of the bevel in the shear flat and the top flange or the fillet weld seam of the steel beam will get a contact when the beam rotation is increased. Strain gauge, g4 in Figs. 4.5 and 4.20, was used in order to obtain this contact. The measured strain is given in Fig. 4.21. The curve exhibits a sudden increase at a rotation of about 13 mrad, which may be explained by a contact starting.

The principal strains in the shear flat, calculated from the strains in the rosette gauges, g1 and g2 in Fig. 4.5, are shown plotted with respect to the joint moments and rotations in Figs. 4.22 and 4.23. The contact developed is also verified by the principal strain curves. The yielding of the shear flat in all the tests was detected simultaneously with the yielding of the slab reinforcement, i.e. when the plastic moment resistance of a joint was reached.

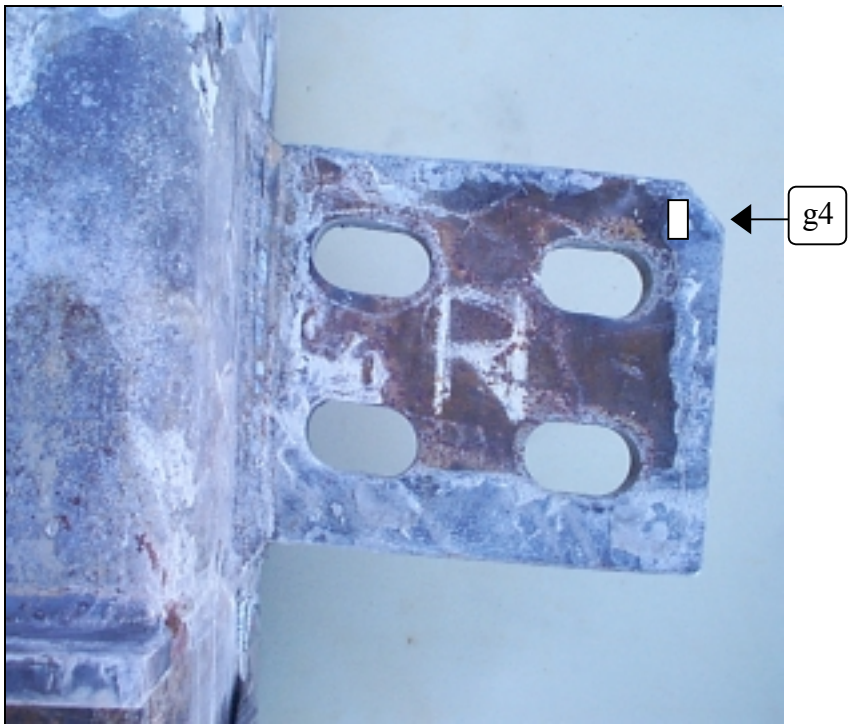

Figure 4.20 Deformed shear flat (specimen CC1 after test).

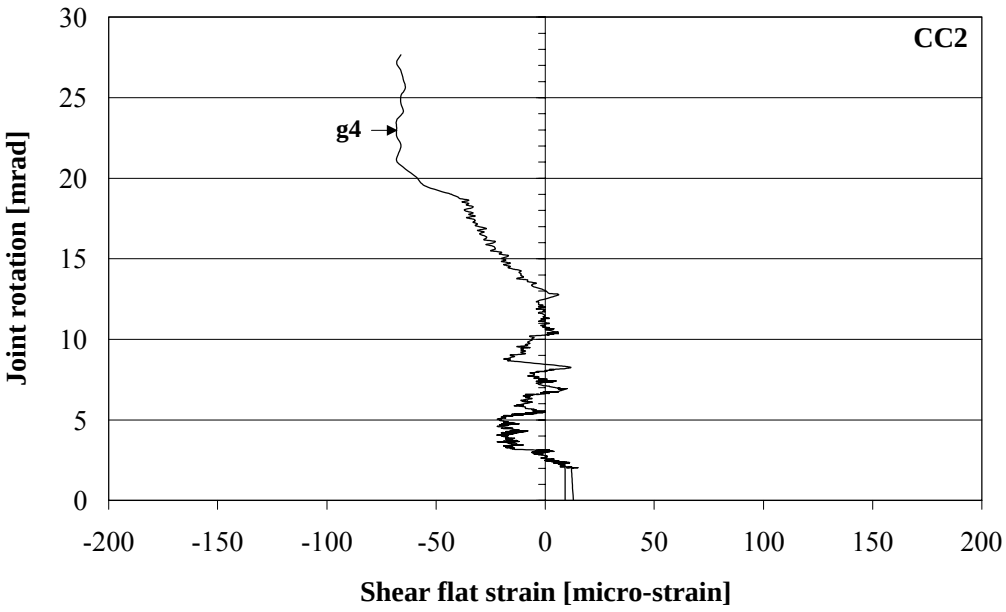

Figure 4.21 Vertical strain at the cantilever end of shear flat, strain gauge g4.

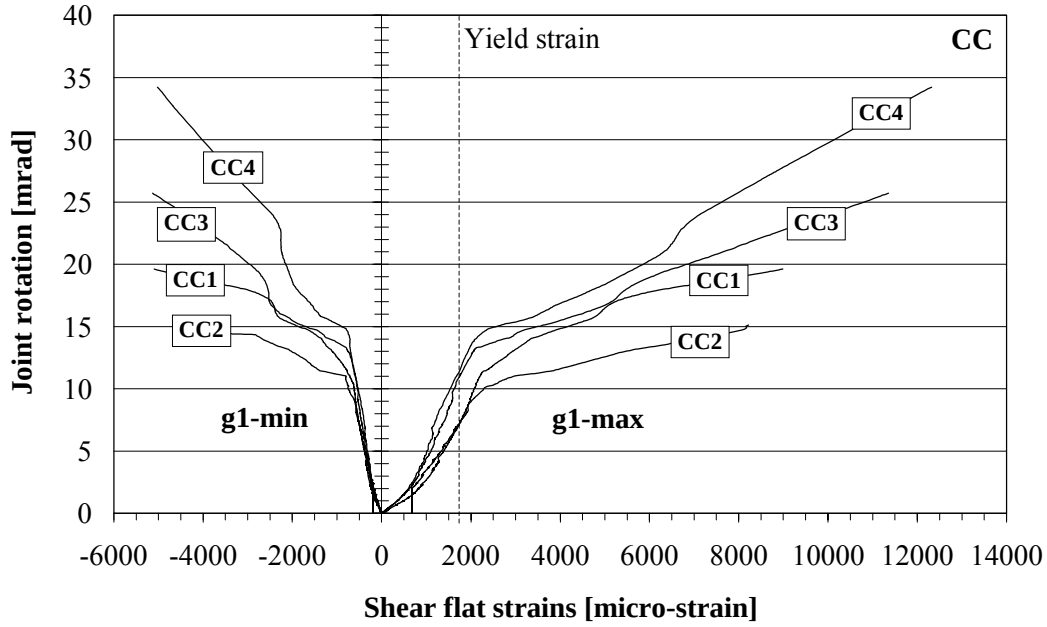

Figure 4.22 Principal strains at shear flats measured by strain gauge rosette g1.

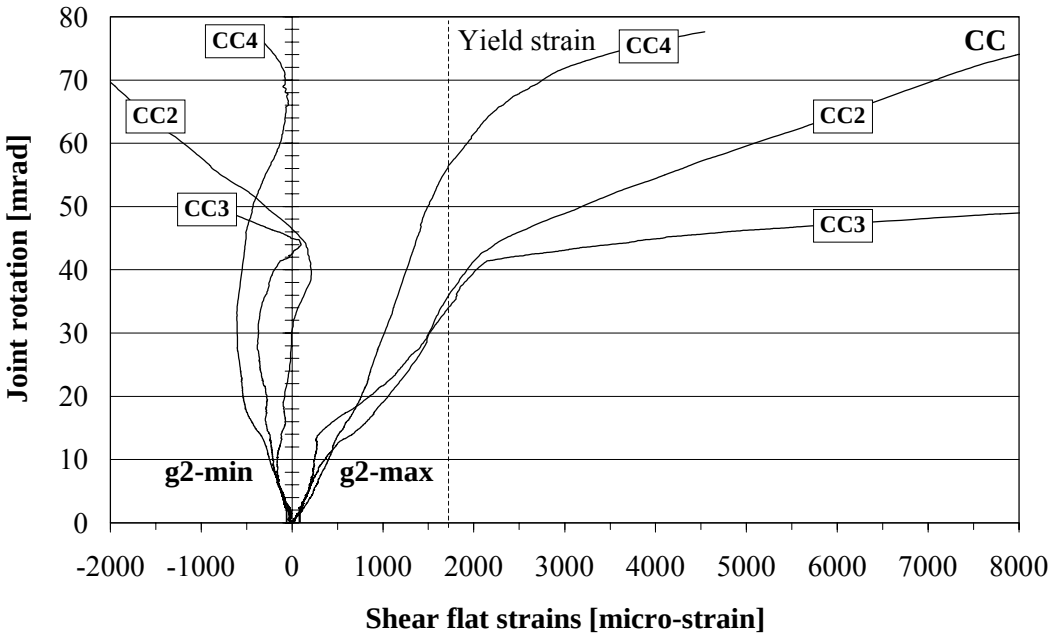

Figure 4.23 Principal strains at shear flats measured by strain gauge rosette g2.

4.8.6 Column web

The vertical strains in the column web were measured at a point directly below the shear flat, as shown in Fig. 4.5. The variations of column web stresses with respect to joint moments and rotations are shown in Figs. 4.24 and 4.25, respectively. The shear-to-moment ratio significantly affected the strain level in the column web when connection moments were similar. This is demonstrated by a faster rate of straining in specimen CC4. This is quite natural, however, as the applied load closer to the column, needs to be higher in order to produce the same moment.

4.9 Discussion of the experimental results

The joint classification according to the Eurocode 4 criteria for braced frames and the experimental moment-rotation curves of the studied composite connections CC1, CC2 and CC4 are shown in Fig. 4.26 (a). A beam span of 9.0 m was assumed consistently for defining the boundaries. A cracked beam section was assumed in the determination of EI_b. It should be noted that all the joints possess high values of elastic stiffness. All three curves are located in the rigid domain and therefore the joints can be classified as rigid. The connections possessed significant strength, which is 67 % of the estimated sagging bending capacity of the composite beam adjacent to the connection on average.

Fig. 4.26 (b) shows the classification and the experimental moment-rotation curve of connection CC3. Again, the curve is located in the rigid domain and the joint can be classified as rigid. The resistance of the connection is 83 % of the estimated sagging bending capacity of the composite beam adjacent to the connection.

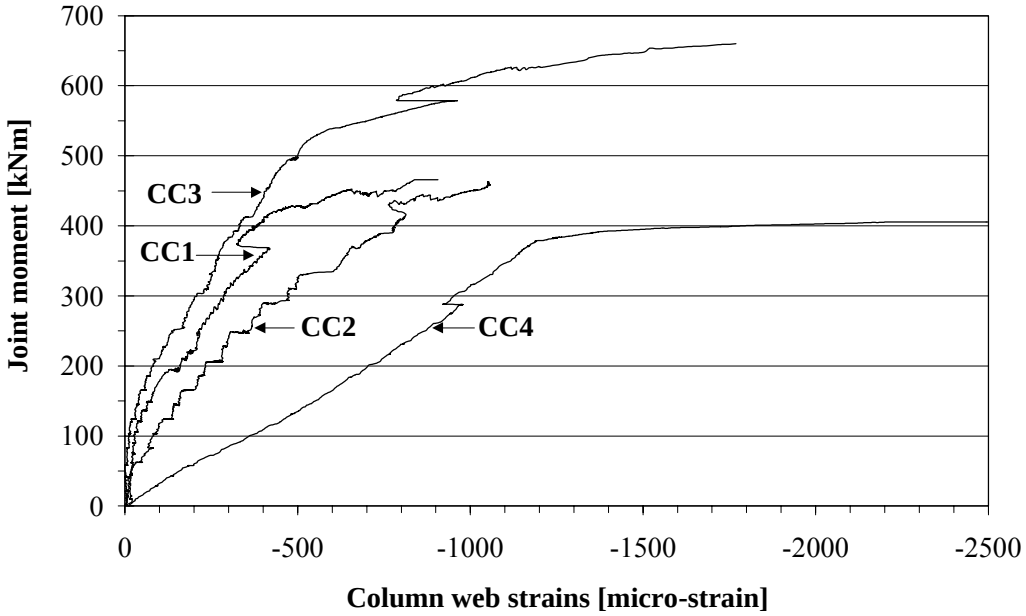

Figure 4.24 Measured column web strains with respect to joint moment.

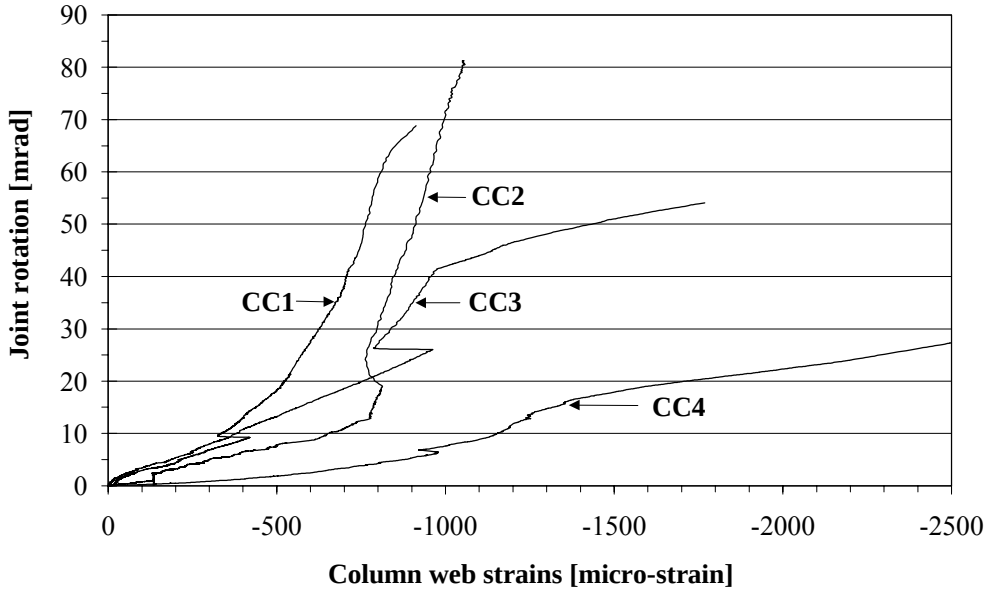

Figure 4.25 Measured column web strains with respect to joint rotation.

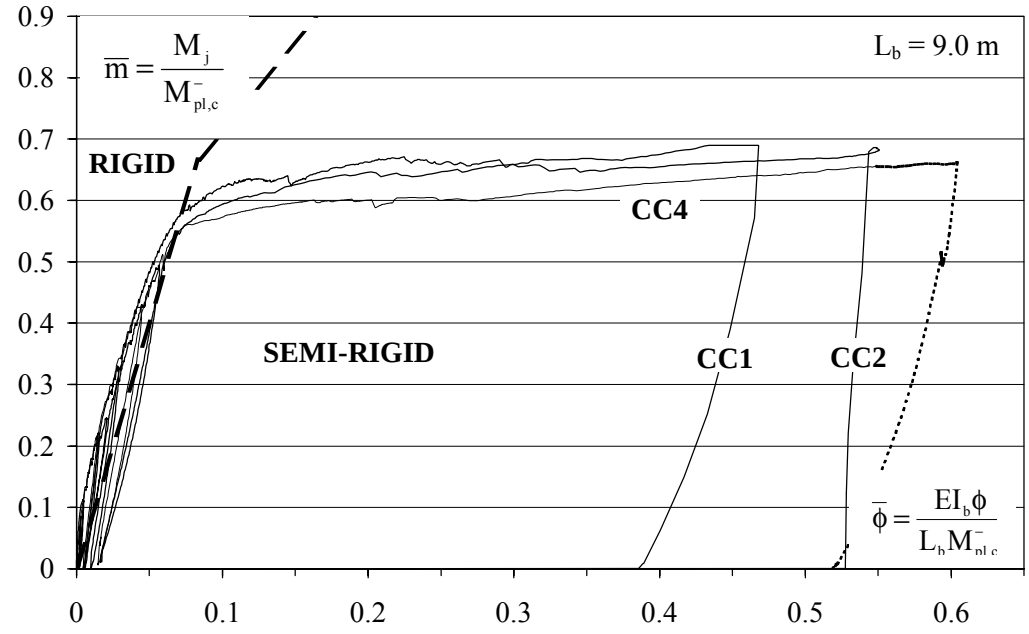

(a) Tests CC1, CC2 and CC4 (slab reinforcement 10 bars ϕ 16 mm).

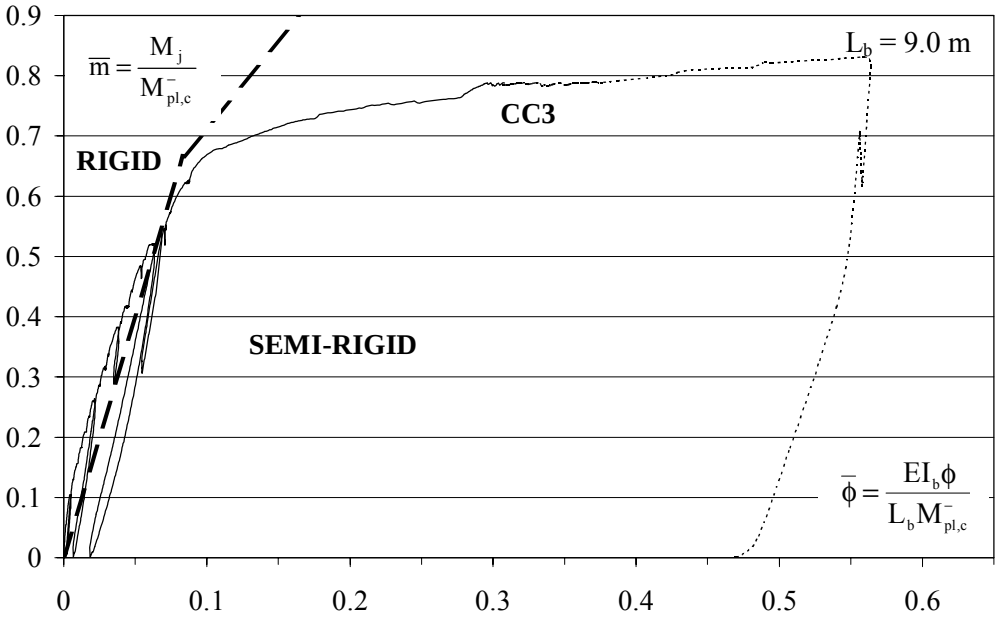

(b) Test CC3 (slab reinforcement 10 bars ϕ 20 mm).

Figure 4.26 The experimental moment-rotation curves and boundaries between the Eurocode 4 domains rigid vs. semi-rigid.

Table 4.6 summarises the main data related to the connections. In the table, M_{pl}^{+} and M_{pl}^{-} are the predicted theoretical sagging and hogging plastic bending resistances of the composite slim floor beam, respectively (assuming full interaction). The initial rotational stiffness $S_{j,ini}$ of a test is taken from the gradient of the unloading and reloading part of the curve. $M_{j,Rd}$ is the moment value that defines the upper limit of the elastic stage and $M_{j,u}$ is the measured ultimate bending resistance of the connection. It can be seen that the increase in the slab reinforcement by 55 %, from ρ=0.92 % to ρ=1.43 %, results in an increase in the bending resistance of the corresponding connection by 40 %.

The experimental results indicate that for the given connection detail the connection characteristics are not influenced by the concrete strength, which is quite natural while there are no concrete components in compression. The connection was tested for two different shear-to-moment ratios in order to investigate the effects of different levels of coincident vertical shear on the connection characteristics. The shear span for tests CC1, CC2 and CC3 was 1.65 m and for test CC3 1.15 m, so the ratios of shear-to-moment were 0.61 and 0.87, respectively. Results from the study show that the flexural stiffness and moment capacity of the joint are not significantly influenced by the shear-to-moment ratio. The increase in shear-to-moment ratio from 0.61 to 0.87, reduce the moment capacity about 4 %, as indicated in Fig. 4.9. The maximum shear force applied was 387 kN and no failure due to the insufficient shear resistance of a shear flat was attained.

In Table 4.7, the values of the ratios between the joint capacity and the sagging and hogging plastic bending resistance of the floor beam are summarised. In terms of the hogging moment resistance of the beam, every connection delivered at least 48 % of this moment, whilst with the reinforcement ratio of 1.43 % the specimen attained 60 %.

The joint moment levels that can be reached before the maximum crack widths exceeded 0.3 mm are reported in Table 4.8. If the maximum crack width is limited to 0.3 mm in the serviceability limit state (Eurocode 2, 1992), then about 70 % of the

plastic moment resistance of a joint can be utilized for connections similar to the test specimens.

Eurocode 4 requires full shear connection in the hogging moment areas. The experimental results indicate that eight 500 mm-long reinforcing bars ϕ 16 mm placed on each cantilever beam and used as flexible shear connectors can develop the required shear force without causing any considerable slip between the steel beam and the concrete slab.

TABLE 4.6

MAIN DATA RELATED TO THE SLIM FLOOR BEAM AND BEAM-COLUMN CONNECTION.

Test (1)	M_{pl}^{-} [kNm] (2)	M_{pl}^{+} [kNm] (3)	$S_{j,ini} = S_{j,unl}$ [kNm/mrad] (4)	$M_{j,Rd}$ [kNm] (5)	ϕ_{Xd} [mrad] (6)	$M_{j,u}$ [kNm] (7)
CC1	675	1132	99.0	375	9.5	466
CC2	675	1132	65.8	347	9.0	460
CC3	793	1132	87.6	489	12.0	659
CC4	675	1132	97.1	371	10.5	446

TABLE 4.7

THE RATIOS BETWEEN THE JOINT CAPACITY AND THE POSITIVE AND NEGATIVE PLASTIC MOMENT CAPACITIES OF THE SLIM FLOOR BEAM.

Test	$M_{j,Rd} / M_{pl}^{-}$	$M_{j,Rd} / M_{pl}^{+}$	$M_{j,u} / M_{pl}^{-}$	$M_{j,u} / M_{pl}^{+}$
CC1	0.53	0.31	0.69	0.41
CC2	0.48	0.29	0.68	0.41
CC3	0.60	0.42	0.83	0.58
CC4	0.53	0.31	0.66	0.39

TABLE 4.8

JOINT MOMENT LEVELS WHEN THE MAXIMUM CRACK WIDTHS EXCEEDED 0.3 MM.

Test	$M_{j,wk=0.3mm}$	$M_{j,wk=0.3mm}$ / $M_{j,Rd}$
CC3	330 kNm	0.67
CC4	290 kNm	0.78

5 PREDICTION METHOD FOR THE MOMENT-ROTATION CHARACTERISTICS OF THE COMPOSITE JOINT

5.1 Objective

After the analyses of the experimental study, the connection behaviour is now simplified and an approximation is made for the response of the key elements of the composite joint. Having identified the active connection components from experimental results, the mechanical properties contributing to the response of these components are determined. The response is described with the concepts of translational stiffness, resistance and deformation capacity, and their quantitative values are estimated. Once these are known, the components are assembled as a system to give the overall characterization of the joint in terms of rotational stiffness, moment resistance and rotation capacity. Simplified approximate calculation procedures to predict the joint moment-rotation design characteristics are derived, and their fit with the experimental test results is tested. The analytical methods proposed follow the standard design concepts as characterized for the composite beam-column joints (Anderson & Najafi, 1994, Tschemmernegg, 1994, Anderson et al., 1999, Huber, 1999) with appropriate modifications made for the composite slim floor beam and a concrete-filled rectangular hollow column section.

5.2 Idealization of connection characteristics

The difficulty in designing semi-continuous frames lies primarily in the non-linear connection behaviour, which leads to complexity in predicting the joint moment-rotation characteristics. The tests enable the measurement of these characteristics, but the use of a non-linear moment-rotation curve is often too complex for design purposes. Therefore, the joint behaviour must be represented with various simplified idealizations of design moment-rotation characteristics, which take into account adequate safety margins. Eurocode 3 and Eurocode 4 permit the use of approximate design characteristics, which are derived by adopting any appropriate curve enveloped totally by the experimental curve, see Eurocode 3 clause 6.9.2 (4). Where the approximate curve proposed is too much below the actual behaviour characteristics,

this would result in a loss of economy without any real impact on safety. In this sense, the proper choice of the approximate curve means attaining the adequate safety margin and a good economic performance at the same time.

The most practical approximation is to represent the joint characteristic by a bi-linear curve, see Fig. 3.7 c, where only two important points of the characteristics need to be calculated for the design. The first one corresponds to the end point of the elastic range of the design characteristic. Up to this point, the joint rotational stiffness is assumed to be constant, S_j, such that the linear approximation of the moment is smaller than the actual moment measured everywhere. The other part of the bi-linear approximation defines the moment $M_{j,Rd}$ that corresponds to the approximate yield plateau. $M_{j,Rd}$ is defined as the design moment resistance. The second point (Point 2) determines the intersection of the yield plateau and the vertical line defining design rotation capacity ϕ_{Cd} of the joint.

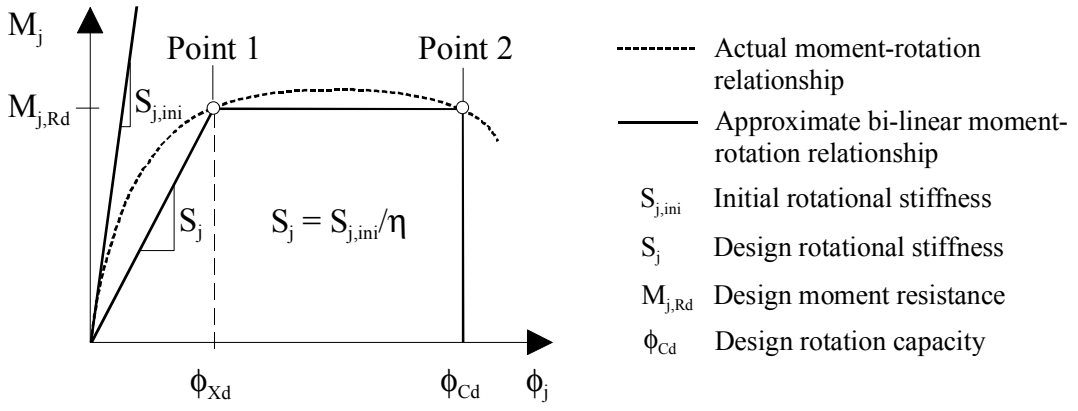

Figure 5.1 Design moment-rotation relationship of a joint approximated by a bi-linear idealization.

The design rotational stiffness S_j to be used in the global analysis of the structure is assumed to be valid to the design moment resistance $M_{j,Rd}$. This secant joint stiffness can be calculated by dividing the predicted initial joint stiffness $S_{j,ini}$ by a modification coefficient, denoted by η. The coefficient results from the non-linearity of the joint

moment-rotation curves as compared to those of the connected members, and it depends on the type of connection and the joint configuration. For example, in Eurocode 3, coefficient values of 1.5 and 2.0 are recommended for connections that utilize a contact plate or a bolted end-plate, respectively.

The prediction of an idealized joint moment-rotation relationship is carried out using a concept known as the *component method*, which is followed in many design codes, in particular in Eurocode 3 Annex J (1993) and in the model code provision for composite joints by Anderson et al. (1999), see Fig. 5.2. In the characterization procedures, a complex joint is divided into simple axial components and it is then treated as a set of these individual components (Mechanical model). The application of the method requires the following steps:

1. Identification of the active joint components, so-called basic components, contributing the rotational behaviour in the joint configuration studied;
2. Evaluation of the mechanical properties of each individual basic component;
3. Assembly of the components in view of the evaluation of the mechanical characteristics of the whole joint.

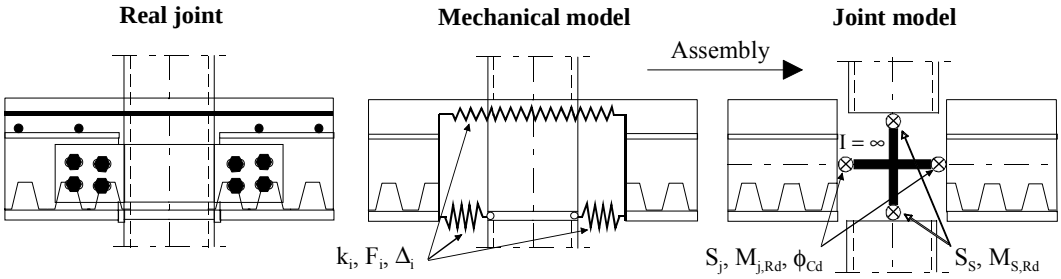

Figure 5.2 Joint modelling using the component method.

In the following, mathematical models aimed at predicting the joint response of a beam-column composite joint configuration between a slim floor beam and a concrete-filled tubular column section are derived following the procedure specified above.

5.3 Identification of the active components

A description of the rotational behaviour of a joint has to take into account all sources of deformations, local plastic deformations and instabilities within the joint area. The analysis of the experimental test results formed the background for the model assumed for force transfer through the components of a connection.

Reflecting the behaviour observed in the tests, simplifications concerning the component interplay have been adopted in the proposed model, resulting in a model, presented in Fig. 5.3. The connection resists applied moments by generating a couple between the tension and compression components of the connection. In the model assumed, the tensile force, F_t, resulting from the bending moment is taken by the reinforcement in the slab, and a contact plate is used to transmit the compressive force resultant, F_c, from the bottom flange of the beam to the column. Any contribution of the bolt connection to the joint moment-rotation behaviour is neglected. The shear connectors on the top flange of the steel beam transfer the longitudinal shear force, F_v, between the concrete slab and the steel beam. Resistance to vertical shear V is assumed to be provided by the four bolts and the shear flat.

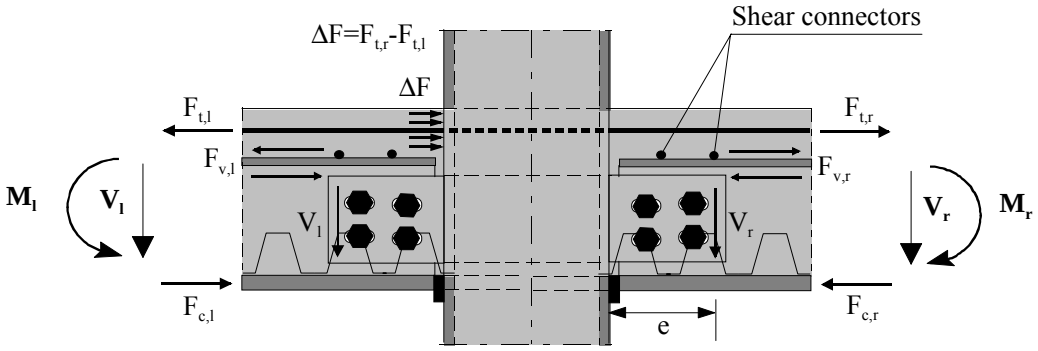

Figure 5.3 Assumed mechanics of force transfer in the joint.

If an internal column joint is exposed to unbalanced hogging moments ($M_l \neq M_r$), the moments will cause a difference in tensile force in the reinforcement at each side of the column ($F_{t,r} \neq F_{t,l}$). This difference of forces, $\Delta F = F_{t,r} - F_{t,l}$, must be redirected

around the column and there then balanced by the interaction between the concrete slab and the column face. Concerning this in Fig. 5.3 it is assumed that the hogging bending moment at the right hand side exceeds that of the left hand side.

5.4 Mechanical model and response of the basic components

Eurocode 3 defines a basic component of a joint as a specific part that makes an identified contribution to one or more structural properties of the joint. Reflecting the behaviour observed in the tests, simplifications concerning the component interplay have been adopted in the proposed model, resulting in a mechanical model, presented in Fig. 5.4. In the particular case of the connection shown in Fig. 5.3, the relevant basic components loaded in compression, tension and shear are the following:

- Compression region:
  - Beam bottom flange in compression (spring No.1)
  - Contact plate in compression (spring No.2)
  - Concrete encasement of the column in local compression (spring No.3)
- Tension region:
  - Slip of composite beam due to incomplete interaction (spring No.4)
  - Longitudinal slab reinforcement in tension (spring No.5)
  - Redirection of unbalanced forces (spring No.6)
- Shear region:
  - Concrete encasement in shear (spring No.7)

The component method is based on the known force-deformation behaviour of the active basic joint components that are derived from the component characterization using the material or component tests. The components are modelled as physical, elastic-plastic translational springs that provide the following properties: coefficient of initial translational stiffness k_i, design resistance $F_{i,Rd}$ and deformation capacity Δ_i corresponding the design resistance. No interaction between the basic components is taken into consideration in the mechanical model proposed.

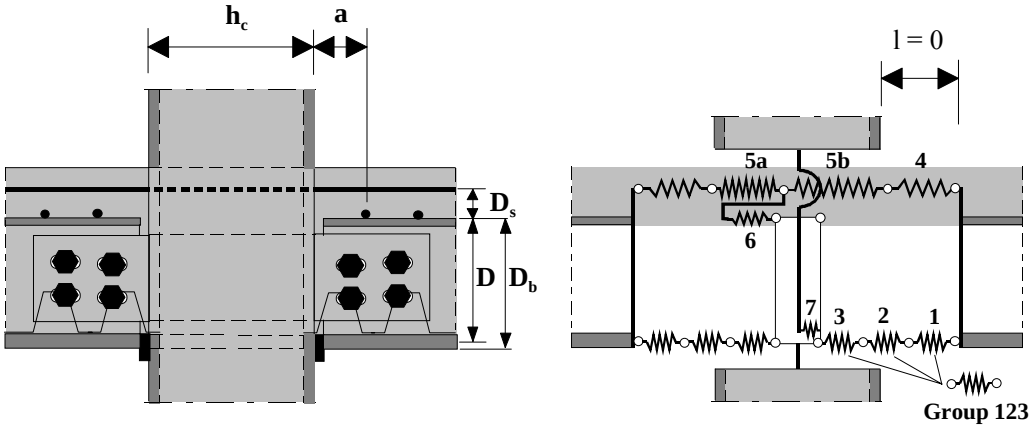

Figure 5.4 Mechanical model of the joint.

The compression region of the joint is modelled by two steel springs and a concrete spring. The compression in the beam flange immediately adjacent to the joint and in the contact plate can be converted to the stiffnesses of compression springs No.1 and No.2, respectively. The spring No.3 represents the concrete encasement in the column acting together with the two steel plates (stiffeners) welded both sides the column and it allows for the influence of the local load introduction. These compression springs are acting in series and they can be combined and represent as a spring group. The translational stiffness, resistance and deformation capacity of the *compression group* may be given as:

$$\frac{1}{k_{123}} = \frac{1}{k_1} + \frac{1}{k_2} + \frac{1}{k_3} \tag{5.1}$$

$$F_{123,Rd} = \min\left(F_{1,Rd}, F_{2,Rd}, F_{3,Rd}\right) \tag{5.2}$$

$$\Delta_{123} = \Delta_1 + \Delta_2 + \Delta_3 \tag{5.3}$$

A shear interaction spring (No.4) is used to simulate the behaviour of shear connectors between the concrete slab and the steel beam. If a full shear interaction exists with no interface slip between the slab and the steel beam, the spring stiffness of the shear interaction should be equal to infinity. According to the experimental results, it may well be assumed that the concrete slab after cracking is incapable of

transferring any tensile force except through the reinforcement. Tension springs (No.5a and No.5b) are used to simulate the behaviour of the reinforced concrete slab in tension.

Springs No.6 and No.7 are only activated when the joint is exposed to unbalanced hogging moments ($M_l \neq M_r$). The behaviour of the tension region of the joint can be described by a mechanical model based on a simple truss idealisation (spring No.6). The compression force (ΔF in Fig. 5.3) has to be introduced also into the column web and the shear region in the concrete core is exposed to opposite horizontal shear forces as shown in Fig. 5.4. This force is transferred by a diagonal concrete strut in compression (spring No.7).

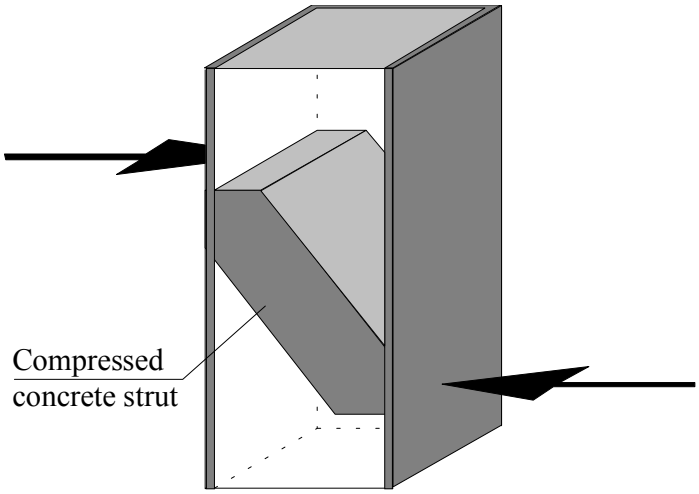

Figure 5.5 Compressed concrete strut.

5.4.1 Theoretical response in the elastic range

The joint response in the elastic range is derived by assuming that the reinforcement, the shear connectors, the steel beam flange, contact plate and the concrete encasement obey Hooke's law. Hence the deformation of the components may be given as:

$$\Delta_5 = \frac{F_5}{k_5}, \tag{5.4}$$

$$\Delta_4 = \frac{F_4}{k_4}, \tag{5.5}$$

$$\Delta_{123} = \frac{F_{123}}{k_{123}}, \tag{5.6}$$

where Δ_5 is the elastic elongation of the reinforced concrete slab, Δ_4 is the slip at the steel concrete interface close to the joint and Δ_{123} is the deformation in the compression region.

Stiffness k_5 of the reinforcement within the effective width of the concrete slab is calculated from:

$$k_5 = \frac{E_s A_s}{L}. \tag{5.7}$$

The stiffness is based on the length L of the reinforcing bars within which the extension is Δ_5. The effective length of the bar considered depends on a considerable number of influencing factors:

- Magnitude of stresses in the reinforcing bars
- Magnitude of bond stresses between the concrete and the reinforcing bars
- Distance between the cracks
- Diameter of the reinforcing bar
- Amount of the reinforcement
- Properties of the concrete

Due to incomplete knowledge of the force-deformation behaviour of the reinforced composite slab in tension, only simplified expressions to determine the effective length of the bar considered are available from the literature:

$$L = D_c/2, \tag{5.8}$$

$$L = D_c/2+a \quad \text{or} \tag{5.9}$$

$$L = D_c/2+a+p, \tag{5.10}$$

where a is the distance of the first shear connector from the column face and p is the distance between the shear connectors. Eq. (5.8) is used by model code provisions for Eurocode 4, Annex J (Anderson et al., 1999) and by Huber (1999). However, it is confirmed by Anderson & Najafi (1994) that if length given by Eq. (5.8) is considered, the resulting model tends to overestimate the stiffness of the reinforcing bar and thus joint stiffness. They proposed that the length of the bar considered should be encreased (Eq. (5.9)). This is because the force in the reinforcement is highest between the centre-line of the column and the position of the first shear connector and, therefore, the reinforcing steel will yield first at this location. Proposed by Ahmed and Nethercot (1997), the effective length may be further encreased for flush endplate connections (Eq. (5.10)).

Eurocode 4 requires full shear connection in the hogging moment areas. However, the influence of slip on the rotational stiffness of the joint is remarkable and the true stiffness of the shear connection should be accounted for in the stiffness model. The stiffness of the shear connection can be determined by push tests. For the load-slip behaviour of the shear connectors used in the joint specimens no test data is available. The experimental results indicated that in all the specimens full shear connection between the steel beam and the concrete slab was achieved and, therefore, full interaction is assumed in the comparison of analytical methods with experimental results.

In elastic range the developed internal forces are low and the stiffnesses of the beam bottom flange and the contact plate can be assumed to be infinitely large (Huber, 1999). This assumption can also be verified by the test results. The maximum strain measured in the bottom flange of the beam at 50 % of the ultimate moment capacity is insignificant compared to the strains measured in reinforcement, see Figs. 4.15 and 4.18. It is also obvious that the local compression from the bottom flange through the contact plate to the concrete encasement is less than compressive strength of the concrete inside the steel column and the concrete can be treated as a form of

strengthening and stiffening. Therefore, the spring stiffness of the compression group, k_{123}, may be assumed equal to infinity in elastic range.

5.4.2 Theoretical response at the ultimate state

The deformation capacity of the joint is provided through inelastic elongation of the slab reinforcement $\Delta_{u,5}$, through slip Δ_4 of the shear connection at the end of the beam and through the plastic deformation Δ_{123} in the compression region.

The deformation capacity of the reinforcement is limited by the rupture of the bars. The bars are most extensively strained and the rupture eventually occurs at locations of the transverse cracks in the joint region. The deformation capacity is influenced by the ductility of the reinforcing bars and by the tension stiffening of concrete between cracks. Due to the tension stiffening effect, the behaviour of the embedded reinforcement provides a higher stiffness and a lower overall ductility than the reinforcement alone. To calculate the deformation capacity of the slab reinforcement, it is necessary to determine the ultimate strain of the reinforcement and the length over which the strain is assumed to act.

The method that takes into account the tension stiffening is adopted from CEB-FIP Model Code 1990 (1993) and is recently included also in the ECCS design recommendations for composite joints (Anderson et al., 1999). The average ultimate strain ε_{smu} in plastic embedded reinforcement (CEB-FIP Model Code 1990, 1993) and the "transmission" length L_t (Hanswille, 1997) is calculated from the expressions:

$$\varepsilon_{smu} = \varepsilon_{sy} - \beta_t \Delta\varepsilon_{sr} + \delta\left(1 - \frac{\sigma_{sr1}}{f_{y,s}}\right)\left(\varepsilon_{su} - \varepsilon_{sy}\right), \tag{5.11}$$

$$L_t = \frac{k_c f_{ctm} \phi}{4\tau_{sm}\rho}. \tag{5.12}$$

In Equation (5.11) β_t is taken as 0.4 for short-term loading and δ is taken as 0.8 for high-ductility deformed bars. $\Delta\varepsilon_{sr}$ is the increase of strain in the reinforcement at the crack, when the crack opens, and σ_{sr1} is the stress in the reinforcement in the crack,

when the first crack has formed. The cracking moment of a composite joint is defined as the moment that causes the mean tensile strength of concrete f_{ctm} to be reached at the top fibre of the uncracked slab. σ_{srl} and $\Delta\varepsilon_{sr}$ are calculated as follows:

$$\sigma_{sr1} = \frac{f_{ctm} k_c}{\rho}\left[1 + \rho \frac{E_s}{E_c}\right], \tag{5.13}$$

$$\Delta\varepsilon_{sr} = \frac{f_{ctm} k_c}{E_s \rho}, \tag{5.14}$$

$$\rho = \frac{A_s}{A_c}, \tag{5.15}$$

$$k_c = \frac{1}{1 + \frac{h_{cs}}{2z_0}}, \tag{5.16}$$

where h_{cs} is the thickness of the concrete flange, excluding any ribs and k_c is a coefficient that allows for the self-equilibrating stresses and the stress distribution in the slab prior to cracking. z_0 is the vertical distance from the centroid of the uncracked concrete flange to the neutral axis of uncracked composite section, which is calculated ignoring the reinforcement and using the modular ratio for short-term effects, E_s/E_{cm}. In Eq. (5.12) ϕ is the diameter of the reinforcing bars and τ_{sm} is the average bond stress along the transmission length. For the bond stress, a value equal to $1.8 \cdot f_{ctm}$ is given in the CEB-FIP Model Code 1990 (1993).

If low amounts of reinforcement are used ($\rho < 0.8$ %), only one main crack in the slab will form at the joint. In such situations the reinforcement will yield directly at the location of this main crack, i.e. only within the transmission length L_t. For higher amounts of reinforcement, it is shown that the elongation length increases and that the length depends on the position of the first shear connector. Considering the above-mentioned, the inelastic extension of the reinforcement is calculated using the formulae (Anderson et al., 1999):

$\rho < 0.8$ %: $$\Delta_{u,5} = 2 \cdot L_t \cdot \varepsilon_{smu}, \tag{5.17}$$

$$\rho > 0.8\ \%\ \text{and}\ a < L_t:\quad \Delta_{u,5} = \left(\frac{h_c}{2} + L_t\right)\cdot \varepsilon_{smu}\,, \tag{5.18}$$

$$\rho > 0.8\ \%\ \text{and}\ a > L_t:\quad \Delta_{u,5} = \left(\frac{h_c}{2} + L_t\right)\cdot \varepsilon_{smu} + (a - L_t)\cdot \varepsilon_{sy}\,, \tag{5.19}$$

where a is the distance from the face of the column to the first shear connector along the beam, h_c is the depth of the column section in the direction parallel to the longitudinal reinforcement, and ε_{sy} is the yield strain of the reinforcement. In Eq. (5.19), the average ultimate strain occurs only within the depth of the column and along the transmission length. The rest of the elongation length is multiplied by only the yield strain of the reinforcement.

The compressive force component F_c in Fig.5.3 is introduced into the column via the bottom flange of a beam and a contact plate. The test results show that plastic elongation in the bottom flange of the beam was small in comparison with the strains in the reinforcement. The load introduction into the column is taken by the concrete encasement inside the steel column and by the steel stiffeners welded both sides the column. It was observed from the tests that the compression force produced negligible local deformation in the column face. The capacity of the column exposed to local compression is calculated assuming that the concrete encasement and steel stiffeners resist the load according to their capacity. If a load distribution shown in Fig. 5.6 is assumed, the compressive resistance may be calculated from:

$$F_{3,Rd} = A_{c1}\cdot\frac{f_{ck}}{\gamma_c} + A_{stiff}\cdot\frac{f_{ay}}{\gamma_a}. \tag{5.20}$$

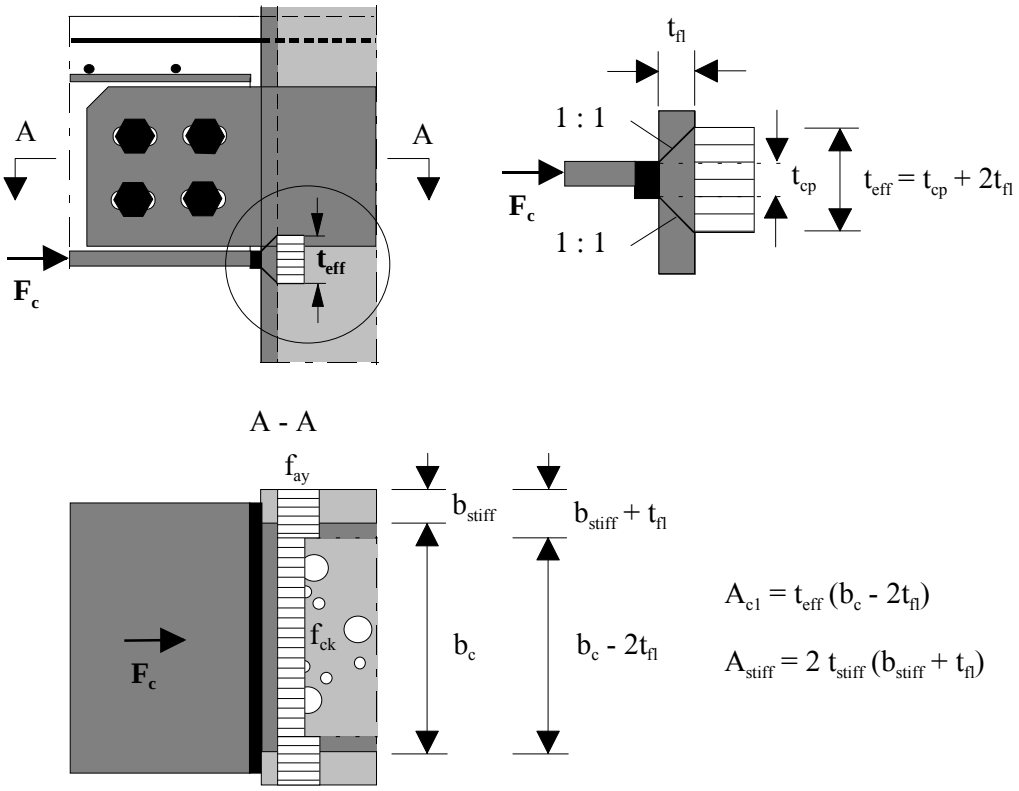

Figure 5.6 Load introduction into the composite column in compression region.

5.5 Assembly of the components and derivation of the bi-linear design characteristics for a joint exposed to a balanced loading

In this work, only the behaviour of joints exposed to balanced hogging moments was experimentally studied. Therefore, the analytical method and design characteristics are derived first for this particular case and validated against the experimental data. A mechanical model for a joint exposed to balanced loading can be derived from the general one simply by omitting the non-existing components, see Fig. 5.7. It is assumed that one half of the total elongation will arise on each side and, therefore, the interplaying translational spring components are combined to rotational joint spring separately for the left and right hand side of the joint.

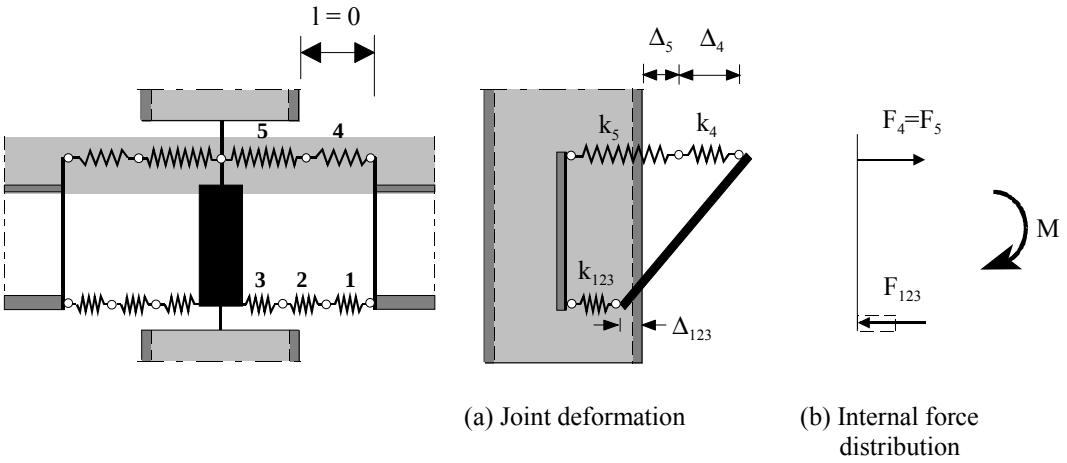

Figure 5.7 A mechanical model for a joint exposed to balanced loading.

The transfer from force-deformation behaviour of the basic joint components to a moment-rotation characteristic of a composite joint is done by joining the individual translational springs together as a system, which fulfils the requirements of compatibility and equilibrium, and the limitations on the resistance of the components, see Fig. 5.2. The assembly of the components to determine the rotational stiffness of the joint, the plastic design moment resistance of the joint and the design rotation capacity of the joint is next explained.

5.5.1 Joint initial rotational stiffness $S_{j,ini}$

The prediction method for calculating the initial rotational stiffness $S_{j,ini}$ is derived from the elastic translational stiffnesses of the basic joint components and it is relation to the elastic bending moment of the cracked composite connection cross-section. Figure 5.7 (a) shows a simplified spring model in which the joint deforms only due to the elastic elongation of the reinforcement in tension, the slip at the steel concrete interface on account of flexibility of the shear connectors and compression in the beam flange, contact plate and concrete core. Considering rotation with respect to the underside of the steel section, the equilibrium and compatibility equations for the joint are:

$$M = F_5 (D_b + D_s), \tag{5.21}$$

$$F_{123} = F_4 = F_5, \tag{5.22}$$

$$\phi = \frac{\Delta_5 + \Delta_4 + \Delta_{123}}{D_b + D_s}, \tag{5.23}$$

where D_b is the height of the steel beam and D_s is the distance between the centroid of the reinforcement and the top of the steel beam, see Fig. 5.4. Using Eqs. (5.4) to (5.6), (5.21) to (5.23) and considering the equilibrium condition of forces, rotation ϕ due to a particular bending moment M is written as:

$$\phi = \frac{\frac{1}{k_5} + \frac{1}{k_4} + \frac{1}{k_{123}}}{(D_b + D_s)^2} M. \tag{5.24}$$

This is expressed in terms of rotational stiffness of the joint as follows:

$$S_{j,ini} = \frac{M}{\phi} = \frac{(D_b + D_s)^2}{\frac{1}{k_5} + \frac{1}{k_4} + \frac{1}{k_{123}}}. \tag{5.25}$$

If a full shear interaction exists, with no interface slip between the slab and steel beam, and if the column section is filled with concrete, the spring stiffnesses of the shear interaction, k_4, and that of the compression group, k_{123}, may be assumed equal to infinity. Further, Eq. (5.25) for the joint stiffness may be written as:

$$S_{j,ini} = k_5 (D_b + D_s)^2 = \frac{E_s A_s (D_b + D_s)^2}{L}. \tag{5.26}$$

5.5.2 Design moment resistance of the joint, $M_{j,Rd}$

The prediction method is based on the simple-plastic theory in which the concept of 'stress blocks', generally accepted and used in major design codes, is employed. It is assumed that the steelwork connection provides no contribution to moment resistance

and therefore the distribution of internal forces may be obtained as shown in Fig. 5.7 (b). The moment resistance is determined by the resistance of reinforcement in tension, ignoring the concrete in tension and assuming that the slab reinforcement is fully yielded. Tension force F_5 is assumed to be transferred at the centroidal axis of the reinforcement, and compression force F_{123} at the centroid of the bottom flange of the beam. The tensile capacity of the reinforced slab, $F_{5,Rd}$, is given by the yield strength of the reinforcement within the effective width of the slab b_{eff}:

$$F_{5,Rd} = \frac{A_s \cdot f_{sy}}{\gamma_s} \tag{5.27}$$

The moment resistance of the composite joint is evaluated by multiplying the tensile resistance of the reinforcement by its distance from the bottom flange of the beam:

$$M_{j,Rd} = F_{5,Rd}(D+D_s). \tag{5.28}$$

When a partial shear connection is used, the effective force in the reinforcement is controlled by the resistance of shear connectors and shear capacity $F_{4,Rd}$ should then be used instead of $F_{5,Rd}$. The tension force used in Eq. 5.28 is limited by the resistance of the compression region.

5.5.3 Rotation capacity of the joint, ϕ_{Cd}

The procedure to calculate the available rotation capacity is similar to that used in determining the initial rotational stiffness of the joint. The joint deformation is determined from the inelastic elongation of the joint components. Assuming that the rotation takes place about the underside of the steel section, the resulting rotation capacity ϕ_{Cd} is determined as (Anderson et al., 2000):

$$\phi_{Cd} = \frac{\Delta_{u,5}}{D_b + D_s} + \frac{\Delta_4 + \Delta_{123}}{D_b}, \tag{5.29}$$

where $\Delta_{u,5}$ is the inelastic elongation of the slab reinforcement, Δ_4 is the slip of the shear connection and Δ_{123} is the plastic deformation of the compression region of the joint, as explained in Section 5.4.2. The design rotation capacity is calculated using characteristic values for material properties.

In determining the rotation capacity of a joint, in general only one component attains its maximum deformation, whilst all other components achieve values lower than their maximum deformation capacity. As the moment resistance of the composite joint, Eq. (5.28), is determined by the resistance of reinforcement, $F_{5,Rd}$, or by the resistance of shear connectors, $F_{4,Rd}$, the resistance of the other components of the joint has to be checked to avoid the premature loss of rotation capacity that would result from their failure.

5.6 Comparison of analytical methods with experimental results

The connection characteristics predicted by the analytical method described above are presented and compared with the values obtained from the experimental observations in Tables 5.1 to 5.4. The experimentally and analytically predicted moment-rotation curves are given for comparison in Figs. 5.8 to 5.11. The values predicted are based on real dimensions and strengths and partial safety factors equal to unity. No slip was observed in the tests and thus it is also ignored in the values. A calculation example of the composite joint used in test CC1 is presented in Appendix V, so as to explain the use of calculation procedures.

The comparison results for the predicted initial rotational stiffness of a joint and those measured from the tests are given in Table 5.1. The joint stiffnesses are given as calculated assuming the length L considered for the bar extension to be equal with the distance between the centre-line of the column and the position of the first shear connector ($L = D_c/2+a = 300/2 + 115$). The rotational stiffness is calculated according to Eq. (5.26) both including and excluding the mesh reinforcement. The results show that equation gives too high stiffnesses compared to the experiments and it is obvious that the straining length L taken as recommended in Eq. (5.9) should be encreased to provide agreement with test results. In Table 5.2, the joint stiffnesses are given as

calculated assuming the length L taken as recommended in Eq. (5.10) ($L = D_c/2+a+p = 300/2 + 115 + 200$). Now the results show that the equation gives too low stiffnesses for specimens CC1 and CC4.

TABLE 5.1

COMPARISON OF THE EXPERIMENTAL AND PREDICTED RESULTS FOR THE INITIAL ROTATIONAL STIFFNESS OF THE JOINT ASSUMING $L = D_c/2+a$ (EQ. (5.26)).

		With mesh reinf.		Without mesh reinf.	
Test (1)	$S_{j,ini,exp}$ [kNm/mrad] (2)	$S_{j,ini,pred}$ [kNm/mrad] (3)	Pred./Test (4)	$S_{j,ini,pred}$ [kNm/mrad] (5)	Pred./Test (6)
CC1	99.0	133.6	1.35	120.5	1.22
CC2	65.8	133.0	2.02	119.8	1.82
CC3	87.6	198.7	2.27	185.3	2.12
CC4	97.1	133.0	1.37	119.8	1.23

TABLE 5.2

COMPARISON OF THE EXPERIMENTAL AND PREDICTED RESULTS FOR THE INITIAL ROTATIONAL STIFFNESS OF THE JOINT ASSUMING $L = D_c/2+a+p$ (EQ. (5.26)).

		With mesh reinf.		Without mesh reinf.	
Test (1)	$S_{j,ini,exp}$ [kNm/mrad] (2)	$S_{j,ini,pred}$ [kNm/mrad] (3)	Pred./Test (4)	$S_{j,ini,pred}$ [kNm/mrad] (5)	Pred./Test (6)
CC1	99.0	76.2	0.77	68.7	0.69
CC2	65.8	75.8	1.15	68.3	1.04
CC3	87.6	113.2	1.29	105.6	1.21
CC4	97.1	75.8	0.78	68.3	0.70

The bending resistance of the connection is calculated using Eq. (5.28) both including and excluding the mesh reinforcement and a comparison with the experimental results

is given in Table 5.3. It is seen that satisfactory agreement exists between the calculated results and actual moments in column (2) when allowance for the mesh is included in column (3). The results show that for test CC3 the moment resistance is overestimated by 4 %. However, it is generally recommended to ignore the mesh reinforcement when calculating the resistance. The resistance values calculated without the mesh in column (5), show that the equation considerably underestimates the bending resistance in tests CC1, CC2 and CC4, and it is obvious that in these specimens the mesh contributes to the actual resistance. In test CC3, the observations during the test and the test results indicate that the mesh has already fractured when the moment resistance of the joint is reached. Therefore, satisfactory agreement exists between the experimental and the calculated moments of resistance where the mesh reinforcement is excluded. It is observed that the analytical prediction underestimates the design moment resistance in all cases, and the ratio of experimental to analytical values of the moment capacity, where the mesh reinforcement is excluded , is 0.85 in average.

TABLE 5.3

COMPARISON OF THE EXPERIMENTAL AND PREDICTED RESULTS FOR THE MOMENT RESISTANCE OF THE JOINT (EQ. (5.28)).

		Mesh included		Mesh excluded	
Test (1)	$M_{j,Rd,exp}$ [kNm] (2)	$M_{j,Rd,pred}$ [kNm] (3)	Pred./Test (4)	$M_{j,Rd,pred}$ [kNm] (5)	Pred./Test (6)
CC1	375	349	0.93	311	0.83
CC2	347	326	0.94	288	0.83
CC3	489	509	1.04	471	0.96
CC4	371	326	0.88	288	0.78

Table 5.4 contains the comparison of calculated and measured rotation capacities of the joints. The experimental values are those recorded when the tests were terminated. The calculation ignores any additional deformation capacity resulting from slip. In-

elastic deformation of the bottom flange of the steel beam immediately adjacent to the column face is included assuming strain ε_1, measured from the experimental results (Fig. 4.19), over a flange length of 40 mm from the outer face of the column (column (5) in Table 5.4). It is seen that the difference between the experimental and analytical predictions is large, and the analytical method underestimates the connection flexibility.

TABLE 5.4

COMPARISON BETWEEN EXPERIMENTAL AND PREDICTED RESULTS FOR THE ROTATION CAPACITY OF THE JOINT (EQ. (5.29)).

Test (1)	$\phi_{Cd,exp}$ [mrad] (2)	L_t [mm] (3)	$\Delta_{u,5}$ [mm] (4)	ε_1 [%] (5)	Δ_1 [mm] (6)	$\phi_{Cd,pred}$ [mrad] (7)
CC1	69	73.0	16.3	0.30	0.1	59
CC2	81	76.0	12.2	0.50	0.2	45
CC3	84	60.6	17.9	0.50	0.2	65
CC4	89	76.2	12.3	1.00	0.4	46

In Figs. 5.8 to 5.11, the predicted bi-linear moment-rotation characteristics are compared with the experimental results. The predicted curves are plotted both including (dashed line) and excluding (solid line) the contribution of the mesh reinforcement. From the results obtained from Tables 5.1 and 5.2, Eq. (5.9) is selected for calculating the length L considered for the bar extension. The rotational stiffness, S_j, is taken as the secant stiffness of the joint when reaching $M_{j,Rd}$. In order to consider the non-linearity of the actual moment-rotation curve of the joint, and to have the approximate curve wholly below the experimental curve, η= 4.5 is selected for the connection of this study.

The results show that the method proposed can predict the overall behaviour fairly well and the bi-linear approximation for the moment-rotation characteristics is entirely enveloped by the experimental curves, as required by the Eurocodes. It is seen

that at the initial stage of loading, the moment rotation relationships exhibit a linear behaviour and the experimental and analytical results are closely related in the majority of the specimens. After the plastic moment has developed, the further increase in the bending moment was possible mainly due to the strain hardening of the reinforcing bars and contribution of the shear flat. The developed model ignores these effects, which explains the difference between the actual moment-rotation characteristics and the yield plateau of the idealization.

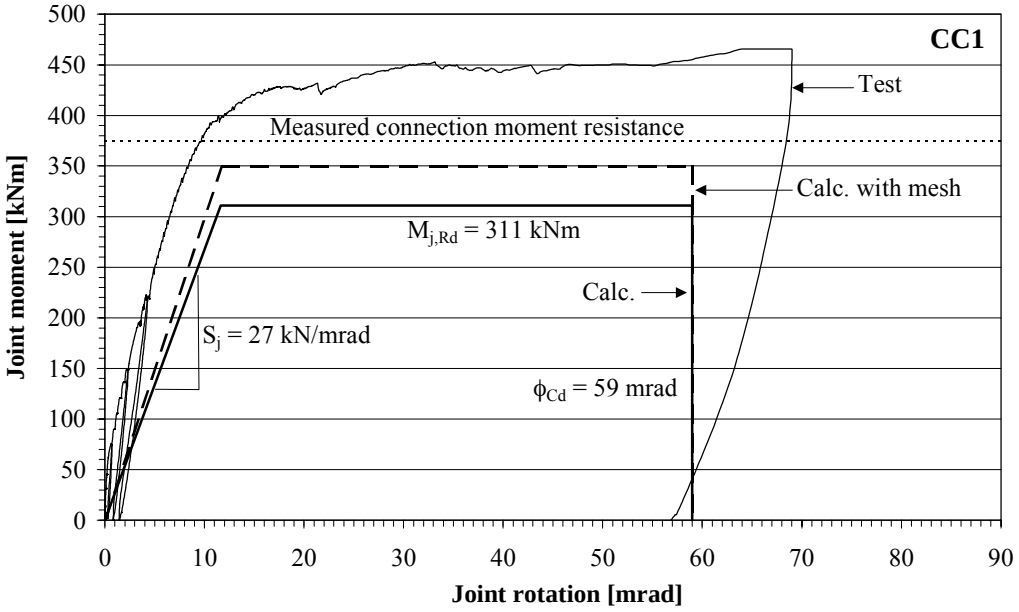

Figure 5.8 Comparison of experimental and calculated connection characteristics of specimen CC1.

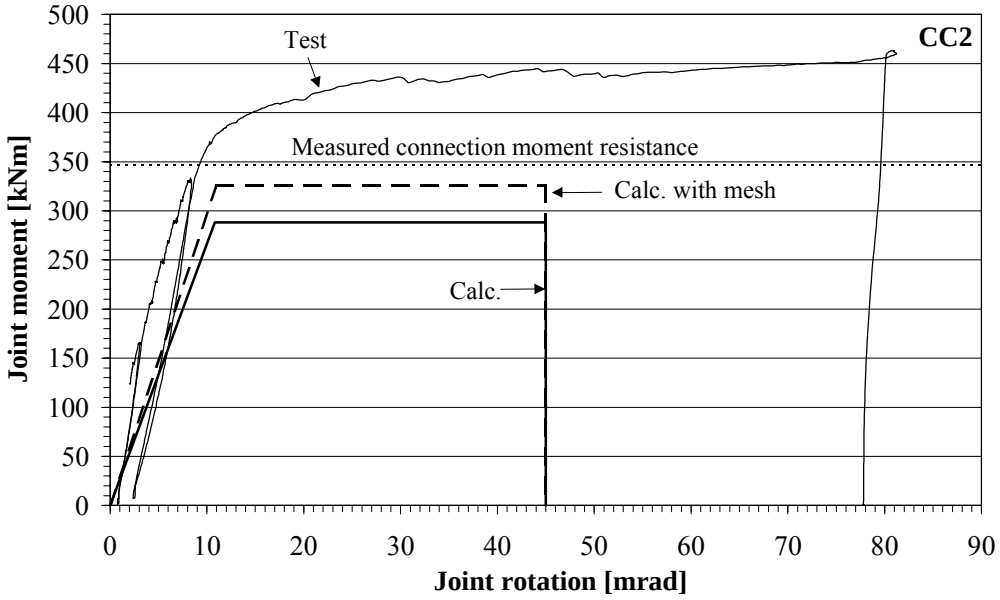

Figure 5.9 Comparison of experimental and calculated connection characteristics of specimen CC2.

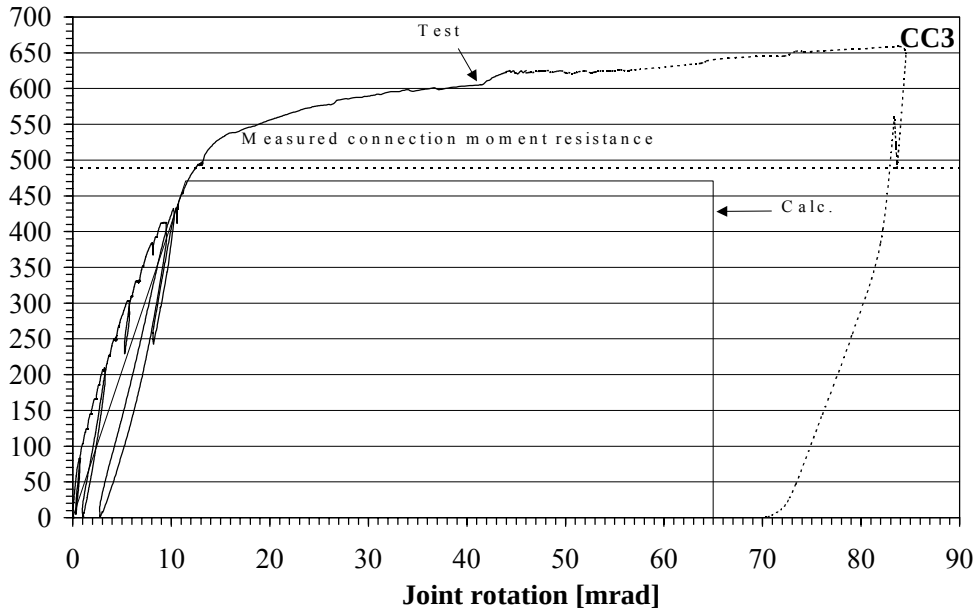

Figure 5.10 Comparison of experimental and calculated connection characteristics of specimen CC3.

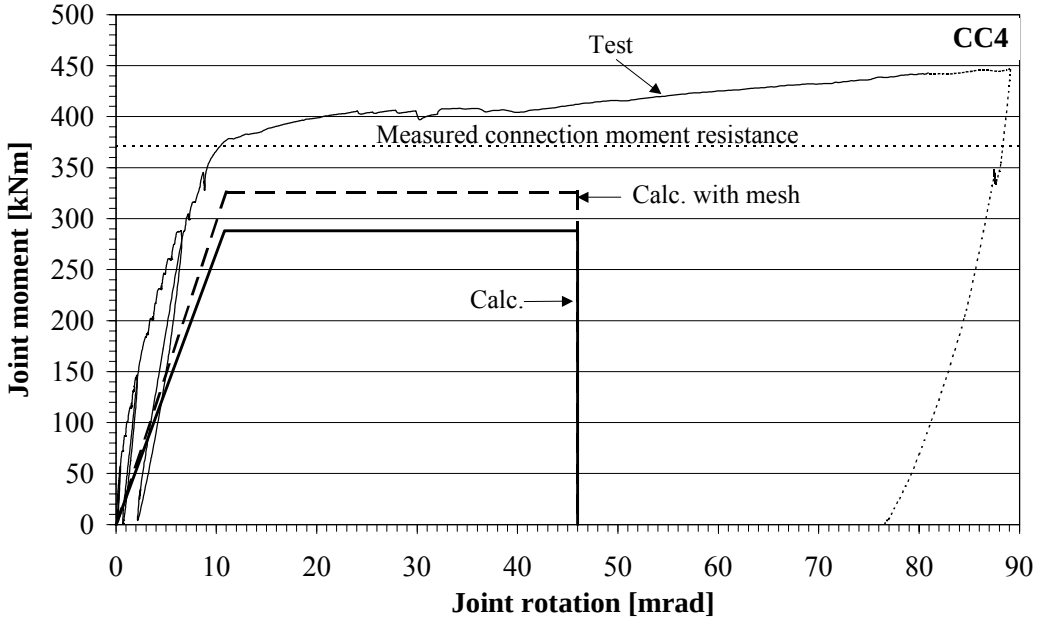

Figure 5.11 Comparison of experimental and calculated connection characteristics of specimen CC4.

5.7 Vertical shear resistance of the connection

The vertical shear resistance of a connection should be checked in order to ensure the desired moment-rotation response in the joint. The governing shear resistance is determined as that of the group of four bolts or the net section of the shear flat reduced by the slotted bolt-holes. Any resistance of the concrete and reinforcement is ignored because of cracking in the slab. In the design of the shear flat, the interaction of shear (V) and moment due to the eccentric load introduction (V·e) from the beam to the shear flat should be taken into account, see Fig. 5.3. A basic ultimate strength formula can be approximately obtained by applying the Von Mises yield criterion, and by accounting for the biaxial state of stress. A combined yield criterion such as:

$$\sigma^2 + 3\tau^2 \le f_y^2, \tag{5.30}$$

may be used, in which σ is the design normal stress in the direction normal to the column face, τ is the design shear stress distributed uniformly throughout the plate section, and f_y is the yield strength of the shear flat.

In the regions of load introduction, it should be ensured that the loads applied to columns at joints can be transferred to the concrete, see Fig. 5.12. Tests (Bergmann et al, 1995) show that the shear flat inserted through the steel section provides a very effective connection because it can transfer large vertical forces to the concrete filled composite column. According to the test results, the stresses below the inserted plate can reach very high values, because the steel section confines the concrete. Based on these results, a design proposal for the resistance of an axially or eccentrically loaded column core is given in a form:

$$f_{u1,Rd} = \left(f_{ck} + 35.0\right)\frac{1}{\gamma_c}\sqrt{\frac{A_c}{A_1}}, \tag{5.31}$$

where

A_c is the area of the concrete core in the column,

A_1 is the area below the plate,

f_{ck} is the characteristic concrete strength in N/mm^2,

γ_c is the material safety factor for concrete (γ_c =1.5) and

$\frac{A_c}{A_1} \leq 20$.

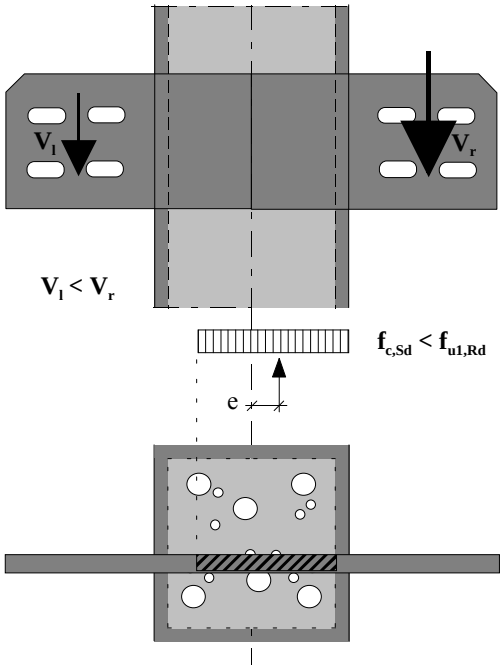

Figure 5.12 Load introduction into a composite column section by an inserted plate.

5.8 Joint exposed to an unbalanced loading

The contribution of unbalanced moments to the mechanical model for a force transfer mechanism in the slab is developed based on proposals by Huber (1999) and Anderson et al. (1999). For joints exposed to unbalanced hogging moments the difference ΔF has to be redirected and account should be taken of the rotational deformation of the connections (spring No.6) and the shear deformation of the shear region (spring No.7). A mechanical model describing this behaviour is derived from a

strut idealisation, which can be seen in Fig. 5.13. It has been assumed that the bigger force is located at right hand side of the joint.

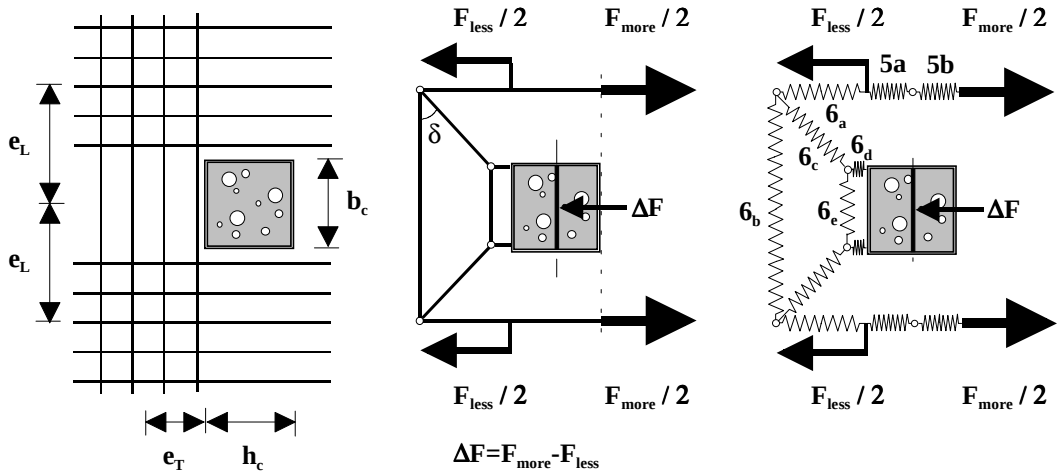

Figure 5.13 Idealisation by a truss model.

Each member within the trussed framework is regarded as a separate translational spring, stressed with an individual load depending on the truss geometry. The strut model, loaded with the force ΔF, consists of the following parts: the longitudinal reinforcement (No.6a) until the centre line of the transverse reinforcement, the transverse renforcement (No.6b) exposed to tension, the diagonal concrete strut (No.6c) as well as the concrete struts No.6d and No.6e in compression. The translational stiffnesses and design resistances of these components in the truss model are given in Table 5.5 (Huber, 1999).

TABLE 5.5

THE TRANSLATIONAL STIFFNESSES AND DESIGN RESISTANCES OF THE BASIC COMPONENTS IN THE TRUSS MODEL (HUBER, 1999).

	Spring	Translational Stiffness $1 / k_i$	Design resistance $F_{i,Rd}$
6a	Longitudinal reinf. In tension	$\frac{e_T}{E_s \cdot A_L}$	$\frac{f_{yL} \cdot A_L}{\gamma_s}$
6b	Transverse reinf. In tension	$\frac{e_L}{2 \cdot \tan^2 \delta \cdot E_s \cdot A_T}$	$\frac{2 \cdot \tan \delta}{\mu} \cdot \frac{f_{yT} \cdot A_T}{\gamma_s}$
6c	Diagonal concrete strut in compression	$\frac{e_L - \frac{b_c}{4}}{b_c \cdot d \cdot E_{cm} \cdot \sin \delta \cdot \cos \delta}$	$\frac{0.8 \cdot \alpha \cdot f_{ck} \cdot bc \cdot d}{\gamma_c \cdot 2 \cdot \sin \delta}$
6d	Concrete strut In compression	$\frac{2.3 \cdot d_{[cm]} - 17.4}{4 \cdot \tan \delta \cdot d \cdot E_{cm}}$	$\frac{1.1 \cdot \alpha \cdot f_{ck} \cdot b_c \cdot d}{\gamma_c}$
6e	Concrete strut In compression	$\frac{1}{4 \cdot \tan \delta \cdot d \cdot E_{cm}}$	$\frac{1.1 \cdot \alpha \cdot f_{ck} \cdot b_c \cdot d}{\gamma_c \cdot 2 \cdot \tan \delta}$

The total redirection spring, spring No.6 in Fig. 5.4, can be set together by the serial springs No.6a to No.6e considering the geometry of the trussed framework. The translational stiffness of the overall tension region is derived from the force F_{more} divided by the corresponding elongation calculated by adding the deformation parts of the truss springs. The deformation is distinguished between the elongation of the longitudinal reinforcement (springs No.5 and No.5b) and the deformation coming from the redirection of the force ΔF around the column (spring No.6). The deformation of spring No.5a is assigned to the less heavily loaded left hand side and that of spring No.5b to the more heavily loaded right hand side of the joint. In the case of fully balanced loading it was assumed that one half of the total elongation of the reinforcement will arise on each side. However, in the case of unbalanced loading the elongation influence is not equally shared between the joint sides. The elongation of springs No.5a and No.5b depend on the actual loading situation given by the factor of imbalance:

$$\mu = 1 - \frac{F_{less}}{F_{more}} \approx 1 - \frac{M_l}{M_r}, \text{ where } M_l < M_r. \qquad (5.32)$$

Translational stiffnesses at less and more heavily loaded sides are calculated from Eqs. (5.32) and (5.33), respectively (Huber, 1999).

$$\frac{1}{k_{5a}} = \frac{1}{k_5} \cdot \frac{1-\mu}{2} \tag{5.33}$$

$$\frac{1}{k_{5b}} = \frac{1}{k_5} \cdot \frac{2-(1-\mu)^2}{2} + \frac{\mu}{k_6} \tag{5.34}$$

where

$$\frac{1}{k_5} = \frac{h_c}{E_s \cdot A_L}, \tag{5.35}$$

$$\frac{1}{k_6} = \sum_{i=a}^{e} k_i = \frac{e_T}{E_s \cdot A_L} + \frac{e_L}{2 \cdot \tan^2 \delta \cdot E_s \cdot A_T} + \\ + \frac{1}{4 \cdot \tan \delta \cdot E_{cm} \cdot d} \cdot \left(\frac{4 \cdot e_L - b_c}{b_c \cdot \cos^2 \delta} + (2.3 \cdot h_{cs}[\text{cm}] - 17.4) + 1 \right), \tag{5.36}$$

$$\tan \delta = \frac{\frac{e_T}{e_L} + \sqrt{\left(\frac{e_T}{e_L}\right)^2 - \frac{1}{\frac{e_L}{b_c}} + \frac{1}{4 \cdot \left(\frac{e_L}{b_c}\right)^2}}}{2 \cdot \left(1 - \frac{1}{4 \cdot \frac{e_L}{b_c}}\right)}, \tag{5.37}$$

The design resistance $F_{more,Rd}$ is reached, when the force in one bar of the truss exceeds its design resistance. The joint detailing needs to ensure that failure in the slab is by yielding of the longitudinal reinforcement. When the resistance of the longitudinal reinforcement (spring No.6a) is assumed to represent the design resistance, we can write the limiting conditions for the maximum cross-sectional area of the longitudinal and transverse reinforcements as follows:

$$F_{more,Rd} = F_{6a,Rd} = \frac{f_{yL} \cdot A_L}{\gamma_s}, \tag{5.38}$$

$$F_{6d,Rd} = \mu F_{more,Rd} \quad \Rightarrow \quad A_L \le \frac{1.1}{\mu} \cdot \frac{\gamma_s}{\gamma_c} \cdot \frac{\alpha \cdot f_{ck}}{f_{yL}} \cdot b_c \cdot d, \tag{5.39}$$

$$F_{6b,Rd} = \mu F_{more,Rd} \qquad \Rightarrow \qquad A_T \le \mu \cdot \frac{A_L}{2 \cdot \tan\delta} \cdot \frac{f_{yL}}{f_{yT}}. \tag{5.40}$$

In the case of an unbalanced loading, the tensile capacity of the reinforced slab, $F_{5,Rd}$, in Eq. (5.28) is assumed to be equal to $F_{more,Rd}$.

The compression force ΔF is introduced also into the column web and the shear region in the concrete core is exposed to opposite horizontal shear forces as shown in Fig. 5.5. This force is transferred by the diagonal concrete strut in compression. The shear influence of the translational spring No.7 is converted into the rotational shear springs S_{sa} and S_{sb} in Fig. 3.6. The resulting modification of the stiffness is shown in Fig. 5.14.

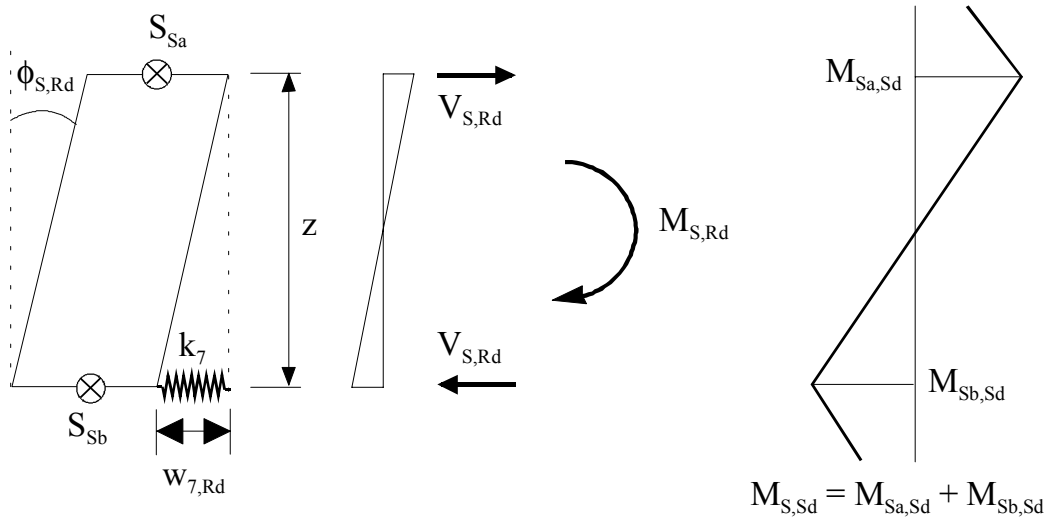

Figure 5.14 Conversion of the translational stiffness in the shear region.

The rotational stiffnesses of the shear springs and the moment resistance can thus be calculated from expressions (Huber and Tschemmernegg, 1998):

$$S_S = \frac{z^2}{\frac{1}{k_7}}, \tag{5.41}$$

$$M_{S,Rd} = V_{S,Rd} \cdot z \;\leq\; M_{Sa,Sd} + M_{Sb,Sd}\,. \tag{5.42}$$

To fulfil a parallel deformation of the upper and lower part of the column, the shear stiffness S_S is shared with a part above and below the joint depending on the moment ratio $M_{Sa,Sd}/ M_{Sb,Sd}$:

$$S_{Sa} = S_S \frac{1}{1 + \dfrac{M_{Sb,Sd}}{M_{Sa,Sd}}} \tag{5.43}$$

$$S_{Sb} = S_S \frac{1}{1 + \dfrac{M_{Sa,Sd}}{M_{Sb,Sd}}}\,. \tag{5.44}$$

The moment resistance of the composite joint exposed to unbalanced loading is determined by the resistance of reinforcement, $F_{more,Rd}$, or by the resistance of shear connectors, $F_{4,Rd}$. and calculated from Eq. (5.28). The resistance of the other components of the joint has to be checked to avoid the premature loss of rotation capacity that would result from their failure. The potential concrete crushing failure in the slab, the failure of the transverse reinforcement and the failure of the concrete core are avoided if the limits given by Eqs. (5.39), (5.40) and (5.42) are satisfied.

5.9 Conclusions

Starting from the basic mechanism of force transfer within the components of a composite connection and using the simplified calculations validated by the experimental results, a simple and yet reliable method is proposed to estimate the moment-rotation characteristics of the new connection-type developed by the author. The analytical method follows existing general design concepts developed for conventional composite connections. According to the results of this study, the general design principles are nevertheless applicable also for composite connections between a slim floor beam and concrete-filled tubular column when the modifications proposed are considered in the design.

The method is validated against the experimental results of joints exposed to balanced loading. Comparison of the models for initial rotational stiffness and moment resistance with experimental data shows a satisfactory agreement. The predicted initial rotational stiffness is overestimated by the analytical model, while predictions on moment capacity and rotation capacity are on the conservative side.

The experimental results indicate that for the given connection detail the connection characteristics are not influenced by the concrete strength, which is quite natural while there are no concrete components in compression. Hence, it is not considered in the methods proposed to predict the rotational stiffness and the moment resistance of the joint.

It was also observed from the experimental results that changes to the shear-to-moment ratio produced negligible effect on the initial rotational stiffness and the moment capacity of the joint. Hence, the method proposed does not predict any reduction in the rotational stiffness and moment capacity due to the presence of coincident vertical shear force. The experimental research of this study show that this assumption may be used when the shear to moment ratio does not exceed value 0.87 m^{-1} and the maximum applied vertical shear load is 387 kN. The influence of the shear effect on joint characteristics should be checked if the above-mentioned shear-to-moment ratio and vertical load are exceeded. The presence of a large amount of longitudinal reinforcement increases the vertical load and, therefore, may lead to the checking.

The mechanical model proposed includes also the case when the joint is exposed to unbalanced loading. The main principles of the unbalanced loading and the component assembly are explained. Owing to the lack of knowledge of the actual behaviour of a joint exposed to unbalanced hogging moments and of the true force–deformation behaviour of the concrete core in compression, these components of the model are not validated and calibration against the test results need be considered in further research.

6 DISCUSSION OF THE RESULTS AND CONCLUSIONS

This study focused on the behaviour of beam-column connections in a building frame consisting of slim floor beams. The principal purpose was to gain a better understanding of the engineering features of semi-continuous composite joints and to apply this design knowledge to the structures frequently used in construction in Finland. The objectives achieved were set as:

- To develop a new structural design connecting a slim floor beam to a tubular steel column section filled with concrete;
- To identify the parameters and determine mechanical properties that govern the connection behaviour;
- To translate this knowledge into simple analytical and numerical methods that can be used by designers.

The following sections summarize the methodology of the study, the principal results, practical applications and conclusions, and propose further research that should be carried out so as to develop the solutions of the problem.

6.1. Methodology

In the preliminary stage and on the course of the study many experts in research, design offices, construction and steel workshops were consulted in order to determine the relevant requirements for the structural and economical features, and to check the author's ideas of design as well as to specify relevant construction conditions. By contributing to international conferences and studying international research reports and other relevant literature the programme was prepared before the test arrangements were designed and carried out.

The research methodology of the study on the connection behaviour and the joint characteristics consisted of well-designed experimental investigations, mathematical modelling resulting in predictions of the characteristics, and deriving design formulae.

The author gained new knowledge with each of the mutually supporting methodological means. The main contributions are summarized below.

6.2 Design of a new advanced connection configuration

A new advanced construction of a composite beam-column connection configuration consisting of a slim floor beam and a concrete-filled tubular column section was designed and implemented for practise. This solution enables a semi-continuous approach to be employed in a new way in slim floor beam design and construction. The design principles and practical aspects are thoroughly reported in the study.

A slim floor system offers many advantages compared to conventional floor systems. It provides a floor system of minimum depth and a flat soffit, which facilitates easy installation of services and the free positioning of partition walls of the building. Both the beam and the steelwork connection are encased in the concrete, which significantly enhances their resistance at ambient and fire temperatures. The new connection configuration of the study enables the application of semi-continuous concept in the design and construction of a floor beam. The semi-continuous design approach increases the overall flexural stiffness of the slim floor beams and allows the use of shallower beam and floor sections, larger column-free floor spans and better performance of beams in service conditions by reducing cracking, deflections and vibrational problems. These advantages offer technical and economical flexibility and a floor system with improved cost-effectiveness.

6.3 Experimental results of joint behaviour

Experimental investigations of bare steel connections were carried out in order to demonstrate the joint behaviour during the erection and casting work of a floor beam. Four composite joints were then tested in order to understand the influence of the slab on the joint behaviour as related to the amount of reinforcement in the slab, the concrete strength and the shear-to-moment ratio. The experimental research resulted in the following main features of the joint responses:

- The bare steel joint can be regarded as a hinge up to rotation of 15-25 mrads.

- At the composite stage, the joints have rotational stiffnesses of 65-99 kNm/mrad, and according to the Eurocode 4 application rules, all the connections may be classified as rigid.

- At the composite stage, the joints had moment resistances of 347-489 kNm, i.e. 48-60 % of the hogging bending resistances of the adjacent composite beam sections. According to application rules of Eurocode 4, the connections are classified as partial-strength.

- Any actual evidence of collapse of the tested composite connections was not really attained even though the connections were tested up to rotations of 80-90 mrads. This confirms that the connections fulfil the rotation requirements implied by plastic methods of the design.

- The experimental tests showed that neither the column nor the compressed flange of the beam fails before the plastic resistance of the reinforcement is reached. The weakest component in all four tested specimens was the reinforcement in tension.

- Tests showed that welded fabric mesh has limited ductility, and therefore its contribution of the mesh reinforcement to the overall flexural stiffness and moment capacity of the joint should be ignored.

- The strength of the concrete had no effect on the joint moment-rotation characteristics as long there are no effective concrete components in compression.

- The connection was tested for two different shear-to-moment ratios in order to investigate the effects of different levels of coincident vertical shear on the connection characteristics. The ratios of shear to moment used were 0.61 and 0.87. Results from the study show that the flexural stiffness and moment capacity of the joint are not significantly influenced by the shear-to-moment ratio. The maximum

shear force applied was 387 kN and no failure due to the insufficient shear resistance of a shear flat was attained.

6.4 Simplified calculation method

The experimental test results form the background for the mathematical model aimed at predicting the moment-rotation characteristics of the joint response based on the geometrical and mechanical joint properties. The mathematical model allows calculation of the initial rotational stiffness $S_{j,ini}$ (Eq. (5.25)), design rotational stiffness S_j, plastic design moment resistance $M_{j,Rd}$ (Eq. (5.28)) and design rotation capacity ϕ_{Cd} (Eq. (5.29)) of the joint. The model is experimentally calibrated against the test results in which the joints were exposed to balanced loading. The design rotational stiffness S_j of the connection, taken as joint secant stiffness at the attainment of $M_{j,Rd}$, is calculated by dividing the predicted initial stiffness value by a coefficient value of η equal to 4.5.

The method proposed does not predict any reduction in the rotational stiffness and moment capacity due to the presence of coincident vertical shear force. Therefore, the method may be used when the shear to moment ratio does not exceed value 0.87 m^{-1} and the maximum applied vertical shear load is 387 kN. The influence of the shear effect on joint characteristics should be checked if the above-mentioned shear-to-moment ratio and vertical load are exceeded.

The mechanical model proposed includes also all the joint components activated when the joint is exposed to unbalanced loading. The main principles and the component assembly considering these joint components are explained. Owing to the lack of knowledge of the actual behaviour of a joint exposed to unbalanced hogging moments and of the true force–deformation behaviour of the concrete core in compression, these components of the model are not validated and the calibrated against the test results need be considered in further research.

6.5 Practical considerations for designers

The capability to predict joint behaviour is a vital need for a new construction to become a real design option. The calculation method presented in this study can be used in the design of following applications:

- Approximation of the form of the moment-rotation curves without the need of testing;
- Classification of joints;
- Calculation of deflections at serviceability limit state;
- Calculation of moment redistribution of continuous composite structures at the ultimate limit state.

Exploiting the semi-continuity in the design, the span of the slim floor beam with a depth of 300 mm (see Fig. 3.1) can be increased from 6-7 m up to 9-10 m. The maximum crack width under service loads, if considered in the design, controls the maximum beam span.

6.6 Further research

In further research, the general form of the mechanical model proposed has to be studied in order to validate the model for cases when the exposed load in a joint is not symmetrical. The model proposed needs to be experimentally calibrated against the test results in which the joints are exposed to unbalanced loading. Also the design methods proposed for the capacity of the column exposed to local compression (Eq. 5.20) and for the capacity of the compressed concrete core below the inserted shear flat (Eq. 5.31) have to be experimentally validated. In order to obtain more insight into the load transfer mechanism and to be able to establish the basic strength formulae for the shear resistance of the shear flat, further investigations are required. From the experiments of this work, a general insight into the static behaviour of the

shear flat has been obtained using electrical strain gauges. However, it is insufficient to understand all the detailed aspects of the distribution of stresses in the plate. For the load-slip behaviour of the shear connectors used in the joint specimens no test data is available. The experimental results indicated that in the specimens full shear connection between the steel beam and the concrete slab was achieved. However, a design method has to be developed for the shear connectors.

7 REFERENCES

Ahmed, B. & Nethercot, D. A. 1997. Prediction of initial stiffness and available rotation capacity of major axis composite flush endplate connections. *Journal of Constructional Steel Research.* Vol. 41. No. 1. Elsevier Science Limited. pp. 31-60.

Anderson, D. & Najafi, A. A. 1994. Performance of composite connections: major axis end plate joints. *Journal of Constructional Steel Research.* Vol. 31. No. 1. Elsevier Science Limited. pp. 31-57.

Anderson, D. (ed) 1997. *Composite steel-concrete joints in braced frames for buildings.* COST-C1. Semi-rigid behaviour of civil engineering structural connections. European Commission. Luxembourg. 197 p.

Anderson, D., Aribert, J.-M., Bode, H., Huber, G., Jaspart, J.-P., Kronenberger, H.-J. & Tschemmernegg, F. 1999. *Design of Composite Joints for Buildings (incl. Model code provisions for composite joints in building frames).* ECCS – Technical Committee 11 – Composite Structures. No. 109. Brussels. Belgium. 140 p. + app. 84 p.

Anderson, D., Aribert, J. M., Bode, H. & Kronenburger, H. J. 2000. Design rotation capacity of composite joints. *The Structural Engineer.* Vol. 78. No. 6. 21 March. pp. 25-29.

Bergmann, R., Matsui, C., Meinsma, C. & Dutta, D. 1995. *Design guide: For concrete filled hollow section columns under static and seismic loading*. CIDECT. Construction With Hollow Sections. No. 5. Verlag TÜV Rheinland. 68 p.

Bernuzzi, C., Gadotti, F. & Zandonini, R. 1995. Semi-continuity in slim floor steel-concrete composite systems. *Steel Structures – Eurosteel '95. Proceedings of the 1st European Conference on Steel Structures.* Athens. Greece. 18-20 May. pp. 287-294.

Charbrolin B. & Bitar, D. 1998. *Unpropped large span floor. Properties and in-service performance*. Technical steel research. Report EUR 18564 EN. Office for Official Publications of the European Communities. Luxembourg. 166 p.

CEB-FIP *Model Code 1990: Design code* 1993. CEB – Comité Euro-International du Beton. Thomas Telford Services, London. Great Britain.

Couchman, G. & Way, A. 1998. *Joints in Steel Construction: Composite connections*. The Steel Construction Institute. SCI-P-213. Ascot. Great Britain. 99 p.

ENV 1993-1-1 Eurocode 3 1992: Design of steel structures: Part 1.1 General rules and rules for buildings. European Prestandard. CEN. Brussels.

ENV 1994-1-1 Eurocode 4 1994: Design of composite steel and concrete structures: Part 1.1 General rules and rules for buildings. European Prestandard. CEN. Brussels.

Hansville, G. 1997. Cracking of concrete: mechanical models of the design rules in Eurocode 4. Composite Construction in Steel and Concrete III: proceedings of an Engineering Foundation conference, Swabian Conference Centre. Irsee. Germany. June 9-14. 1996. Edited by C.D. Buckner & B.M. Shahrooz. ASCE. New York, pp. 421-433.

Harris, H. G. & Sabnis, G. M. 1999. *Structural modeling and experimental techniques*, Second Edition, CRC Press. U.S.A. 789 p.

Huber, G. & Tschemmernegg, F. 1998. Modelling of beam-to-column joints. *Journal of Constructional Steel Research.* vol 45. No. 2. Elsevier Science Limited. pp. 199-216.

Huber, G. 1999. *Non-linear calculations of composite sections and semi-continuous joints*. Dissertation. Institut für Stahlbau. Holzbau und Mischbautechnologie. Universität Innsbruck. Austria.

Leino, T. 1994. Results from two series of tests on typical Finnish steel beam to composite column connections. Semi-Rigid Behaviour of Civil Engineering Structural Connections. *COST C1 Proceedings of the Second State of the Art Workshop*. 28-28 October. Prague. Czechoslovakia. pp. 165-174.

Leon, R. T. & Zandonini, R. 1992. Composite connections. In *Constructional Steel Design: An International Guide.* ed. P. J. Dowling, J. E. Harding and R. Bjorhovde. Elsevier Applied Science. London. pp. 501-522.

Malaska, M. & Mäkeläinen, P. 1999. *Study on composite slim floor beams*. TKK-TER-9. Laboratory of Steel Structures. Department of Civil and Environmental Engineering. Helsinki University of Technology. Espoo. Finland. 37 p.

Malaska, M., Ma, Z. & Mäkeläinen, P. 2000. *Steel-Concrete Composite Slim Floor Frame System.* TKK-TER-14. Laboratory of Steel Structures. Department of Civil and Environmental Engineering. Helsinki University of Technology. Espoo. Finland. 58 p.

Mäkeläinen, P. & Malaska, M. 1999. Study on a Frame System with Composite Slim Floors. IABSE Symposium, Structures for the Future – The Search for Quality. Rio de Janeiro. Brazil. August 25-27. pp. 308-309.

SFS-EN 10 002-1:1990. *Metallic materials. Tensile testing. Part 1: Method of test (at ambient temperature).* CEN European Committee for Standardization. March 1990

SFS 4474 1988. *Concrete. Compressive strength.*

Tschemmernegg, F. 1994, Deformation of semi-rigid composite joints. *Semi-rigid behaviour of civil engineering structural connections.* COST C1. Proceedings of the Second State of the Art Workshop. Prague. 26.-28. October. pp. 195-207.

Tschemmernegg, F. 1998, Composite Frames with Slim Floors. *Journal of Constructional Steel Research*. Vol. 46. No. 1-3. 1998. Paper No. 107. Elsevier Science. 14 p.

Vuolio, A. 2000, *Numerical Study on a Semi-Continuous Beam-to-Column Connection in a Slim Floor Frame System*, Master's Thesis. Laboratory of Steel Structures. Department of Civil and Environmental Engineering. Helsinki University of Technology. Espoo. Finland. 83 p. + app. 30 p.

Zandonini, R. 1989. Semi-rigid composite joints. *Structural connections – stability and strength*. Chapter 3. Elsevier Applied Science. London. Great Britain. pp. 63-20

APPENDIX I

MATERIAL TEST RESULTS OF STRUCTURAL STEEL AND REINFORCING STEEL

The mechanical properties of the structural steel and reinforcing steel components were determined from coupon tests in accordance with standard SFS-EN 10 002-1 "*Metallic materials. Tensile testing. Part 1: Method of test (at ambient temperature)"* (1990). The definitions of the measured material properties of the structural and reinforcing steels are given in Fig. I.1.

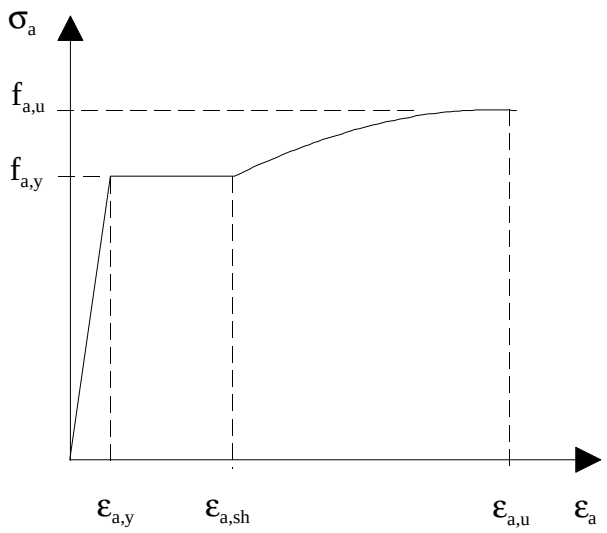

Figure I.1 Definitions of the material properties of the steel.

I.1 Structural steel

Material for tensile test coupons was gas-cut from the shear flat and from the beam bottom flange and web of a specimen not tested. The dimensions of the tensile test specimens are shown in Fig. I.2. The shear flat and the asymmetric steel beam sections used for the tests were all of steel grade S355K2G3 (Raex moniteräs). The

experimental stress-strain curves are plotted in Figs. I.3 to I.5 and the average values are concluded in Table 4.2 in Section 4.4.1.

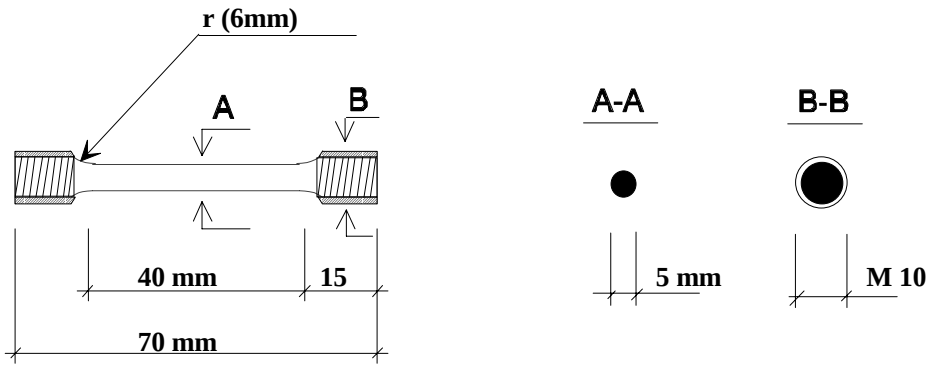

Figure I.2 Dimensions of the test specimen.

I.2 Reinforcing steels

The reinforcement used in the slab and column was achieved with hot-finished bars of grade A500HW. The specimen lengths of 300 mm and 350 mm were used for reinforcing bars and mesh, respectively. The strain of a specimen was measured from the bar lenth of 100 mm. The experimental stress-strain curves are plotted in Figs. I.6 to I.12 and the measured average values for material characteristics are concluded in Tables 4.4 and 4.5 in Section 4.4.3. The surfaces of the reinforcing bars were ground smooth where the strain gauges were fixed, which reduces the cross-sectional area of the bars locally. Therefore, also longitudinal bars ground equally were tested so as to interpret the reduction in strength and ductility, see Figs. I.10 and I.12.

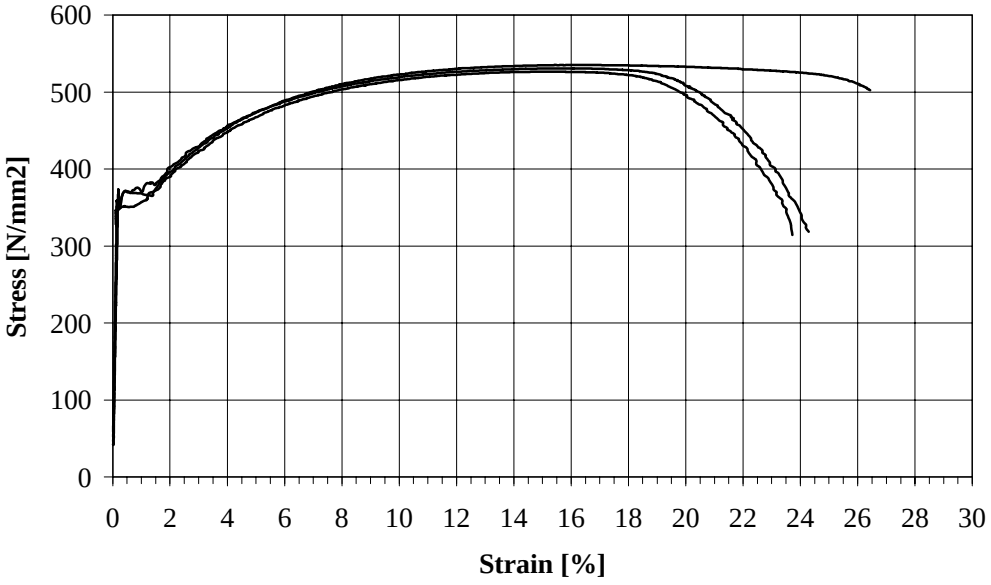

Figure I.3 Measured stress-strain curves for structural steel in shear flat.

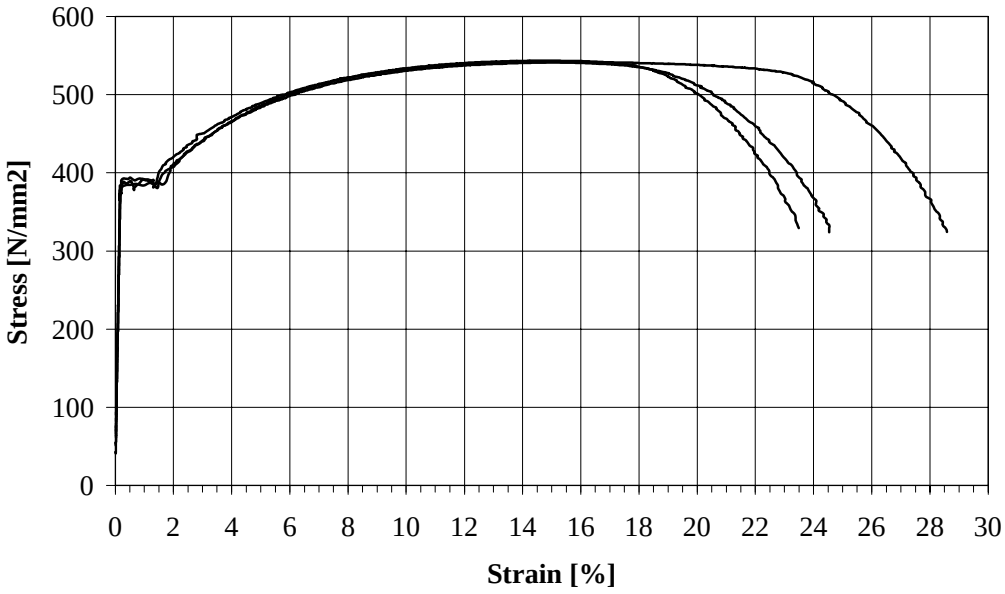

Figure I.4 Measured stress-strain curves for structural steel in beam flange.

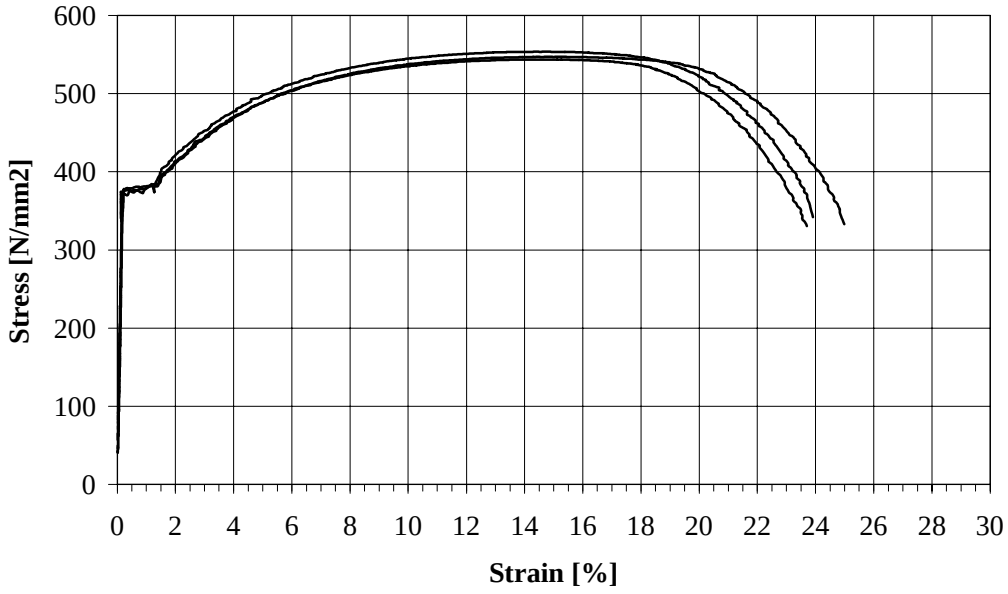

Figure I.5 Measured stress-strain curves for structural steel in beam web.

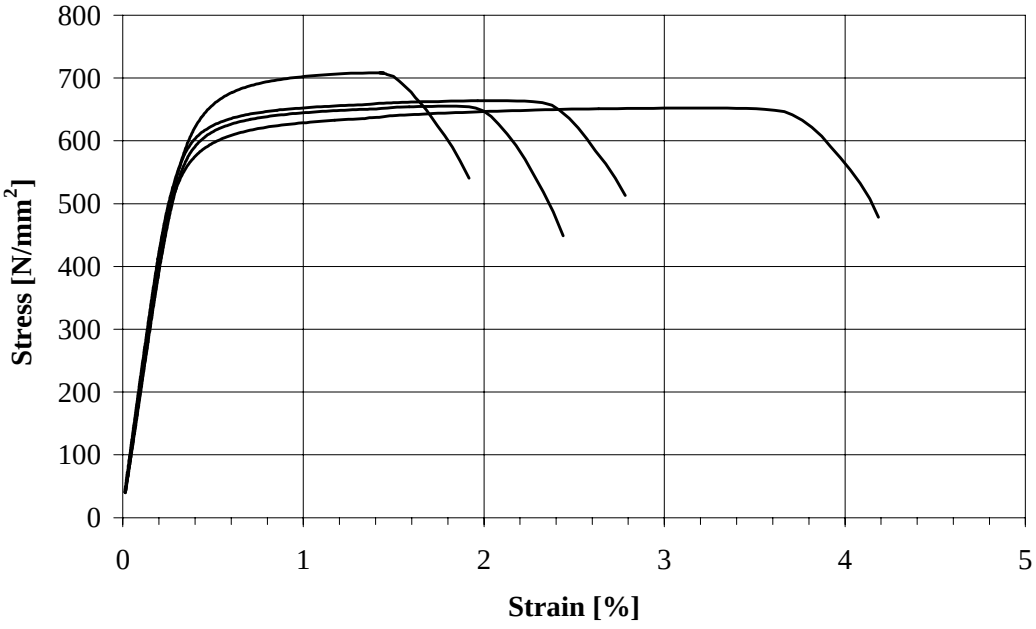

Figure I.6 Measured stress-strain curves for reinforcing bars with a 6 mm diameter.

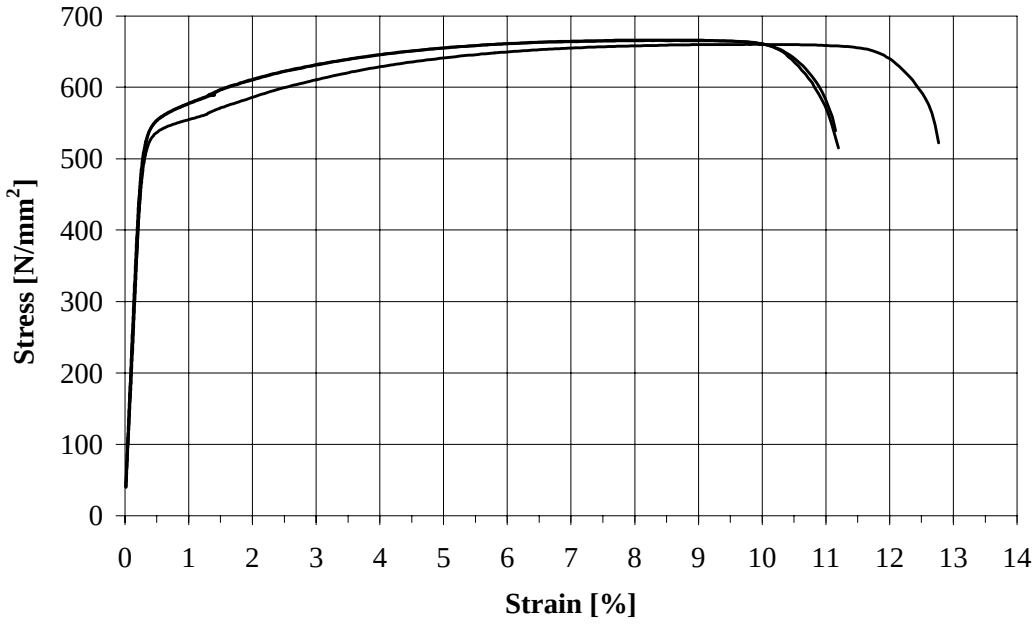

Figure I.7 Measured stress-strain curves for reinforcing bars with a 12 mm diameter.

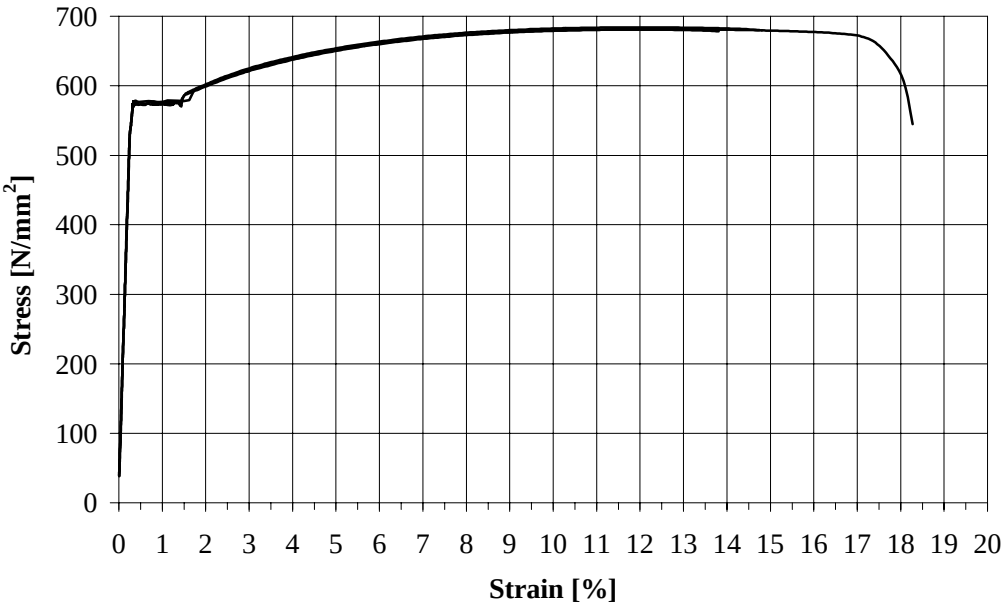

Figure I.8 Measured stress-strain curves for reinforcing bars with a 16 mm diameter (specimen CC1).

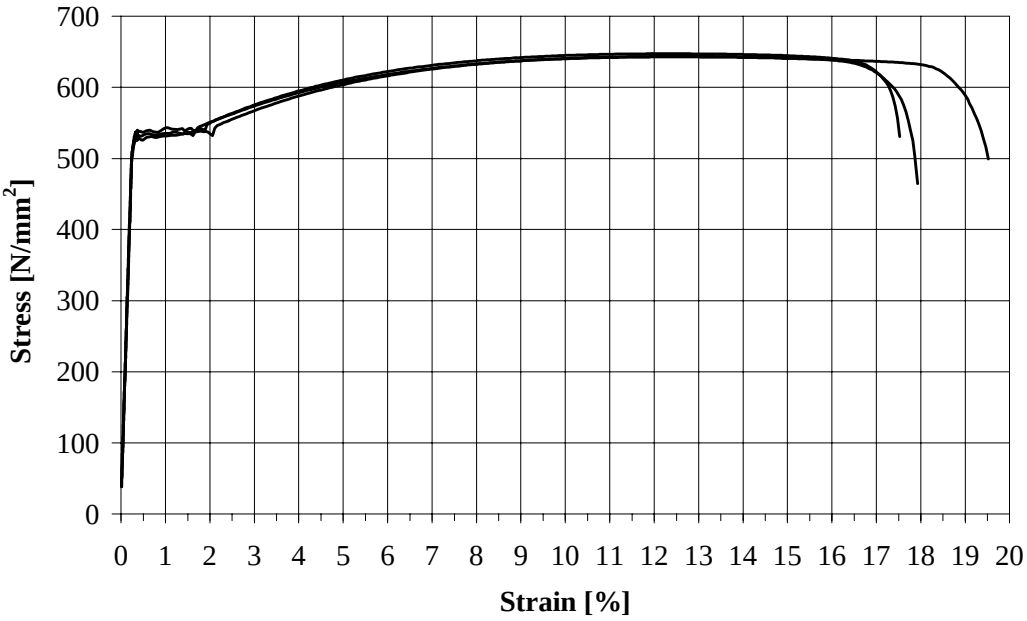

Figure I.9 Measured stress-strain curves for reinforcing bars with a 16 mm diameter (specimens CC2, CC3 and CC4).

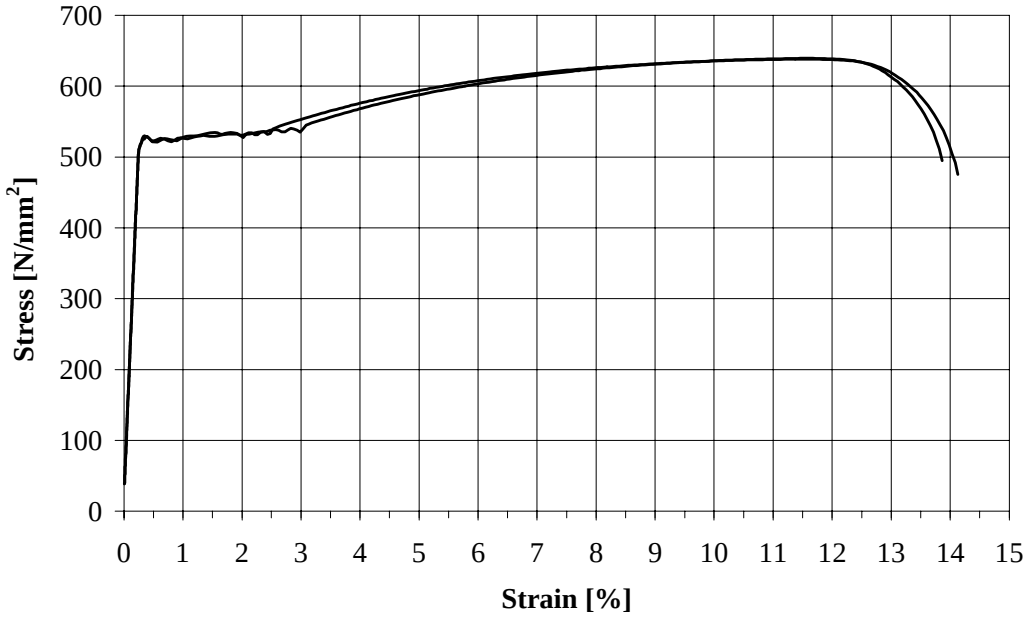

Figure I.10 Measured stress-strain curves for grounded reinforcing bars with a 16 mm diameter (specimens CC2, CC3 and CC4).

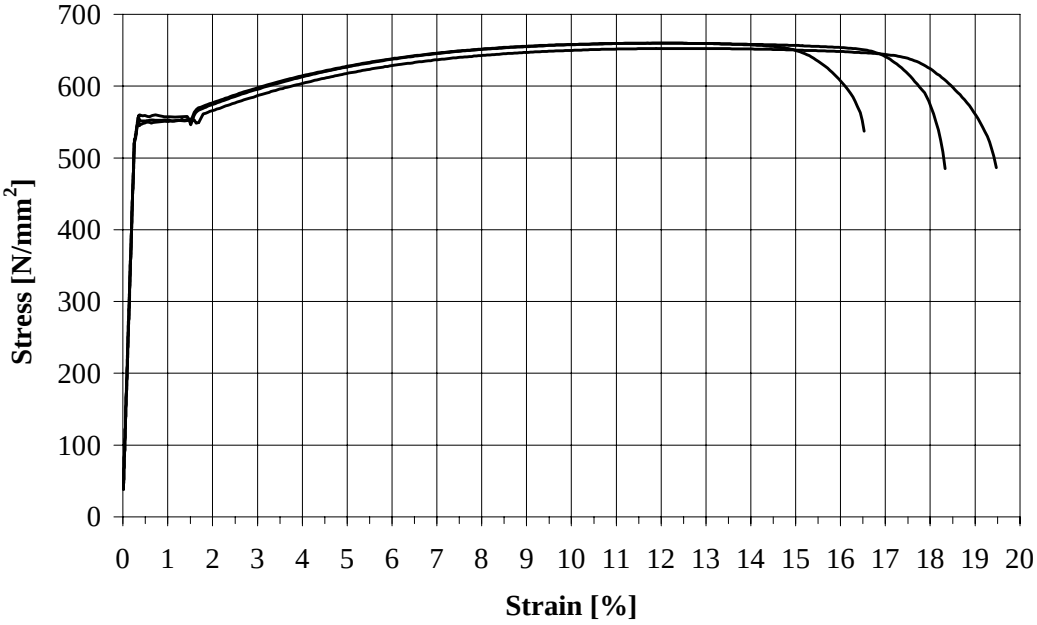

Figure I.11 Measured stress-strain curves for reinforcing bars with a 20 mm diameter.

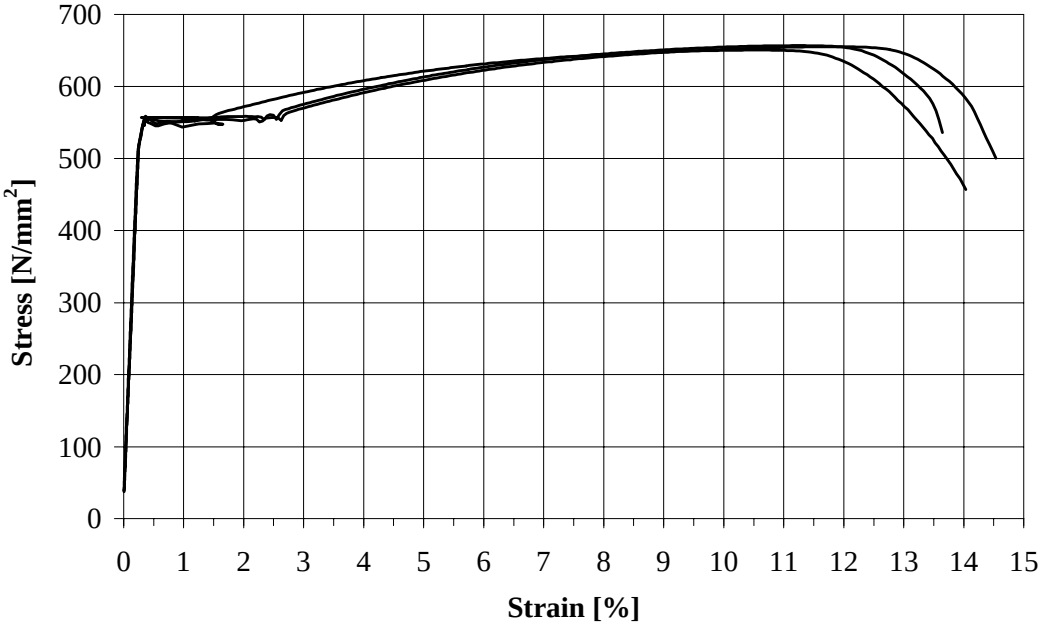

Figure I.12 Measured stress-strain curves for grounded reinforcing bars with a 20 mm diameter.

APPENDIX II

EXPERIMENTAL MOMENT-ROTATION CURVES

In Figs. II.1 to II.6, the moment-rotation curves for bare steel connection specimens (SC1, SC2) and for composite connection specimens (CC1, CC2, CC3 and CC4) are presented. The curves were determined at the surface of the column flange as described in Section 3.3.1.

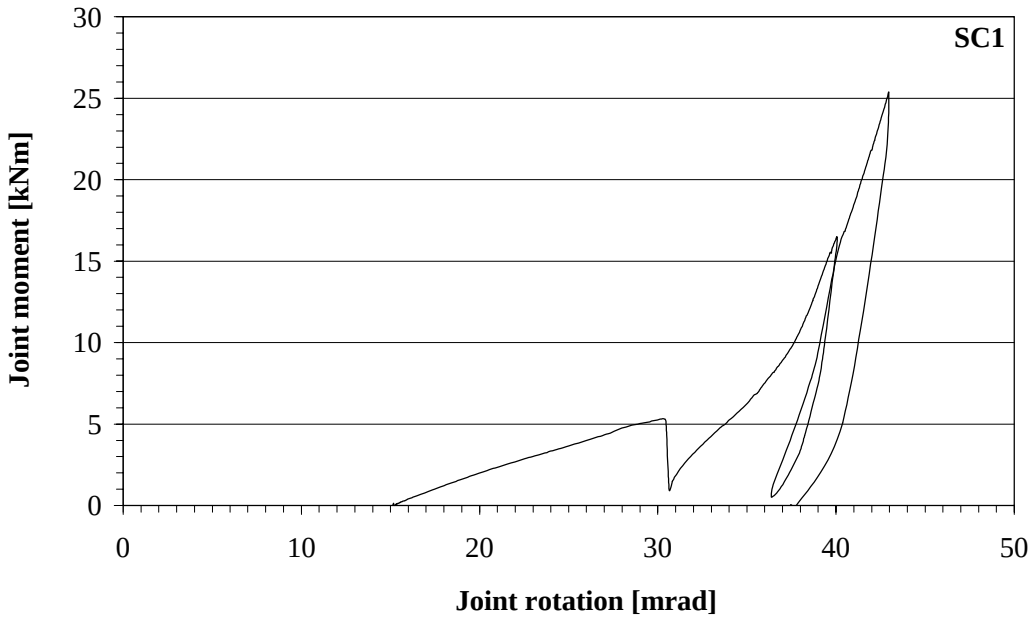

Figure II.1 Measured moment-rotation ($M_{j,exp}$-$\phi_{j,exp}$) curve for specimen SC1.

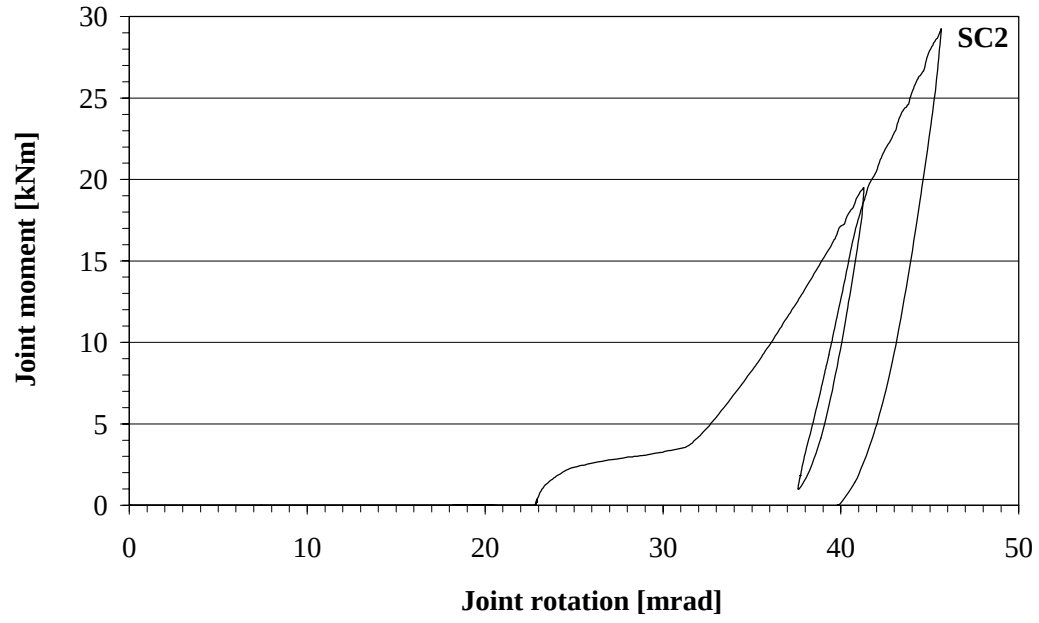

Figure II.2 Measured moment-rotation ($M_{j,exp}$-$\phi_{j,exp}$) curve for specimen SC2.

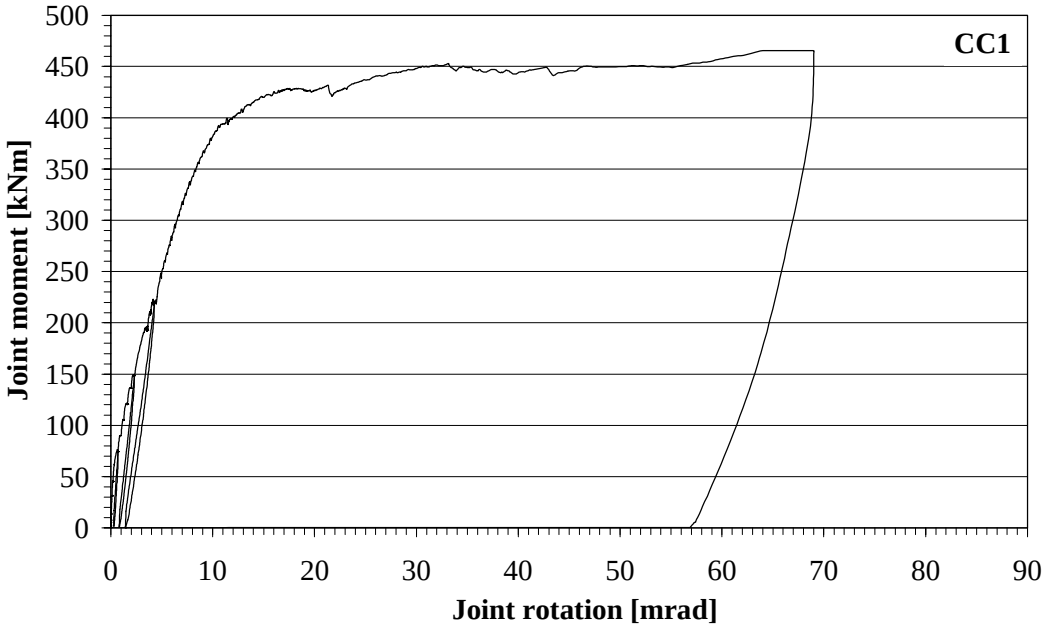

Figure II.3 Measured moment-rotation ($M_{j,exp}$-$\phi_{j,exp}$) curve for specimen CC1.

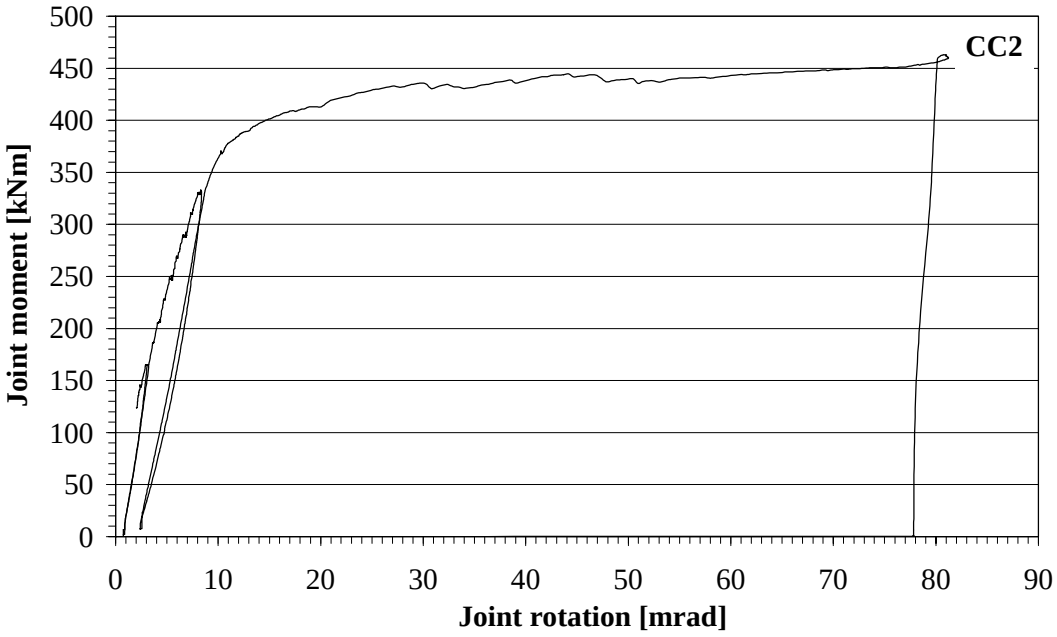

Figure II.4 Measured moment-rotation ($M_{j,exp}$-$\phi_{j,exp}$) curve for specimen CC2.

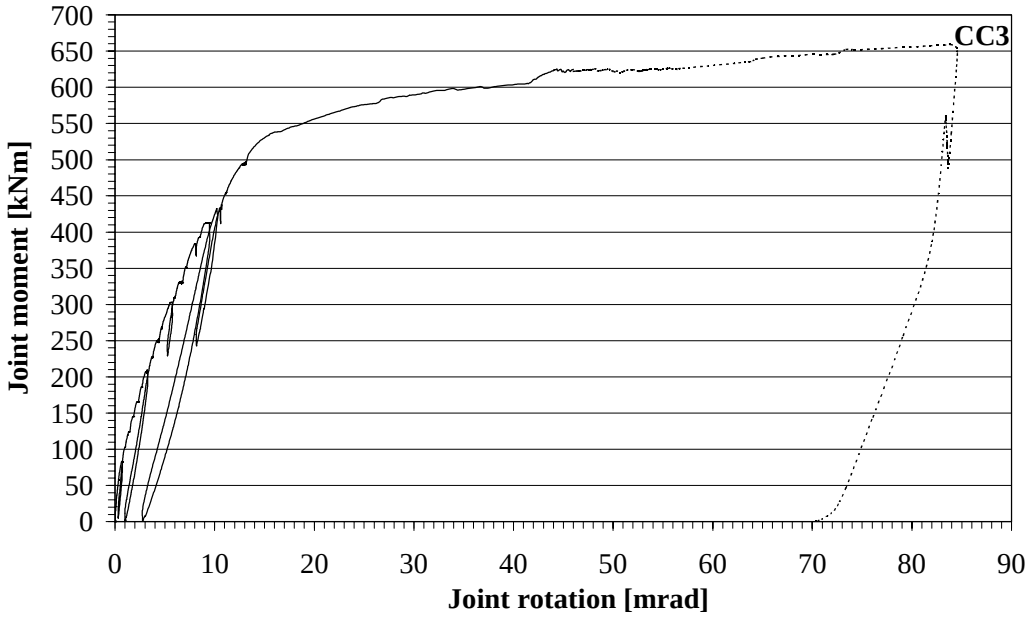

Figure II.5 Measured moment-rotation ($M_{j,exp}$-$\phi_{j,exp}$) curve for specimen CC3.

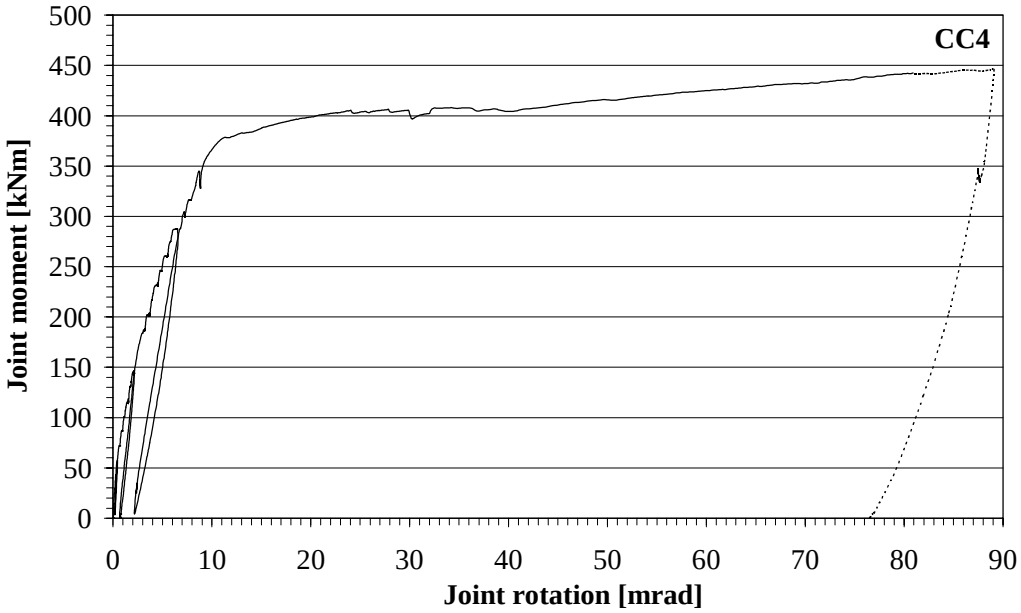

Figure II.6 Measured moment-rotation ($M_{j,exp}$-$\phi_{j,exp}$) curve for specimen CC4.

APPENDIX III

MEASURED REINFORCEMENT STRAINS

Electrical strain gauges were used to monitor the variation in stress distribution in the longitudinal reinforcing bars during testing. Sixteen strain gauges were placed on the innermost and outermost bars at four sections, as indicated in Fig. III.1. The four sections selected (A,B,C and D) are: the column centre-line and the cross-sections at 175 mm, 332 mm and 482 mm apart from it.

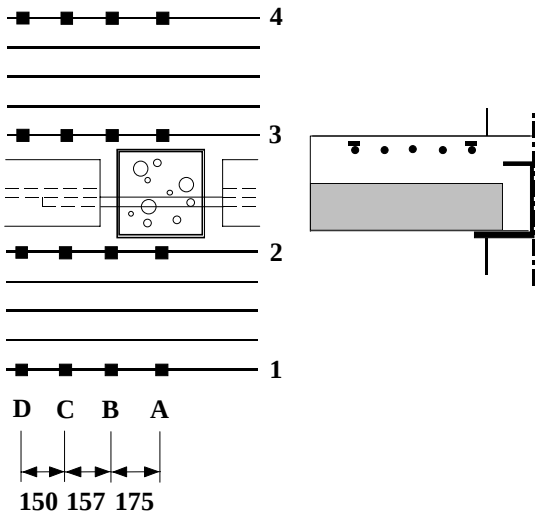

Figure III.1 Strain gauges on reinforcing bars.

In Figs. III.2 to III.5, the average strains on the beam sections are presented with respect to the joint moment. The results indicate that reinforcement yields first on section B in the specimens CC1, CC2 and CC3 and on section A in specimen CC4. The strains in the reinforcement on these first yielded beam sections are presented with respect to the joit moment in Figs. III.6 to III.9. The joint moment when all the reinforcing bars in the slab section are plastic is assumed to define the threshold of the inelastic stage of the joint, i.e. it is the plastic moment capacity $M_{j,Rd}$ of the joint. The joint rotations measured at $M_{j,Rd}$

can be measured from Figs. III.10 to III.13. The plastic moment capacities and the corresponding joint rotation values measured are given in Table III.1.

TABLE III.1
PLASTIC MOMENT CAPACITIES OF THE JOINTS

Specimen	CC1	CC2	CC3	CC4
Plastic moment capacity $M_{j,Rd}$ [kNm]	375	347	489	371
Joint rotation $\phi_{j,Xd}$ [mrad] at $M_{j,Rd}$	9,5	9,0	12,0	10,5

In Figs. III.14 to III.17, the average strains on the beam sections are presented with respect to the joint rotation. In all the specimens, the yielding of the reinforcement spreaded over the sections A to C when the plastic moment capacity $M_{j,Rd}$ was reached.

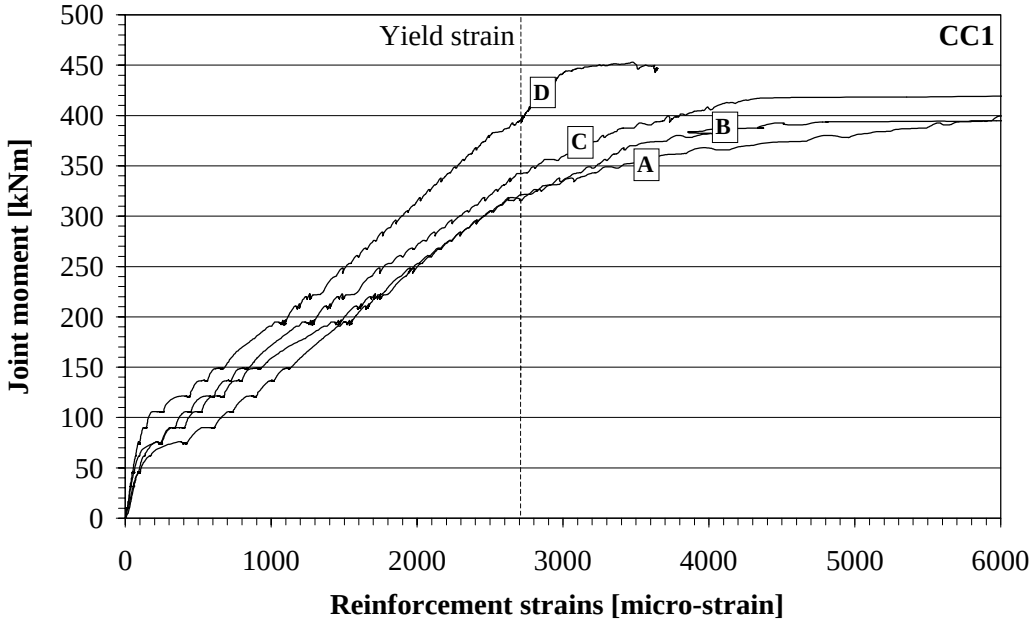

Figure III.2 Average reinforcement strains with respect to joint moment in specimen CC1.

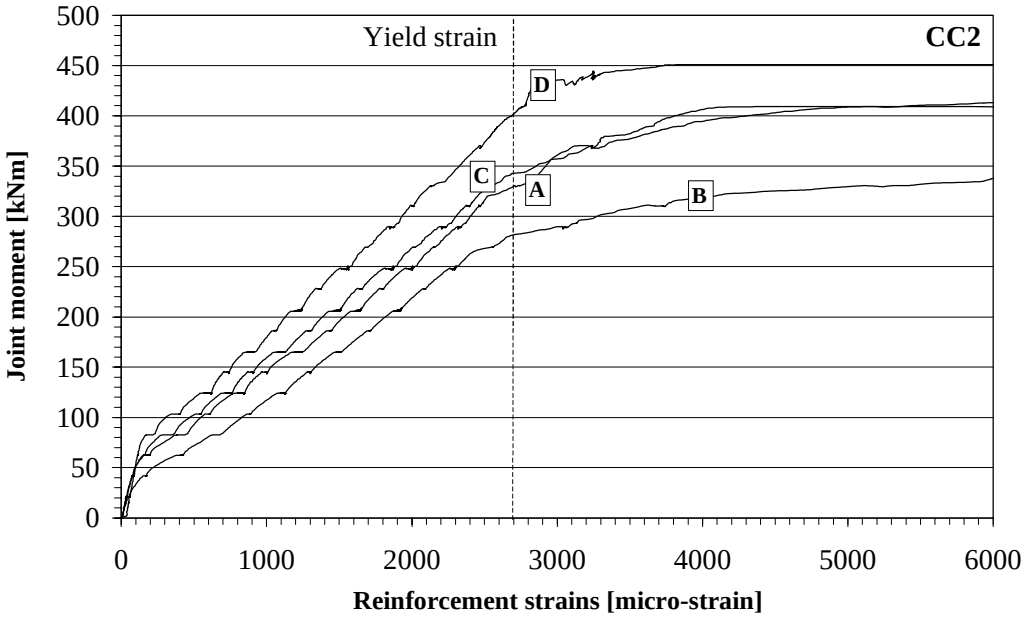

Figure III.3 Average reinforcement strains with respect to joint moment in specimen CC2.

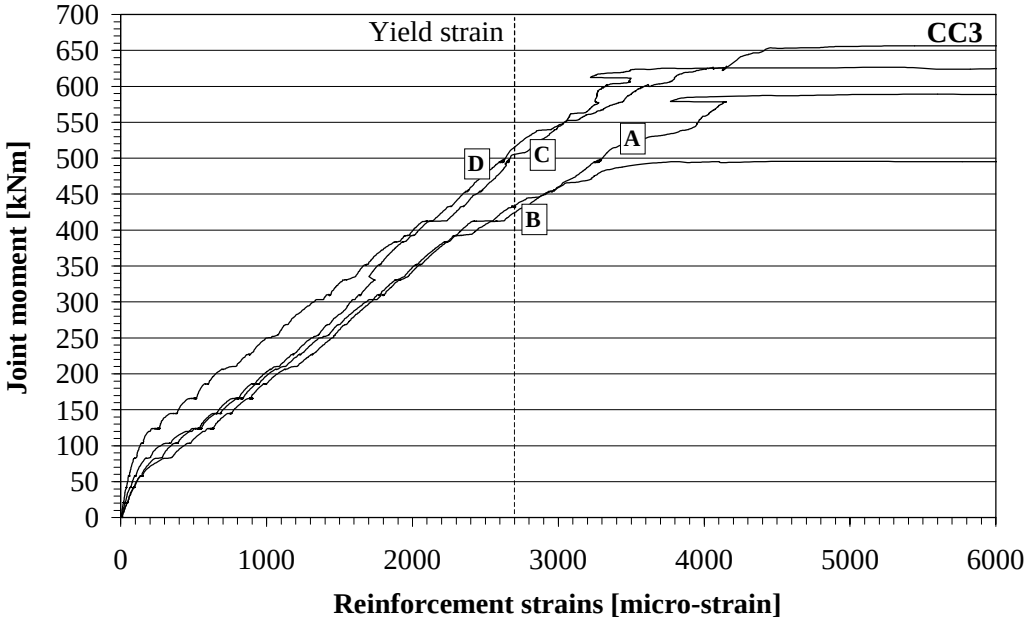

Figure III.4 Average reinforcement strains with respect to joint moment in specimen CC3.

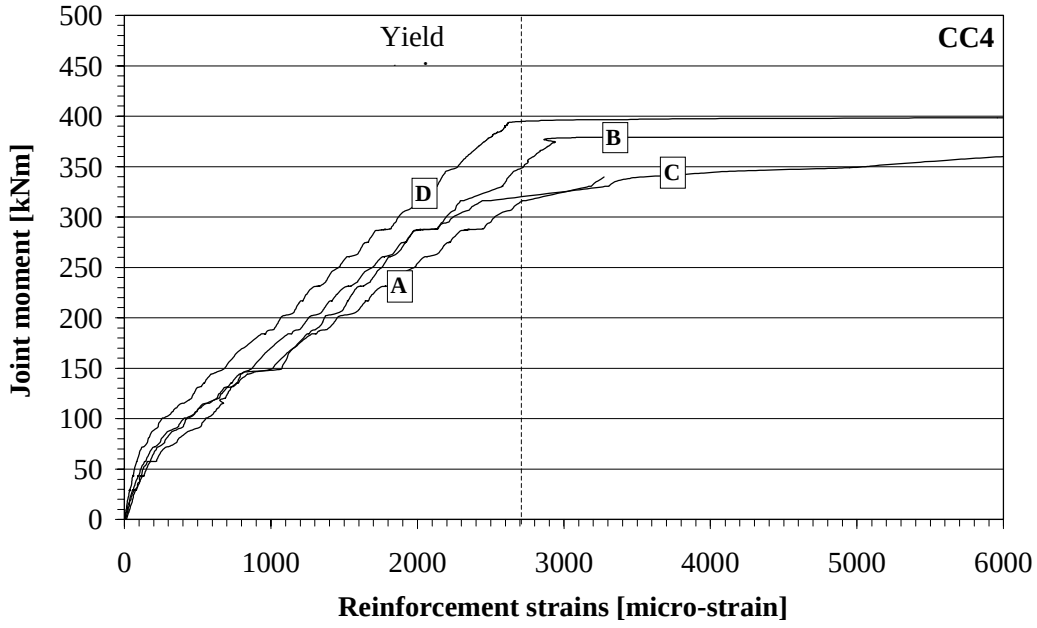

Figure III.5 Average reinforcement strains with respect to joint moment in specimen CC4.

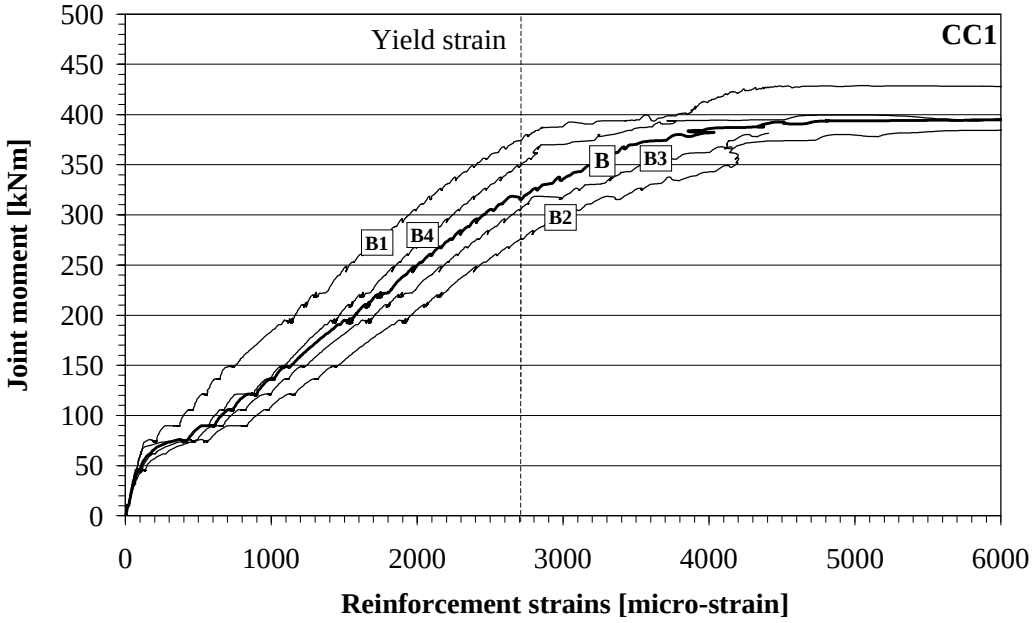

Figure III.6 Reinforcement strains with respect to joint moment in section B in specimen CC1.

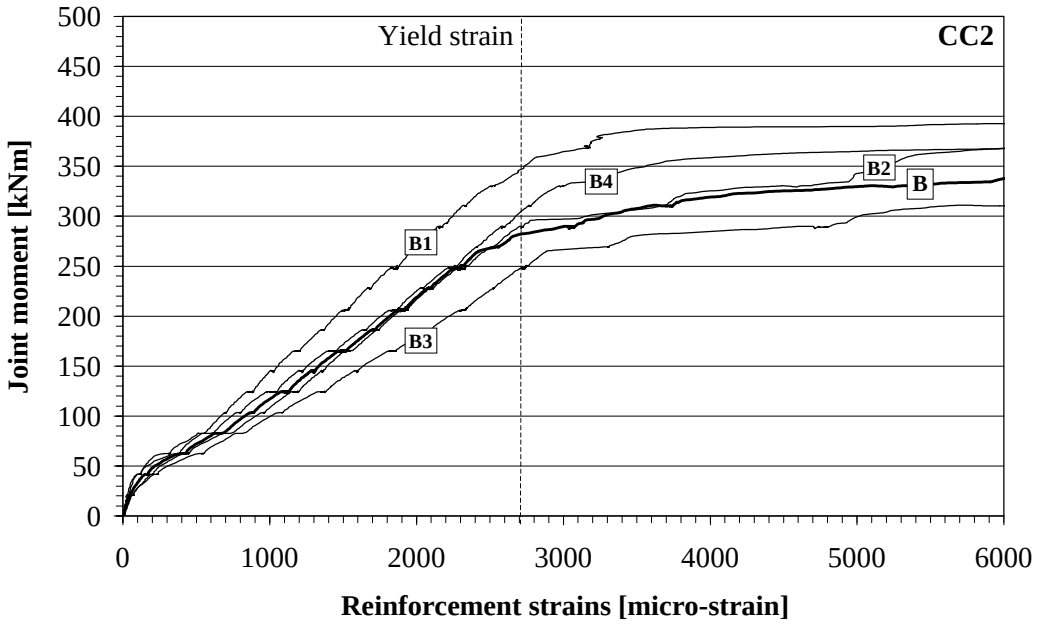

Figure III.7 Reinforcement strains with respect to joint moment in section B in specimen CC2.

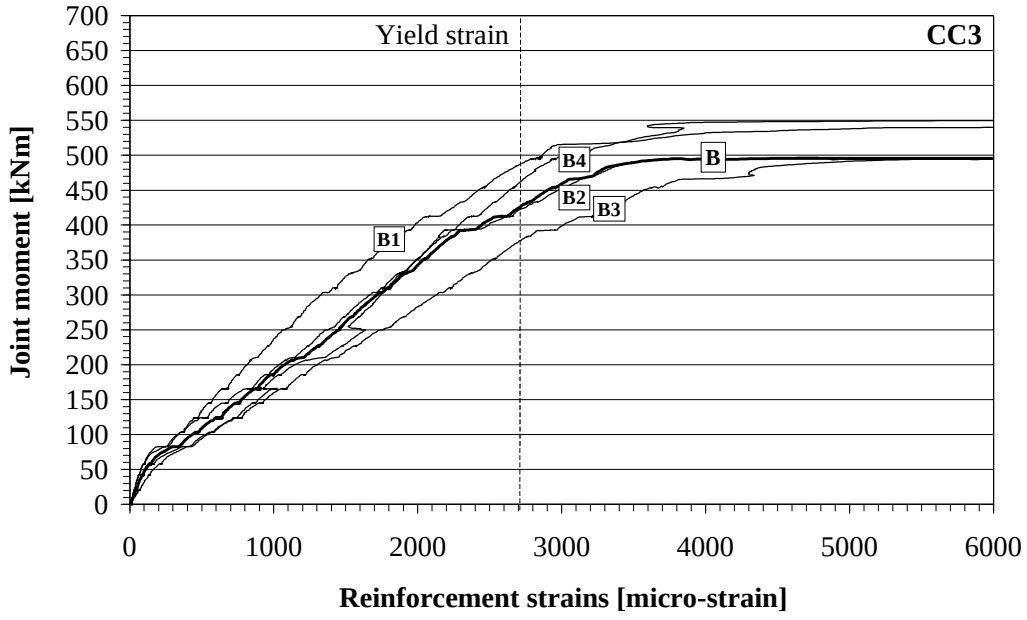

Figure III.8 Reinforcement strains with respect to joint moment in section B in specimen CC3.

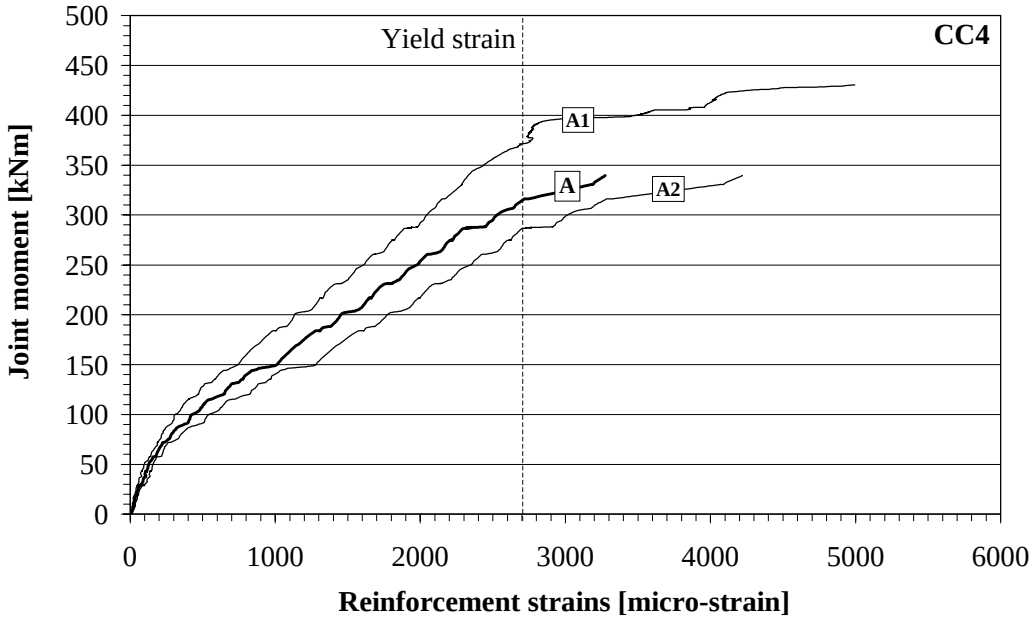

Figure III.9 Reinforcement strains with respect to joint moment in section A in specimen CC4.

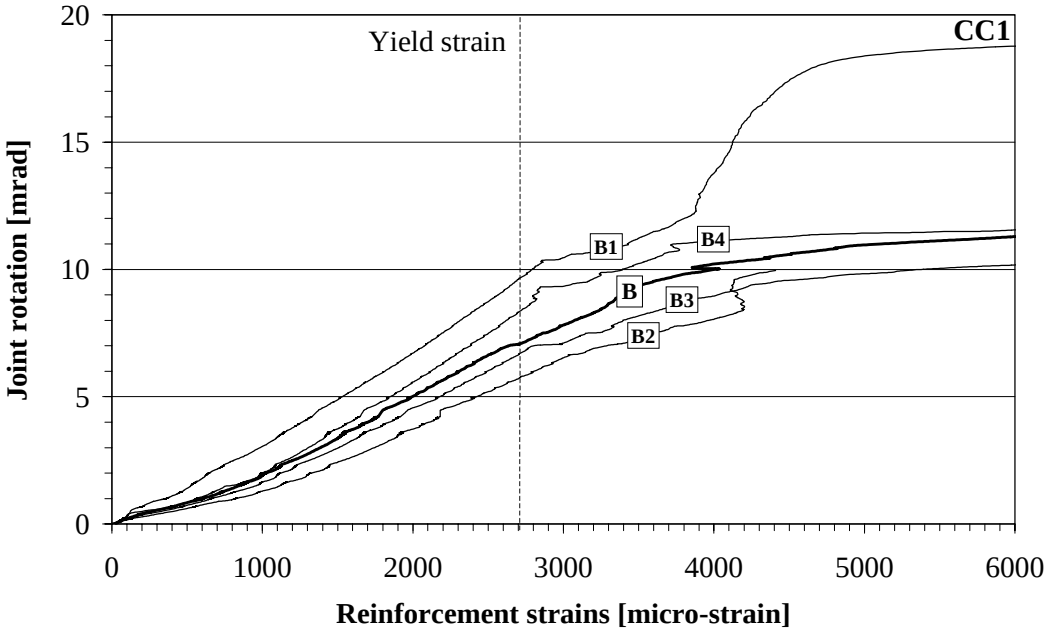

Figure III.10 Reinforcement strains with respect to joint rotation in section B in specimen CC1.

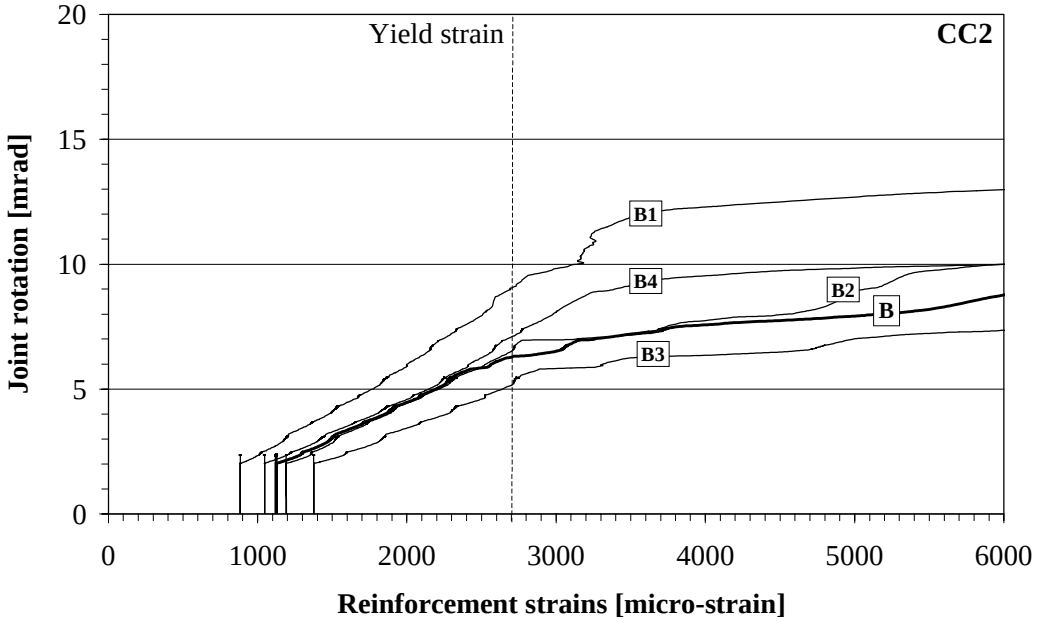

Figure III.11 Reinforcement strains with respect to joint rotation in section B in specimen CC2.

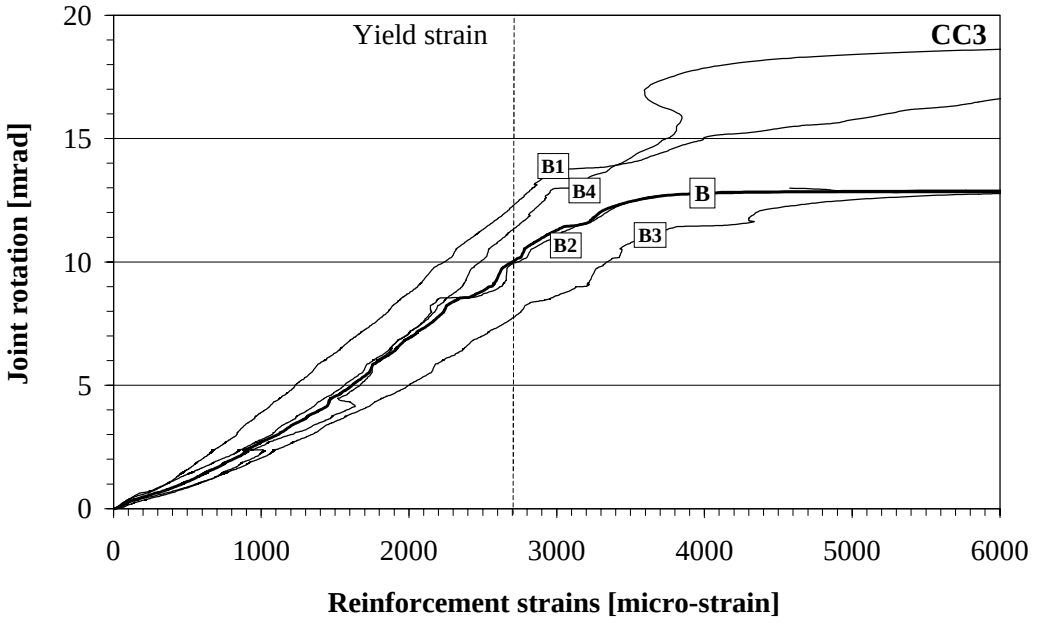

Figure III.12 Reinforcement strains with respect to joint rotation in section B in specimen CC3.

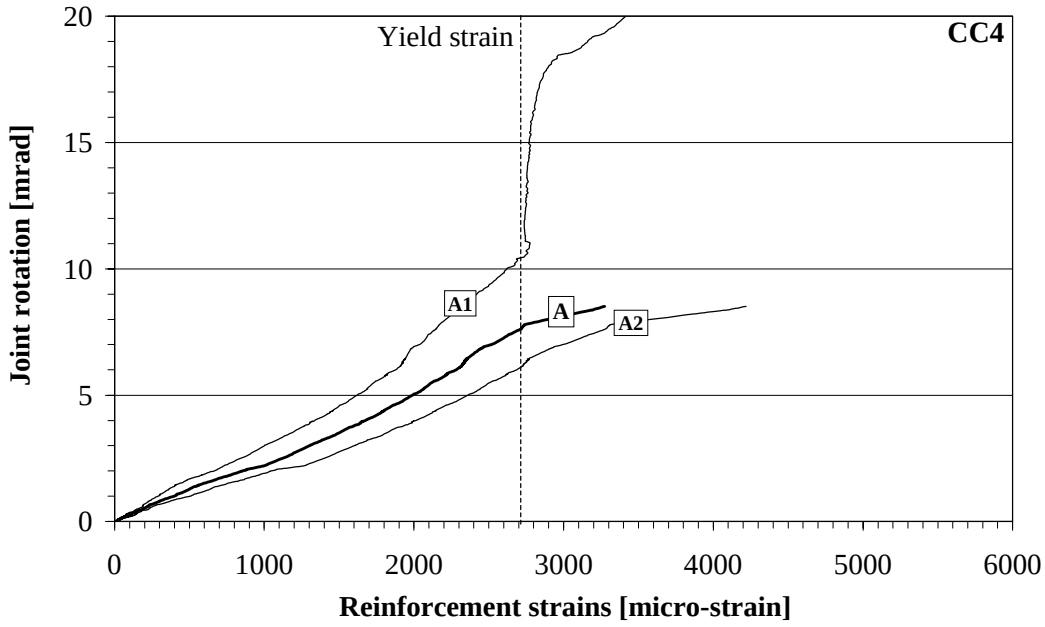

Figure III.13 Reinforcement strains with respect to joint rotation in section A in specimen CC4.

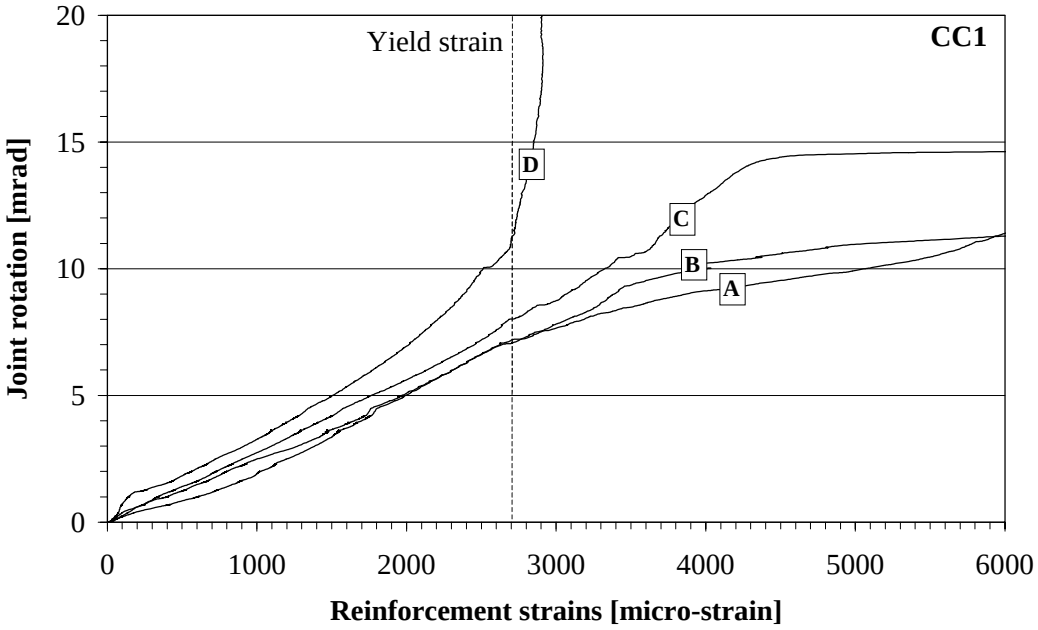

Figure III.14 Average reinforcement strains with respect to joint rotation in specimen CC1.

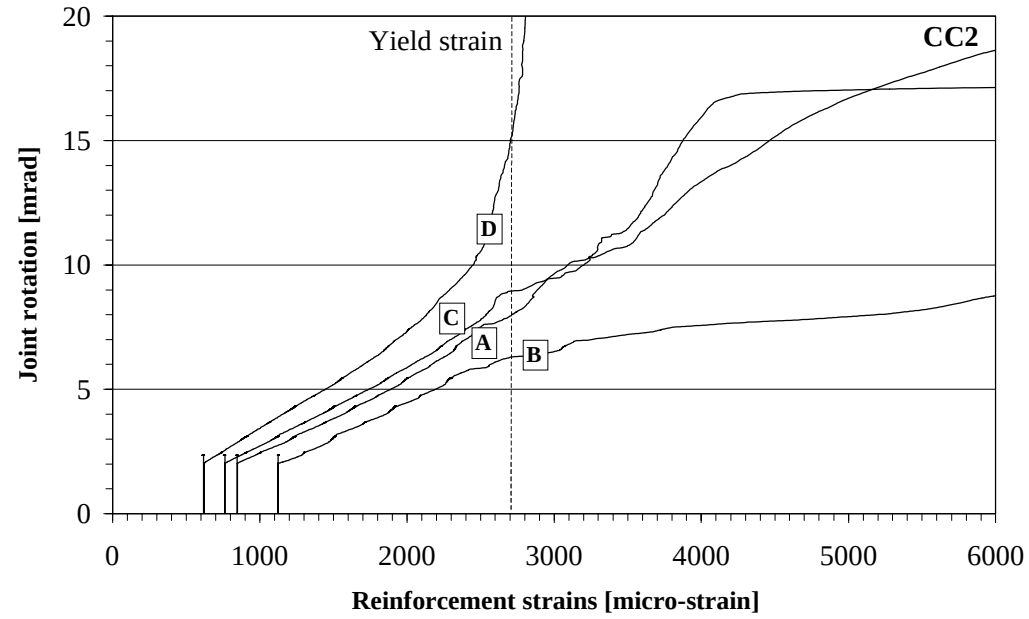

Figure III.15 Average reinforcement strains with respect to joint rotation in specimen CC2.

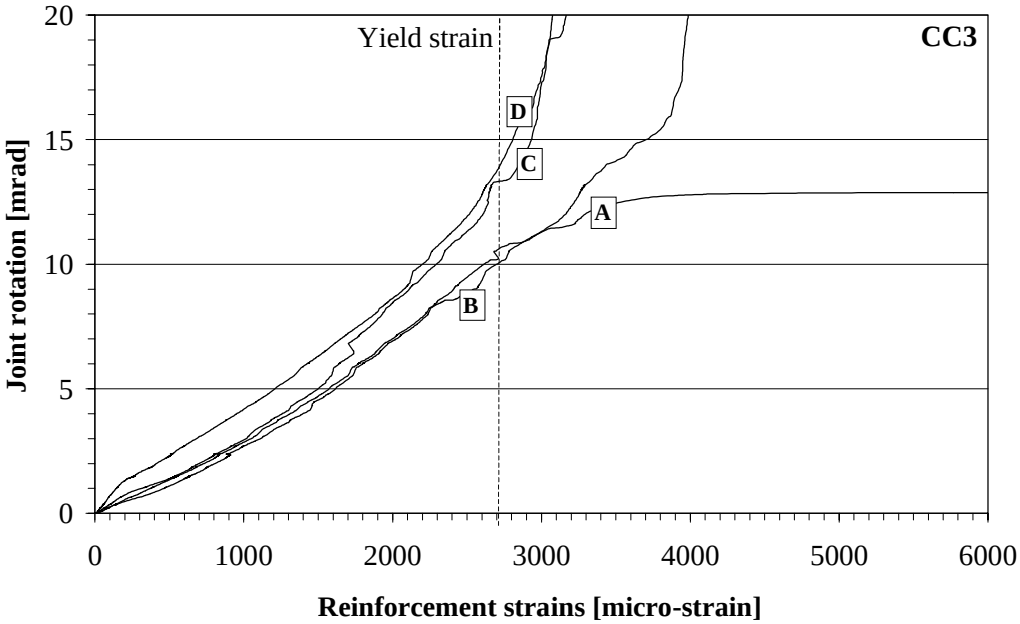

Figure III.16 Average reinforcement strains with respect to joint rotation in specimen CC3.

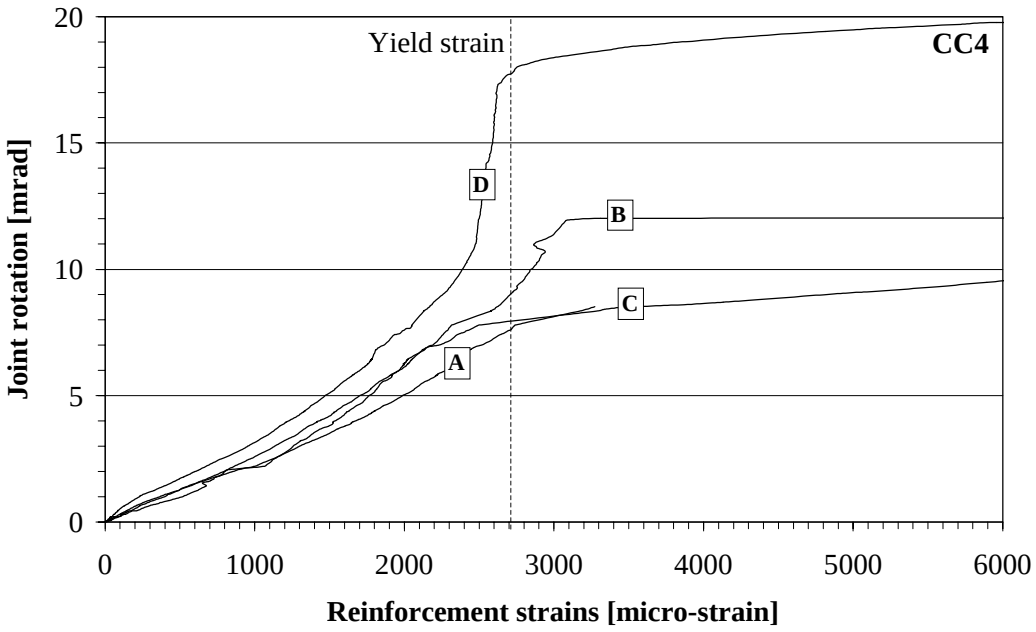

Figure III.17 Average reinforcement strains with respect to joint rotation in specimen CC4.

MEASURED STRAINS IN THE SHEAR FLAT

Strain gauge rosettes (gauges g1 and g2) and strain gauges (gauges g3 and g4) were used in order to resolve the strain state in the shear flat, see Fig. IV.1. The strains were measured only one side of the shear flat.

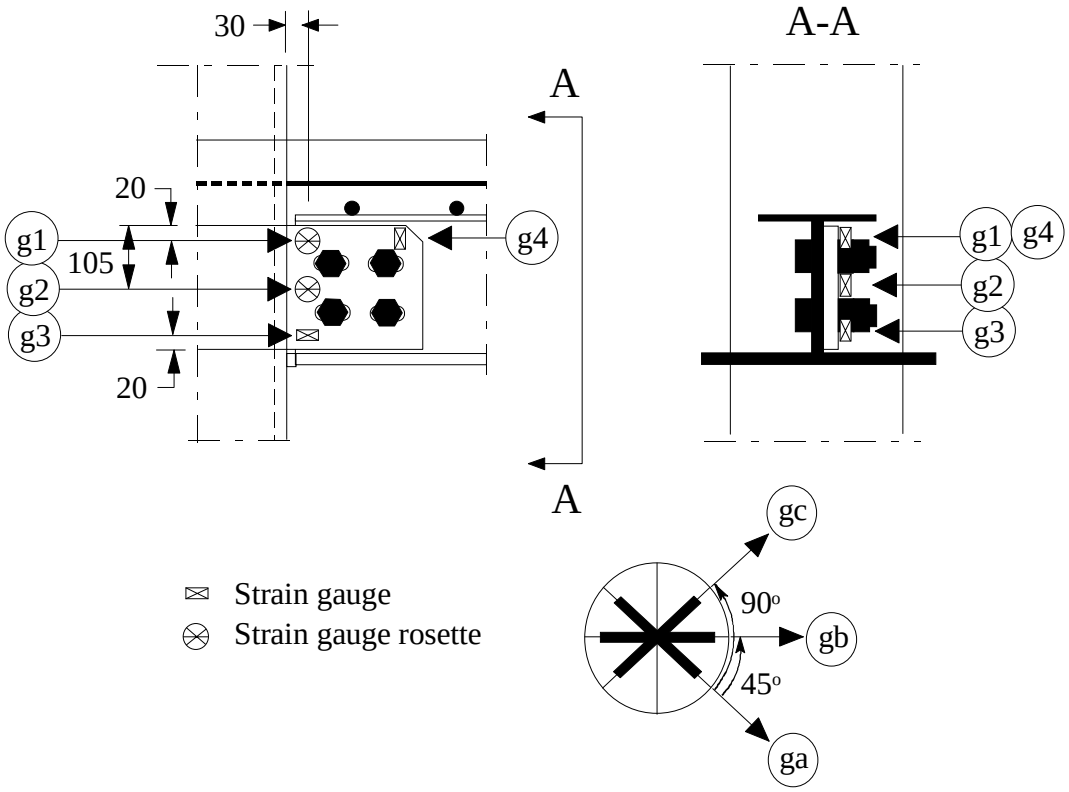

Figure IV.1 Strain gauges on the shear flat.

The principal strains in the shear flat were calculated from the strains in the rosette gauges. In the rectangular strain gauge rosette used in the tests, the orientations for gauges ga, gb and gc are 45°, as shown in Fig. IV.1. If ε_{ga}, ε_{gb} and ε_{gc}, are known, the principal strains $\varepsilon_{g\text{-}max}$, and $\varepsilon_{g\text{-}min}$, can be obtained from the following equation (Harris & Sabnis, 1999):

APPENDIX IV

$$\varepsilon_{g-max,g-min} = \frac{\varepsilon_{ga} + \varepsilon_{gc}}{2} \pm \frac{1}{2}\sqrt{\left(\varepsilon_{ga} - \varepsilon_{gc}\right)^2 + \left[2\varepsilon_{gb} - \left(\varepsilon_{ga} + \varepsilon_{gc}\right)\right]^2} \,. \qquad \text{(IV.1)}$$

In Figs. IV.2 to IV.5, the principal strains, calculated from the strains in the rosette gauges g1 and g2, are shown plotted with respect to the joint rotations. The strain components ε_{ga}, ε_{gb} and ε_{gc}, measured by the strain gauge rosettes g1 and g2, are plotted with respect to the joint moments in Figs. IV.6 to IV.9. The same strain components with respect to the joint rotations are plotted in Figs. IV.10 to IV.13. In Fig. IV.14, the horizontal strain measured by the strain gauge g3 in the specimen CC4 is plotted with respect to the joint rotation. Strain gauge g4 was used in order to obtain the contact between the corner of the bevel in the shear flat and the top flange or the fillet weld seam of the steel beam. The measured strain is given in Fig. IV.15.

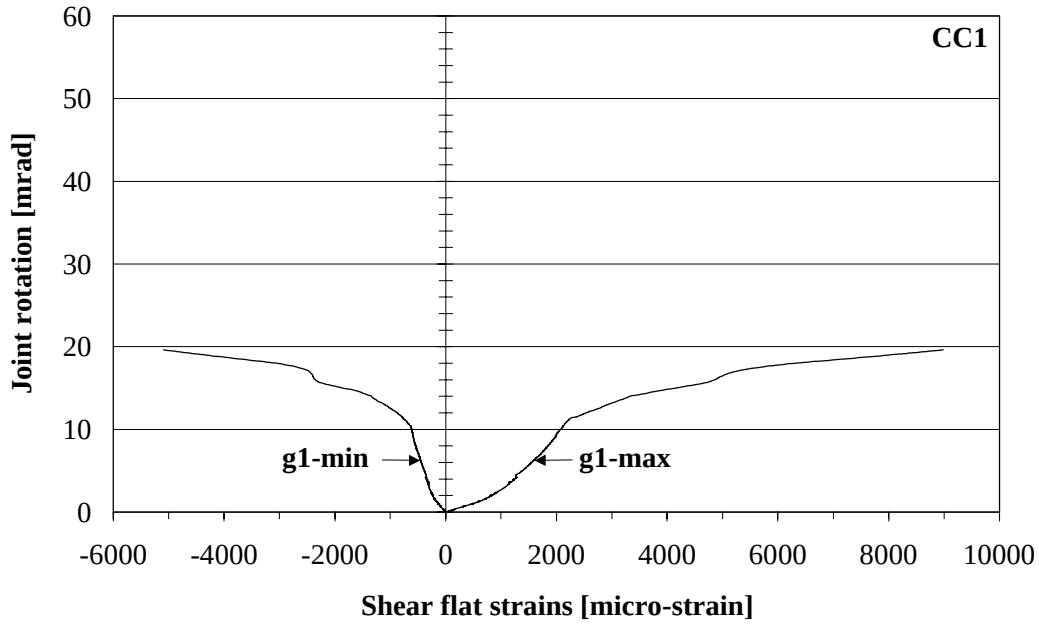

Figure IV.2 Principal strains in the shear flat calculated from strains in the rosette gauge g1 (specimen CC1).

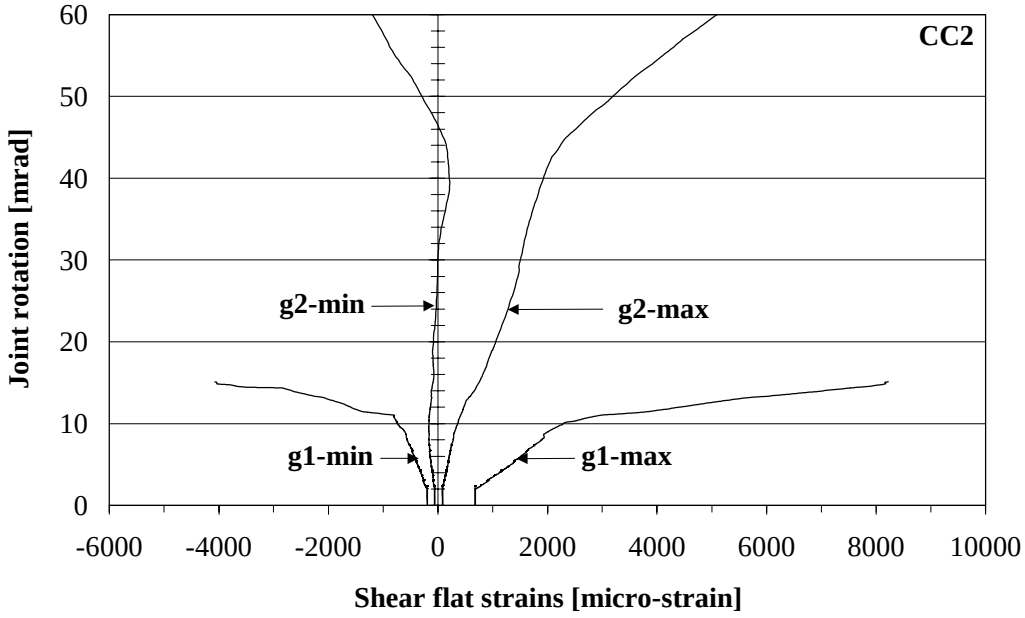

Figure IV.3 Principal strains in the shear flat calculated from strains in the rosette gauges g1 and g2 (specimen CC2).

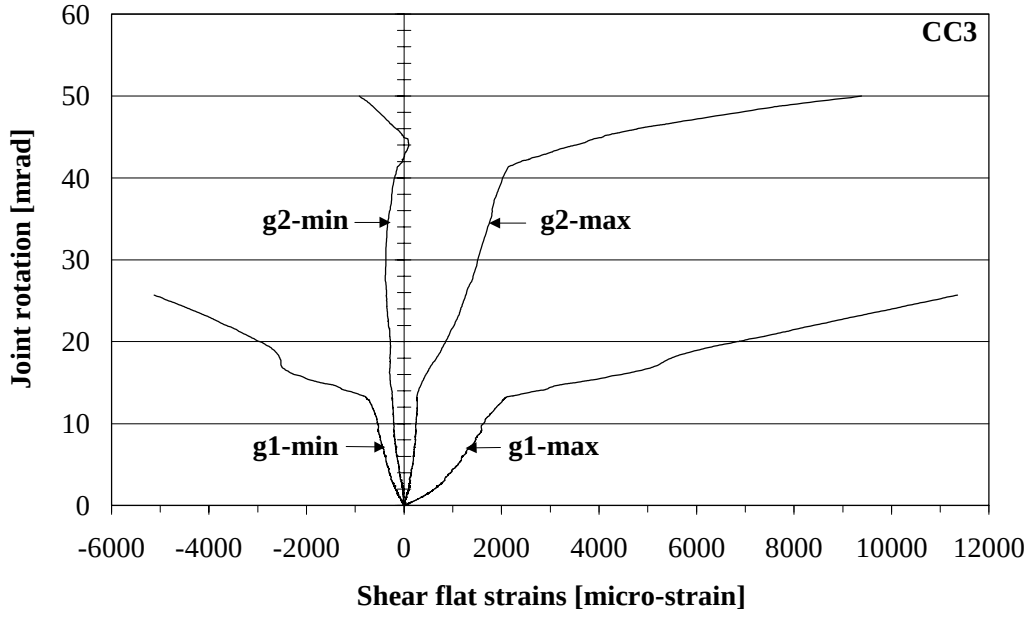

Figure IV.4 Principal strains in the shear flat calculated from strains in the rosette gauges g1 and g2 (specimen CC3).

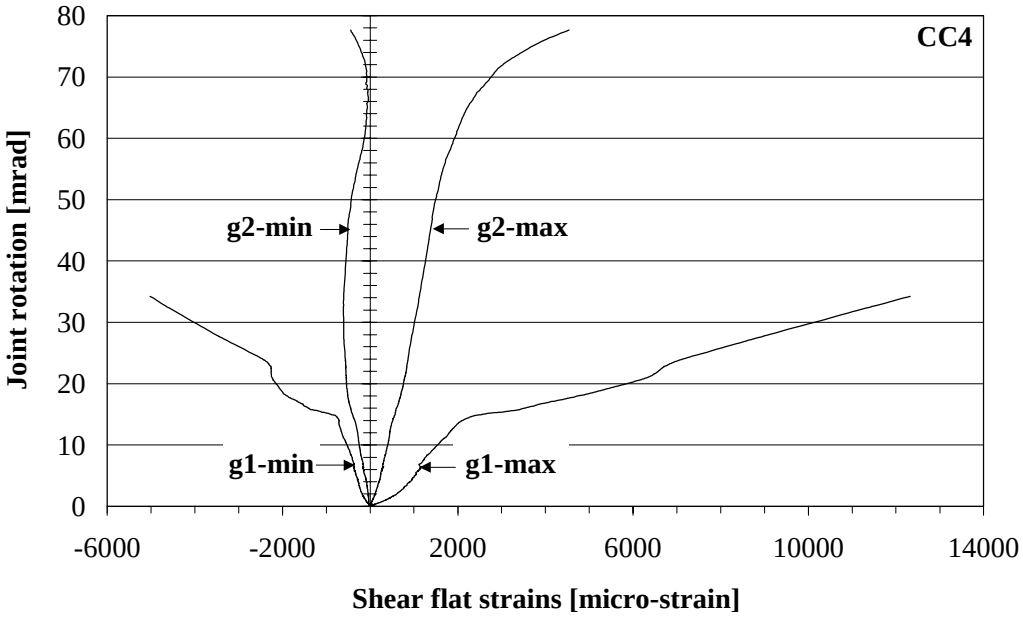

Figure IV.5 Principal strains in the shear flat calculated from strains in the rosette gauges g1 and g2 (specimen CC4).

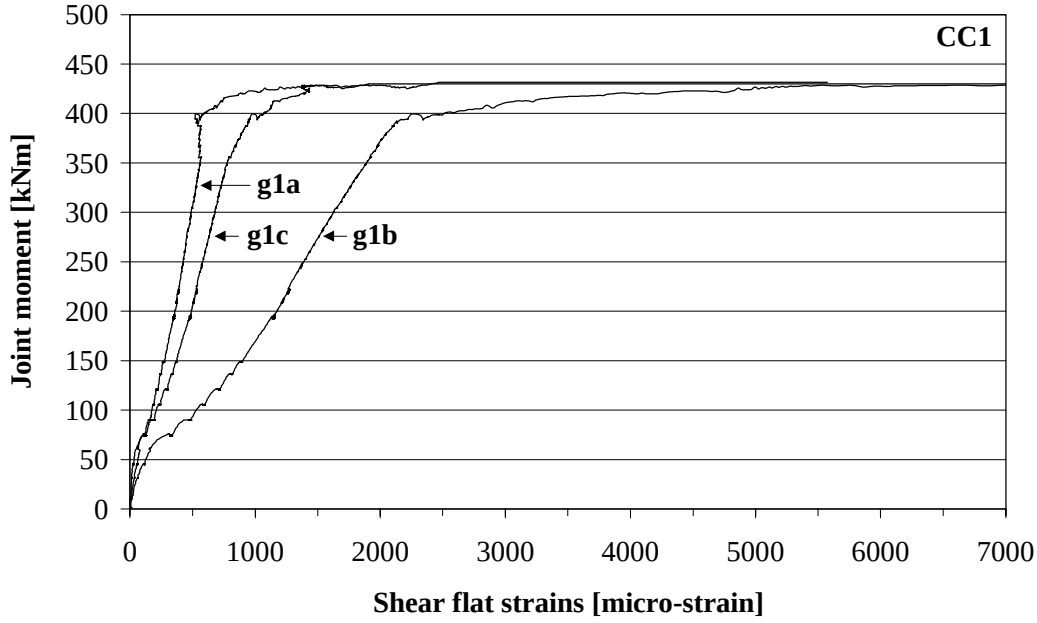

Figure IV.6 Strains in the shear flat measured by the strain gauge rosette g1 (specimen CC1).

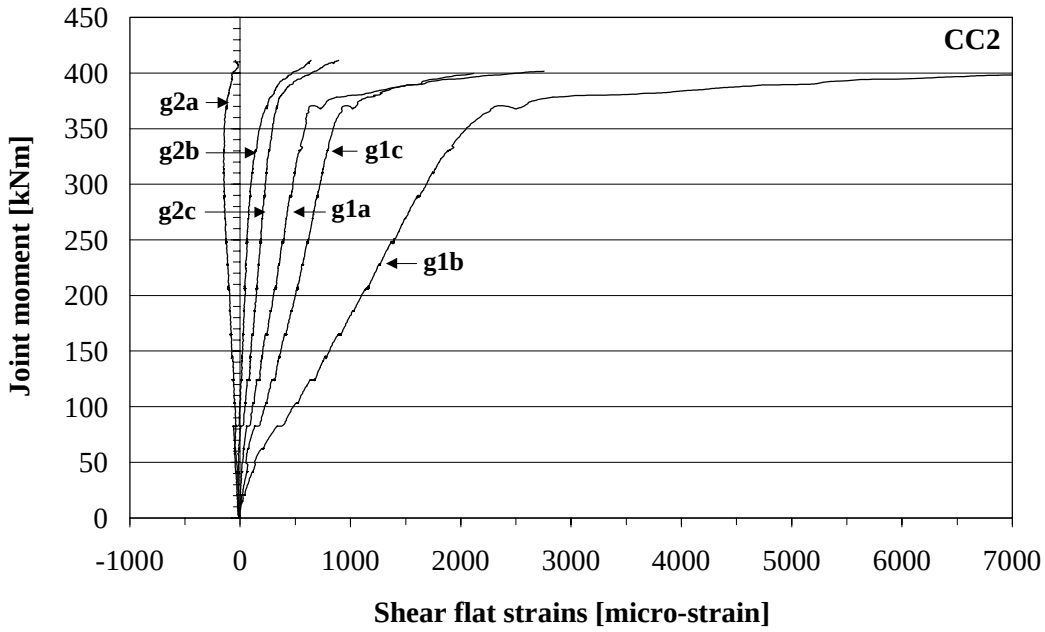

Figure IV.7 Strains in the shear flat measured by the strain gauge rosettes g1 and g2 (specimen CC2).

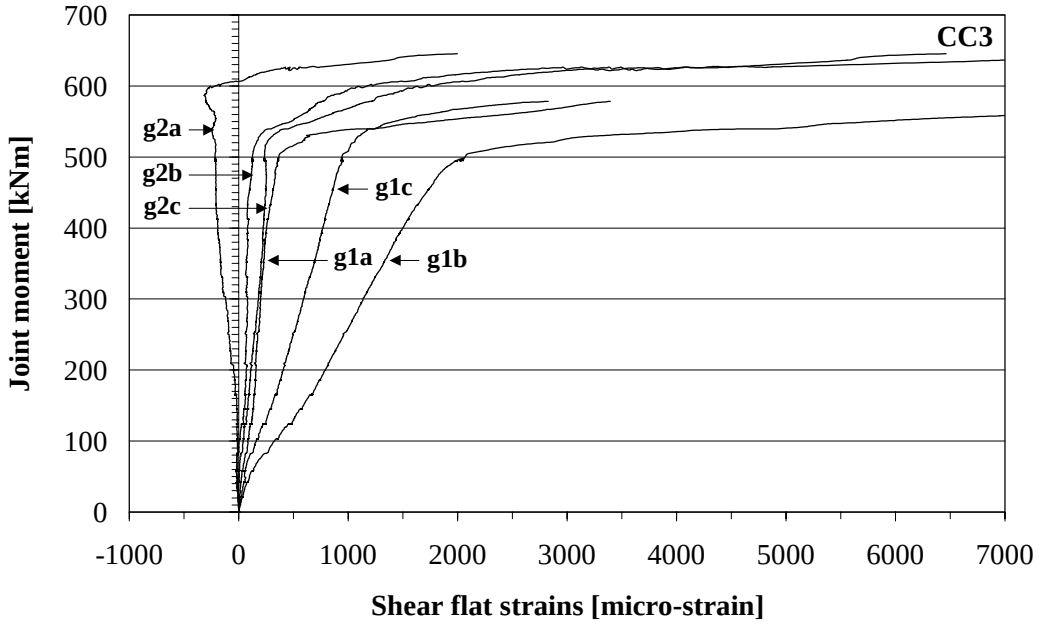

Figure IV.8 Strains in the shear flat measured by the strain gauge rosettes g1 and g2 (specimen CC3).

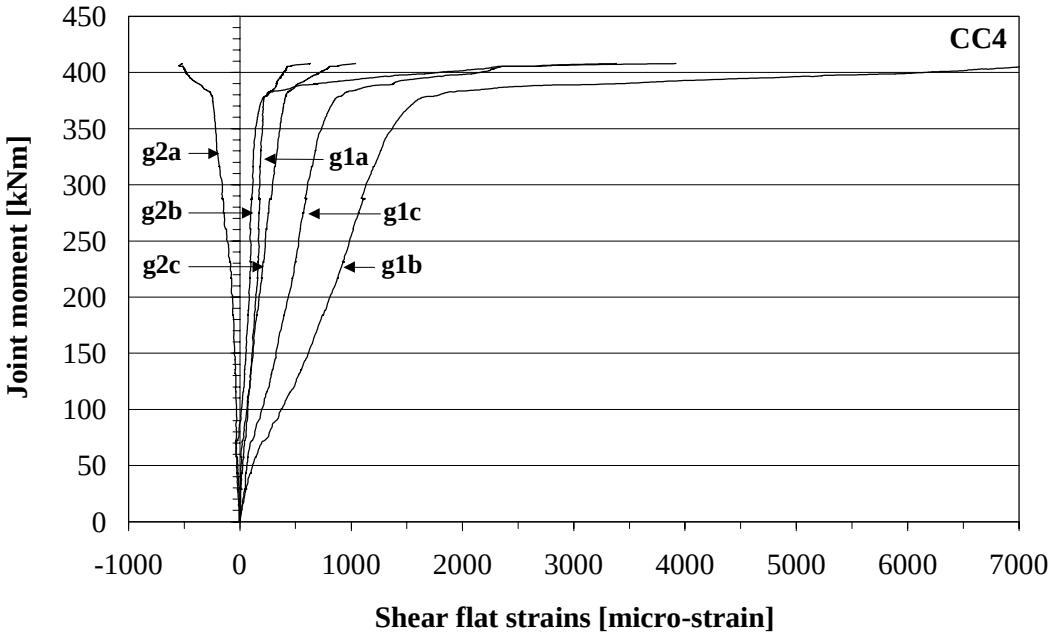

Figure IV.9 Strains in the shear flat measured by the strain gauge rosettes g1 and g2 (specimen CC4).

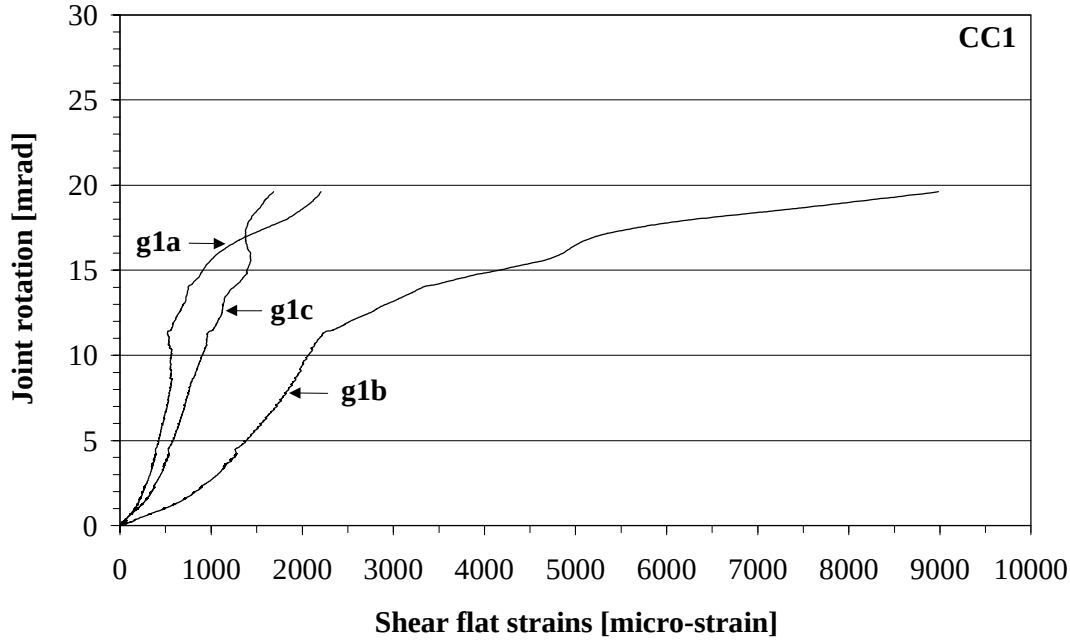

Figure IV.10 Strains in the shear flat measured by the strain gauge rosette g1 (specimen CC1).

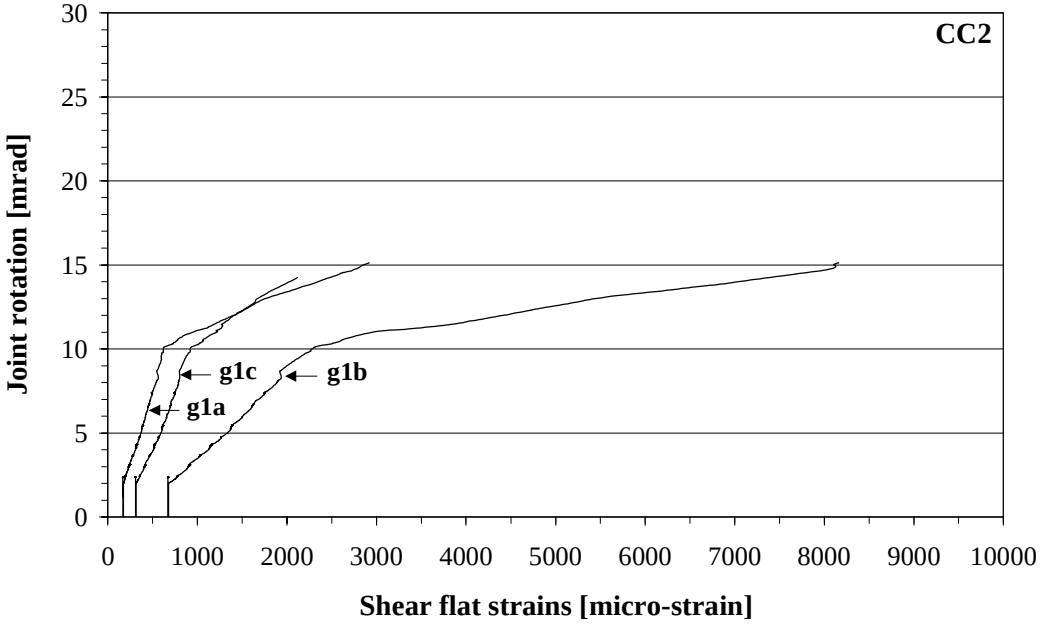

(a) Strains measured by the strain gauge rosette g1.

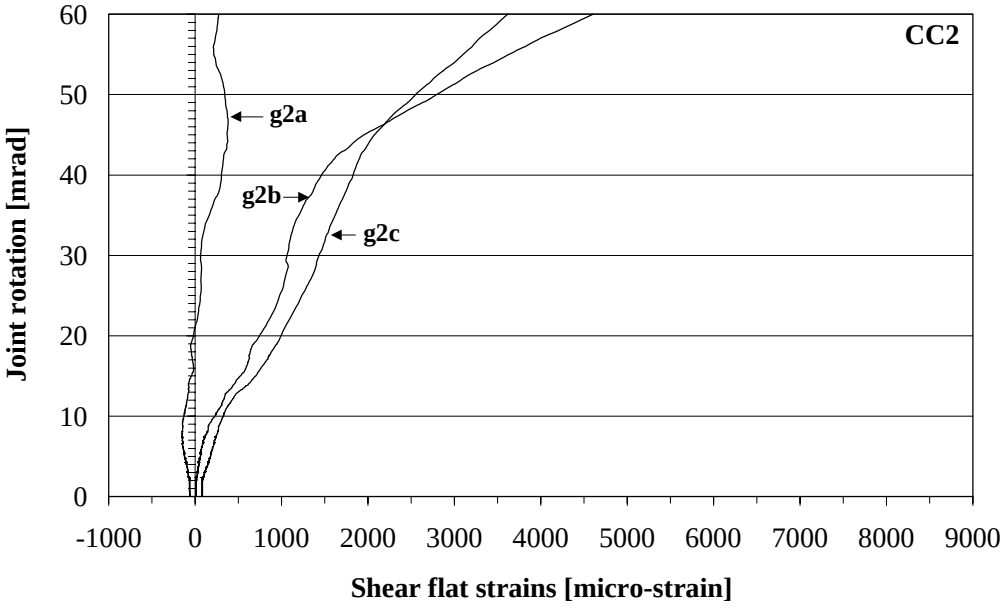

(b) Strains measured by the strain gauge rosette g2.

Figure IV.11 Strains in the shear flat (specimen CC2).

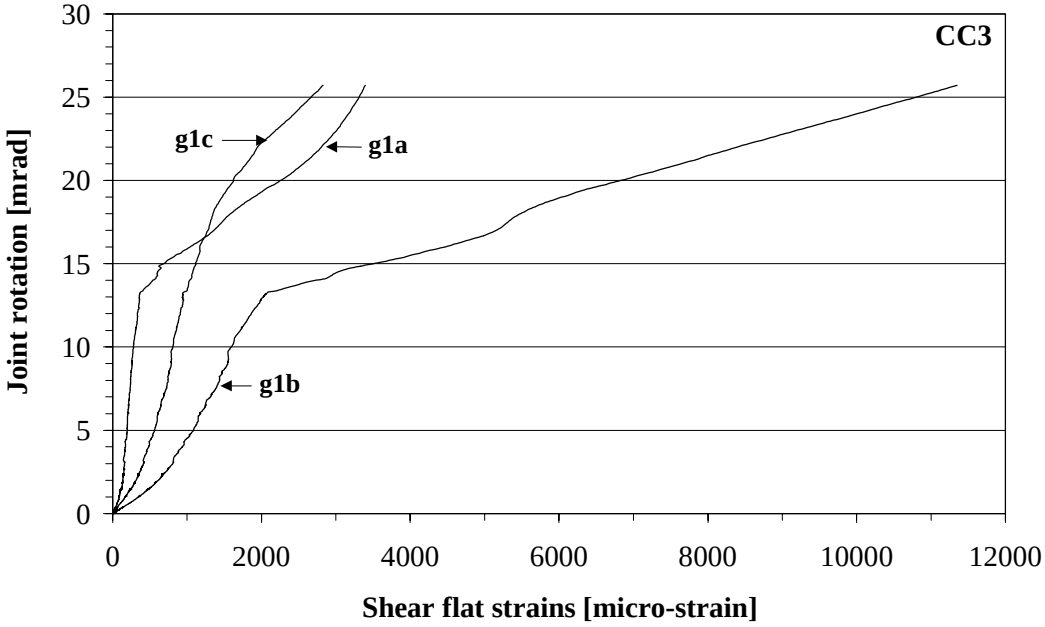

(a) Strains measured by the strain gauge rosette g1.

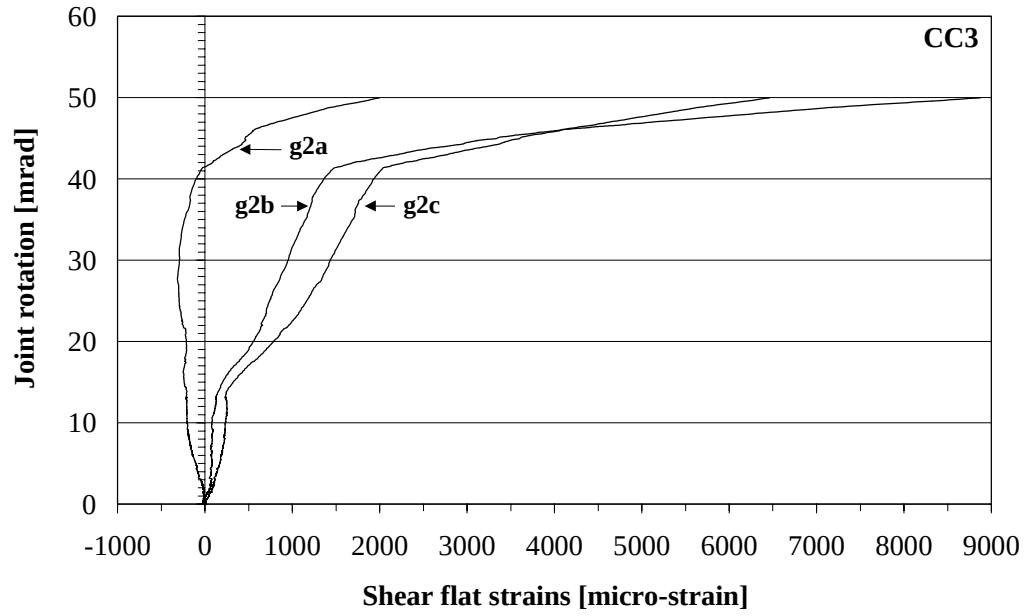

(b) Strains measured by the strain gauge rosette g2.

Figure IV.12 Strains in the shear flat (specimen CC3).

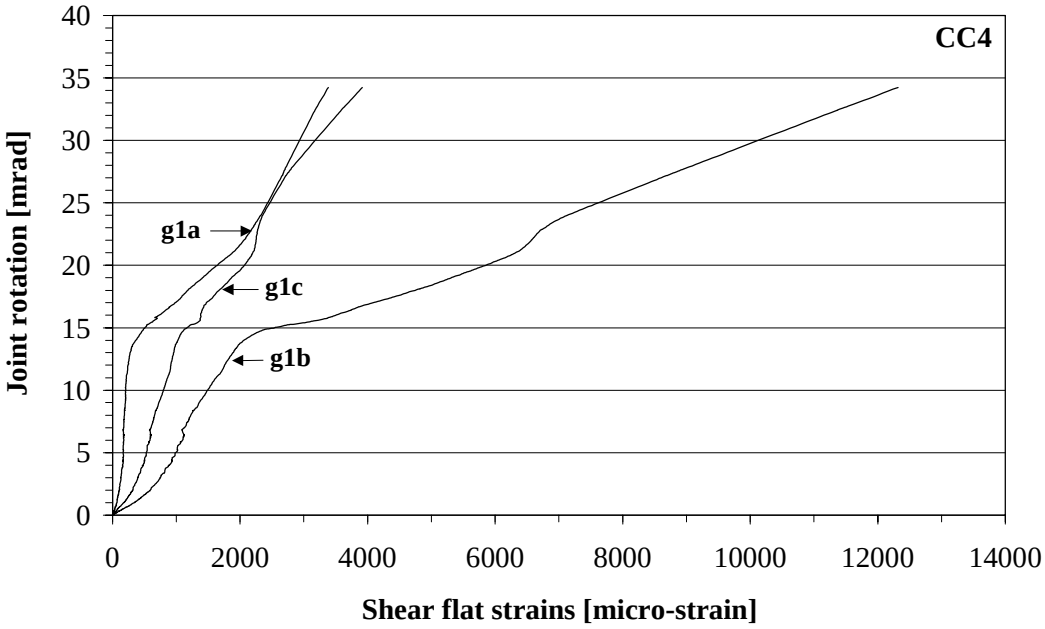

(a) Strains measured by the strain gauge rosette g1.

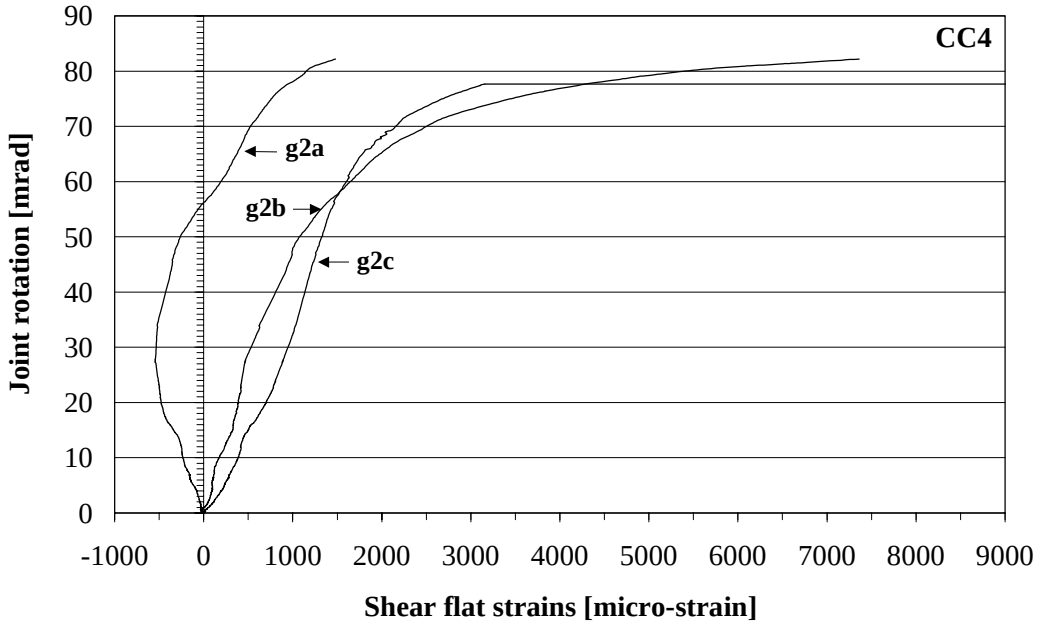

(b) Strains measured by the strain gauge rosette g2.

Figure IV.13 Strains in the shear flat (specimen CC4).

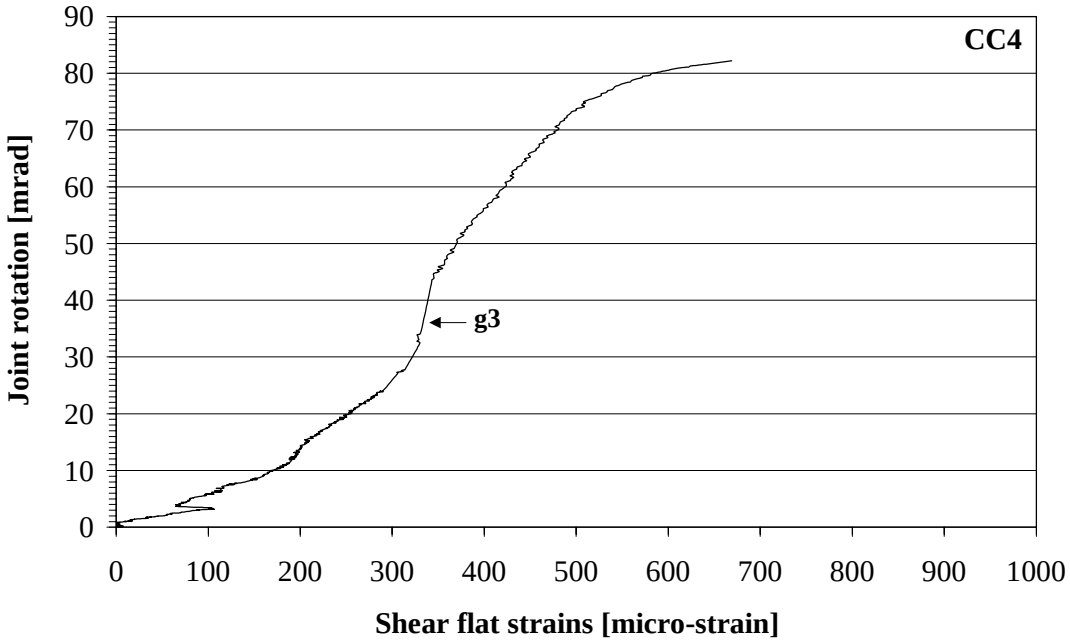

Figure IV.14 Horizontal strain measured by the strain gauge g3 in the specimen CC4.

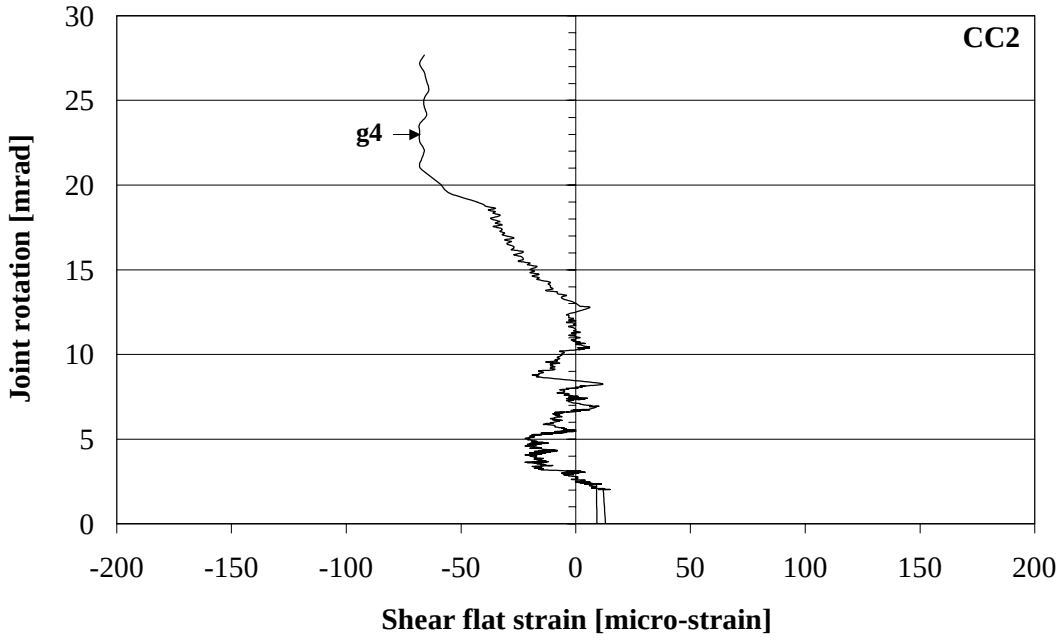

Figure IV.15 Vertical strain measured by the strain gauge g4 in the specimen CC2.

APPENDIX V

CALCULATION EXAMPLE

A calculation example of the composite joint used in test CC1 is presented so as to explain the use of the proposed calculation procedure to predict the moment-rotation characteristics of the joint response. The values predicted are based on real dimensions and strengths and partial safety factors equal to unity. No slip was observed in the tests and thus it is also ignored in the values. The dimensions of the steel beam section are given in Fig. 3.1. Calculations are done excluding the mesh reinforcement.

$A_a = 13800$ mm^2 Cross-sectional area of the steel beam.

$y_a = 85.7$ mm Vertical distance between the centroid and the bottom surface of the steel beam section.

$E_a = 212567$ N/mm^2 Elasticity modulus of the steel beam flange.

$f_{ck,K150} = 46.8$ N/mm^2 Measured concrete cube strength.

$f_{ck,C150} = 39.8$ N/mm^2 Cylinder strength of concrete ($f_{ck,C150} = 0.85\ f_{ck,K150}$).

$f_{ctm} = 3.8$ N/mm^2 Tensile strength of concrete ($f_{ctm}=0.33\text{MPa}\cdot (f_{ck,C150}/1\text{MPa})^{2/3}$).

$E_c = 34473$ N/mm^2 Elasticity modulus of concrete ($E_c=9500\text{MPa}(f_{ck,C150}/1\text{Mpa}+8)^{1/3}$).

Longitudinal reinforcement: 10 bars ϕ 16 mm

$A_s = 2011$ mm^2 Cross-sectional area of the reinforcement.

$E_s = 205437$ N/mm^2 Modulus of elasticity of the reinforcement.

$f_{ys} = 575$ N/mm^2 Yield stress of the reinforcement.

$\varepsilon_{ys} = 0.0028$ Yield strain of the reinforcement.

$\varepsilon_{us} = 0.117$ Ultimate strain of the reinforcement.

$D_b = 258$ mm Height of the steel beam.

$D_s = 20$ mm Distance between the centroid of the reinforcement and the upper layer of the steel beam.

$D_c = 300$ mm Column width.

$a = 115$ mm Position of the first shear connector.

$b_{eff} = 1500$ mm Effective breadth of the concrete slab.

$h_{cs} = 183$ mm Depth of the solid concrete slab above the metal decking.

ROTATIONAL STIFFNESS

$L = D_c/2+a = 300/2 + 115 = 265$ mm

$$S_{j,ini} = \frac{E_s A_s (D_b + D_s)^2}{L} = \frac{205437 \cdot 2011 \cdot (258+20)^2}{265} = 120.5 \text{ kNm/rad}$$

$$S_j = \frac{S_{j,ini}}{\eta} = \frac{120.5}{4.5} = 26.8 \text{ kNm/rad}$$

MOMENT RESISTANCE

$D = 258 – 0.5 \cdot 18 = 249$ mm

$M_{j,Rd} = A_s f_{sy}(D+D_s) = 2011 \cdot 575 \cdot (249 + 20) = 311.0$ kNm

ROTATION CAPACITY

$A_c = (b_{eff}-b_c)h_{cs} = (1500-300) \cdot 183 = 219600$ mm^2

$$\rho = \frac{A_s}{A_c} = \frac{2011}{219600} = 0.0092$$

Centroid of the uncracked unreinforced concrete flange:

$y_{cs} = 18 + 117 + 0.5 \cdot 183 = 226.5$ mm

APPENDIX V

3(4)

Centroid of the uncracked unreinforced composite section:

$$y_{comp} = \frac{A_a y_a + \frac{E_c}{E_a} A_c y_{cs}}{A_a + \frac{E_c}{E_a} A_c} = \frac{13800 \cdot 85.7 + \frac{34473}{212567} \cdot 219600 \cdot 226.5}{13800 + \frac{34473}{212567} \cdot 219600} = 187.2 \text{ mm}$$

$z_0 = y_{cs} - y_{comp} = 226.5 - 187.2 = 39.3$ mm

$$k_c = \frac{1}{1 + \frac{h_{cs}}{2z_0}} = \frac{1}{1 + \frac{183}{2 \cdot 39.3}} = 0.3006$$

$$\sigma_{sr1} = \frac{f_{ctm} k_c}{\rho} \left[1 + \rho \frac{E_s}{E_c} \right] = \frac{3.8 \cdot 0.3006}{0.0092} \left[1 + 0.0092 \frac{205437}{34473} \right] = 133.1 \text{ N/mm}^2$$

$$\Delta\varepsilon_{sr} = \frac{f_{ctm} k_c}{E_s \rho} = \frac{3.8 \cdot 0.3006}{205437 \cdot 0.0092} = 0.000615$$

$\beta_t = 0.4$

$\delta = 0.8$

$$\varepsilon_{smu} = \varepsilon_{sy} - \beta_t \Delta\varepsilon_{sr} + \delta \left(1 - \frac{\sigma_{sr1}}{f_{y,s}} \right) \left(\varepsilon_{su} - \varepsilon_{sy} \right)$$

$$= 0.0028 - 0.4 \cdot 0.000615 + +0.8 \cdot \left(1 - \frac{133}{575} \right) \cdot \left(0.117 - 0.0028 \right) = 0.07276$$

$$\tau_{sm} = 1.8 f_{ctm} = 1.8 \cdot 3.8 = 6.9 \text{ N/mm}^2$$

$$L_t = \frac{k_c f_{ctm} \phi}{4 \tau_{sm} \rho} = \frac{0.3006 \cdot 3.8 \cdot 16}{4 \cdot 6.9 \cdot 0.0092} = 73.0 \text{ mm}$$

$$\Delta_{u,s} = \left(\frac{h_c}{2} + L_t\right)\varepsilon_{smu} + (a - L_t)\varepsilon_{sy} = \left(\frac{300}{2} + 73\right)\cdot 0.07276 + (115 - 73)\cdot 0.0028$$

$$= 16.3 \text{ mm}$$

In-elastic deformation of the bottom flange of the steel beam immediately adjacent to the column face is included assuming strain ε_a=0.0030, measured from the experimental results (Fig. 4.19), over a flange length of 40 mm from the outer face of the column.

$\Delta_a = \varepsilon_a L_a = 0.0030 \cdot 40 = 0.1$ mm

$$\phi_{Cd} = \frac{\Delta_{u,s}}{D_b + D_s} + \frac{\Delta_a}{D_b} = \frac{16.3}{258 + 20} + \frac{0.1}{258} = 0.0592\text{rad} = 59.2 \text{ mrad}$$

HELSINKI UNIVERSITY OF TECHNOLOGY LABORATORY OF STEEL STRUCTURES PUBLICATIONS

TKK-TER-4	Malaska, M., Korhonen, E., Vuolio, A., Lu, W., Outinen, J., Myllymäki, J., Ma, Z., Seminar on Steel Structures: Design of Steel-Concrete Composite Structures, 1998.
TKK-TER-5	Tenhunen, O., Ohutlevyorsien asennustarkkuus, 1998.
TKK-TER-6	Sun, Y., The Shear Behaviour of a Composite Floor Slab with Modified Steel Sheeting Profile, 1998.
TKK-TER-7	Lu, W., Kesti, J., Mäkeläinen, P., Shear and Cross-Tension Tests for Press-Joins, 1998.
TKK-TER-8	Lu, W., Segaro, P., Kesti, J., Mäkeläinen, P., Study on the Shear Strength of a Single-Lap Rosette-Joint, 1998.
TKK-TER-9	Malaska, M., Mäkeläinen, P., Study on Composite Slim Floor Beams, 1999.
TKK-TER-10	Ma, Z., Mäkeläinen, P., Temperature Analysis of Steel-Concrete Composite Slim Floor Structures Exposed to Fire, 1999
TKK-TER-11	Ma, Z., Mäkeläinen, P., Numerical Analysis of Steel-Concrete Composite Slim Floor Structures in Fire, 1999.
TKK-TER-12	Kaitila, O., The Behaviour of Steel-Concrete Composite Frames in Fire Conditions, 1999.
TKK-TER-13	Kesti, J., Mäkeläinen, P. (toim./ eds.), Viidennet teräsrakenteiden tutkimus- ja kehityspäivät 18.-19.1.2000.
TKK-TER-14	Malaska, M., Ma, Z., Mäkeläinen, P., Steel-Cocrete Composite Slim Floor Frame System, 2000.
TKK-TER-15	Hara, R., Kaitila, O., Kupari, K., Outinen, J., Perttola, H. Seminar on Steel Structures: Design of Cold-Formed Steel Structures, 2000.
TKK-TER-16	Lu, W. Neural Network Model for Distortional Buckling Behaviour of Cold-Formed Steel Compression Members ,2000.
TKK-TER-17	Kaitila, O., Kesti, J., Mäkeläinen, P. Rosette-Joint and Steel Trusses, 2000.

ISBN 951-22-5224-4

ISSN 1456-4327